MOLECULAR PARTITIONING AND APPROXIMATE COUPLING TECHNIQUES IN MULTIPLE SCATTERING THEORY

by

FRANCISCO ALEXANDER LEON

B.S., University of Michigan
(1977)

SUBMITTED TO THE DEPARTMENT OF
PHYSICS
IN PARTIAL FULFILLMENT OF THE REQUIREMENTS
FOR THE DEGREE OF

DOCTOR OF PHILOSOPHY

at the

MASSACHUSETTS INSTITUTE OF TECHNOLOGY
February, 1984

Signature of Author Signature redacted
Department of Physics
January 13, 1984

Certified by Signature redacted
Keith H. Johnson
Thesis Supervisor

Accepted by Signature redacted
George Koster
Chairman, Departmental Committee on Graduate Students

MOLECULAR PARTITIONING AND APPROXIMATE COUPLING TECHNIQUES IN MULTIPLE SCATTERING THEORY

by

FRANCISCO ALEXANDER LEON

Submitted to the Department of Physics on January 13, 1984
in partial fulfillment of the requirements for the Degree
of Doctor of Philosophy.

ABSTRACT

A theoretical study was carried out on two techniques for improving the accuracy and extending the range of applicability of the self-consistent-field $X\alpha$ scattered-wave (SCF-$X\alpha$-SW) method for electronic structure calculations. The purpose of the molecular partitioning technique, which involves the division of a molecule or a cluster into spherical sub-clusters, is to minimize the effects of the constant potential region of the standard SCF-$X\alpha$-SW method. The molecular partitioning technique was applied to methanol, yielding better agreement with published photoemission data than the standard SCF-$X\alpha$-SW method. In particular, the molecular partitioning method gave the correct relative ordering of the methanol sigma and pi orbitals. The purpose of the approximate coupling technique is to allow calculations to be performed on molecules or clusters which are too large for the standard SCF-$X\alpha$-SW method. The molecule is divided into a principal sub-cluster and its environment; the electronic interactions between these two regions are treated approximately. This technique was applied to methanol with excellent results.

The chemisorption of carbon monoxide on supported rhodium catalysts was studied using the molecular partitioning and approximate coupling techniques. A notable result of the calculation was the relative weakness of the "back donation" to the carbon monoxide pi antibonding orbital. In addition, it was demonstrated that the approximate coupling technique is effective in the study of chemisorption.

Finally, a study of Zr-Cu and Pd-Si metallic glasses was carried out using the standard SCF-$X\alpha$-SW method. The resulting densities of states are in quantitative agreement with, and provide an interpretation of, published photoelectron spectra.

Thesis Supervisor: Dr. Keith H. Johnson

Title: Professor of Materials Science

TABLE OF CONTENTS

The self-consistent-field Xα scattered wave (SCF-Xα-SW or simply Xα-SW) method of calculating molecular orbitals has proved to be an important tool for investigating electronic structure problems in chemical and solid state physics. The usefulness and popularity of this method is due to its computational efficiency as well as its facility in treating transition metal and other relatively heavy atoms. These two characteristics arise from the combined use of the Xα statistical approximation to the exchange energy and the SCF-Xα-SW model potentials. The statistical (or local density) exchange approximation provides a substantial simplification of the complete Hartree-Fock equations; yet, when the resultant one-electron energies are compared to experiment, they are generally as good as, or better than, those obtained from Hartree-Fock calculations. The SCF-Xα-SW model potentials provide an additional computational simplification compared to calculations using the "true" molecular potential. At the same time, the model potentials allow the use of what is essentially a numerical basis set, which provides the flexibility needed for accurate treatment of inner shell electrons in heavy atoms. This flexible basis set is a distinguishing feature of the SCF-Xα-SW method, and in this respect it compares quite favorably to other techniques, such as LCAO or pseudo-potential methods.

There are, of course, limitations to the SCF-Xα-SW method; two general types of limitations, and possible procedures to overcome them, will be addressed in this dissertation. First, molecules (or clusters representing solids) with very open structures present a problem for the model potentials used in the SCF-Xα-SW method. The SCF-Xα-SW potentials (described more fully in Chapter 1) consist of

spherically averaged regions about the atoms and volume averaged regions in the space between the atoms. The volume averaged regions represent the more severe approximation; therefore, inaccuracies may be expected when performing an SCF-Xα-SW calculation on a system with a great deal of open space, such as an organic or biological molecule. A second type of limitation is encountered with molecules or clusters containing relatively large numbers of atoms. Often such calculations are impractical, because of the amount of computer time involved, or impossible because of numerical difficulties inherent with large matrices. Again, biological molecules provide a good example of this type of problem. Another example is the difficulty of providing realistic boundary condition of a cluster that represents a portion of a solid, the so-called "embedding" problem. In this thesis the techniques of molecular partitioning, first suggested by Kjellander, are described that attempt to solve these problems. Chapter 1 briefly reviews the standard SCF-Xα-SW theory and gives the formalism for the partitioned multiple scattering problem. In Chapter 2, calculations using these techniques are presented and compared with standard SCF-Xα-SW calculations as well as published experimental results. Chapter 3 describes the approximate coupling procedure for partitioned systems and presents some results of test calculations using this procedure. Chapter 4 is a study of carbon monoxide chemisorbed on a supported rhodium catalyst using the techniques described in the previous chapters. Chapter 5 is a study of metallic glasses using the standard SCF-Xα-SW method.

CHAPTER 1 - MOLECULAR PARTITIONING THEORY

In the calculation of molecular orbitals in the SCF-Xα-SW method, the model potential consists of spherically averaged regions about the atoms and a volume averaged region in the space between the atomic spheres [1-3]. While this approximation is a primary reason for the computational efficiency of the SCF-Xα-SW method, it is generally recognized that these model potentials are the most important source of inaccuracies [4-6]. The most severe approximation is the use of a single constant potential in the intersphere region, a region in the "true" molecular potential may vary widely. As a result, since the introduction of the SCF-Xα-SW method there have been many attempts to improve the model potential, particularly in the intersphere region [7-11]. Although the technique of molecular partitioning was introduced by Kjellander primarily to facilitate approximate calculations, it has the additional effect of improving the representation of the potential in the interatomic region [12-15]. In this chapter, the standard Xα-SW method is briefly reviewed, and the theory for molecular partitioning is presented.

1.Review of Standard SCF-Xa-SW Theory

The SCF-Xα-SW method is a way of calculating molecular orbital energies and wavefunctions for molecules or clusters consisting of as

many as fifty atoms. The $X\alpha$ statistical approximation to the exchange energy replaces the exchange term in the full Hartree-Fock equations. This simplification allows each eigenstate to be calculated independently, unlike the full Hartree-Fock case in which all one-electron wavefunctions are coupled through the exchange interaction.

An additional simplification is obtained through the use of a model potential (similar to a "muffin tin" potential of band theory). In the standard $X\alpha$-SW method, the space surrounding a molecule or cluster of atoms is divided into three types of regions (see Fig. 1.1). The potential is treated differently in each of the three types of regions. Region I consists of spheres which are centered on the atoms of the molecule. The potential of the molecule is spherically averaged in this region. Region II consists of the space between the atomic spheres and the outer sphere, which is a sphere surrounding the entire molecule. In region II the potential is represented by a single constant value, which is obtained by volume averaging the true potential throughout the intersphere region. Region III consists of the space outside of the outer sphere. In this region the potential is spherically averaged, and provides a way for the wavefunctions to decay smoothly at large distances from the molecule.

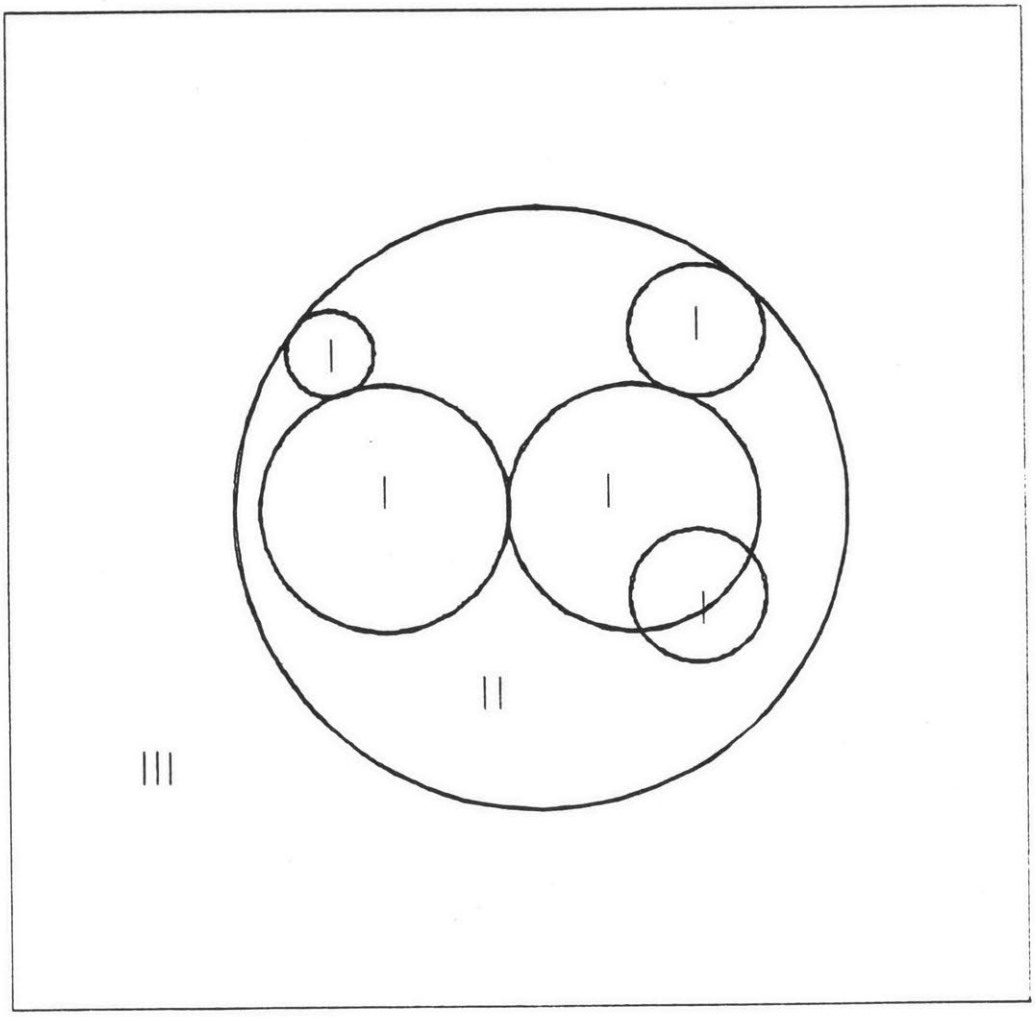

Figure 1.1 - Division of a molecular cluster into (I) atomic, (II) interatomic, and (III) extramolecular (or outer sphere) regions.

Corresponding to each type of region is a different representation of the molecular orbital wavefunction.

REGION I: $$\Psi_I^\alpha(\vec{r}) = \sum_L C_L^\alpha R_\ell^\alpha(E,r) Y_L(\hat{r}) \qquad (1.1)$$

where L=(l,m) is the angular momentum index, alpha is a label for the atom, $R_\ell^\alpha(E,r)$ is the solution to the radial Schrodinger equation in sphere alpha at energy E, $Y_L(\hat{r})$ is a real spherical harmonic, and C_ℓ^α is a coefficient which will be determined in the course of the calculation.

Region II: $$\Psi_{II}(\vec{r}) = \sum_\alpha \sum_L A_L^\alpha \phi_\ell(\kappa r_\alpha) Y_L(\hat{r}_\alpha) + \sum_L A_L^\circ \chi_\ell(\kappa r_\circ) Y_L(\hat{r}_\circ) \qquad (1.2)$$

where $r_\alpha = |\vec{r} - \vec{R}_\alpha|$ ($\vec{R}_\alpha$ is the position of atom alpha)

$$\phi_\ell(\kappa r_\alpha) = \begin{cases} k_\ell^{(1)}(\kappa r_\alpha) & \text{if } E < \overline{V}_{II} \\ n_\ell(\kappa r_\alpha) & \text{if } E > \overline{V}_{II} \end{cases}$$

$$\chi_\ell(\kappa r_\alpha) = \begin{cases} i_\ell(\kappa r_\alpha) & \text{if } E < \overline{V}_{II} \\ j_\ell(\kappa r_\alpha) & \text{if } E > \overline{V}_{II} \end{cases}$$

$\kappa = |E - \overline{V}_{II}|^{\frac{1}{2}}$ (where E is the energy eigenvalue, and $\overline{V}_{II}$ is the value of the constant potential in Region II), $j_\ell(x)$ is a spherical Bessel function, $n_\ell(x)$ is a spherical Neumann

function, $i_\ell(x)$ is a modified spherical Bessel function, and $k_\ell^{(1)}(x)$ is a modified spherical Hankel function of the first kind (see Ref. [3]) The A_L^α are coefficients which are determined in the course of the calculation.

REGION III: $$\Psi_{III}(\vec{r}) = \sum_L C_L^\circ R_\ell^\circ(E, r_\circ) Y_L(r_\circ) \qquad (1.3)$$

Here the quantities are analogous to those of region I.

The problem of finding the eigenstates or molecular orbitals of the system can be considered as a boundary value problem in which an energy is found that allows the wavefunction and its first derivative to be matched across all the sphere boundaries, or it can be considered as a scattering problem in which the scattering of an electron wave from a given atom alpha is consistent with the subsequent re-scatterings by all the other atoms of the molecule. The latter approach will be used here as it can be more easily generalized to the approximation techniques to be described later.

Consider the wavefunction just outside a given atomic sphere alpha. It can be written in a multi-center representation as in (1.2), or it can be described as an expansion of spherical bessel functions about sphere alpha alone:

$$\Psi_{II}(\vec{r}) = \sum_L A_L^\beta \phi_\ell(Kr_\beta) Y_L(\hat{r}_\beta) + \sum_L B_L^\beta \chi_\ell(Kr_\beta) Y_L(\hat{r}_\beta) \qquad (1.4)$$

The first sum in the above expression can be described as the outgoing or scattered wave from sphere alpha, while the second sum can be described as the incoming wave arriving from all the other atoms of the molecule. The ratio of the components of the incoming wave to the outgoing wave is given by a scattering matrix:

$$A_L^\beta = \sum_{L'} \tau_{LL'}^\beta(E)\, B_{L'}^\beta \qquad (1.5)$$

For scattering from spherically symmetric potentials, a simple application of the Wigner-Eckart theorem shows that the l-components are not mixed; the T-matrix (1) is therefore diagonal and independent of m:

$$A_L^\beta = \tau_l^\beta\, B_L^\beta \qquad (1.6)$$

Now the incoming waves in (1.4) can be related to the outgoing waves from all spheres other than beta:

$$B_L^\beta = \sum_{\alpha\neq\beta} \sum_{L'} G_{LL'}^{\beta\alpha}(E)\, A_{L'}^\alpha \qquad (1.7)$$

---

(1) Because the waves in this theory are actually standing rather than traveling waves, what is here called a T-matrix or scattering matrix corresponds to what is often called the K-matrix or reaction matrix in other works dealing with scattering theory [10].

where $G^{\beta\alpha}_{LL'}(E)$ is a matrix element of the one-particle unperturbed Green's function in the intersphere region and the basis is the set of spherical bessel and neumann functions:

$$G^{\alpha\beta}_{LL'}(E) = \langle \chi_\ell(\kappa r_\alpha) Y_L(\hat{r}_\alpha) \,|\, G^\circ(E) \,|\, \phi_\ell(\kappa r_\beta) Y_L(\hat{r}_\beta) \rangle \qquad (\alpha \neq \beta) \tag{1.8}$$

If beta is the outer sphere,

$$G^{\alpha\beta}_{LL'}(E) = \langle \chi_\ell(\kappa r_\alpha) Y_L(\hat{r}_\alpha) \,|\, G^\circ(E) \,|\, \chi_{-\ell}(\kappa r_\beta) Y_L(\hat{r}_\beta) \rangle \qquad (\alpha \neq \beta) \tag{1.9}$$

The precise analytical forms of these matrix elements can be found in Reference [3]. A bound state solution to the scattering problem is obtained when an energy is found for which the outgoing wave from sphere beta is equal to the transformation of the incoming wave by the T-matrix:

$$\sum_L A^\beta_L \phi_\ell(\kappa r_\beta) Y_L(\hat{r}_\beta) = \sum_L \sum_{L'} t^\beta_{LL'}(E) B^\beta_{L'} \chi_{\ell'}(\kappa r_\beta) Y_{L'}(\hat{r}_\beta)$$

$$= \sum_L \sum_{L'} \sum_\alpha \sum_{L''} t^\beta_{LL'}(E) G^{\beta\alpha}_{L'L''}(E) A^\alpha_{L''} \chi_{\ell'}(\kappa r_\beta) Y_{L'}(\hat{r}_\beta) \tag{1.10}$$

The above relation must be true for all atoms beta in order for E to be the energy of a bound state. The problem is finally cast as a system of coupled linear equations for the unknown

coefficients A_L^α :

$$\sum_\beta \sum_{L'} \left\{ \left[t^\alpha(E) \right]^{-1}_{LL'} \delta_{\alpha\beta} - G^{\alpha\beta}_{LL'}(E) \right\} A^\beta_{L'} = 0 \qquad (1.11)$$

For the case of spherically averaged potentials inside the atomic spheres, the T-matrix is simplified:

$$\sum_\beta \sum_{L'} \left\{ \left[t^\alpha(E) \right]^{-1}_{\ell} \delta_{LL'} \delta_{\alpha\beta} - G^{\alpha\beta}_{LL'}(E) \right\} A^\beta_{L'} = 0 \qquad (1.12)$$

The $\left[t^\alpha(E) \right]^{-1}_\ell$ are found by equating the logarithmic derivatives of (1.4) and (1.1) at the boundary of atomic sphere alpha; they are given explicitly by:

$$\left[t^\alpha(E) \right]^{-1}_\ell = \begin{cases} -\dfrac{\left[\chi_\ell(\kappa b_\alpha), R^\alpha_\ell(E, b_\alpha) \right]}{\left[\phi_\ell(\kappa b_\alpha), R^\alpha_\ell(E, b_\alpha) \right]} & (\text{for } \alpha \neq \text{outer sph.}) \qquad (1.13) \\ -\dfrac{\left[\phi_\ell(\kappa b_\alpha), R^\alpha_\ell(E, b_\alpha) \right]}{\left[\chi_\ell(\kappa b_\alpha), R^\alpha_\ell(E, b_\alpha) \right]} & (\text{for } \alpha = \text{outer sph.}) \qquad (1.14) \end{cases}$$

Here b_α is the radius of atomic sphere alpha, and the following notation for the Wronskian is used:

$$[F(x), G(x)] = F(x)\frac{dG(x)}{dx} - G(x)\frac{dF(x)}{dx} \tag{1.15}$$

In order to find bound states of the system, the energy of (1.12) is varied until the determinant of the matrix of the linear system of (1.12) vanishes. The coefficients A_L^α can then be found with standard matrix manipulation techniques. These A_L^α are the coefficients of the wavefunction in the interatomic region (see (1.2)). The coefficients C_L^α for the wavefunction inside the atomic spheres are obtained from the A_L^α and the following relationships (which arise from demanding the continuity of the wavefunction and its first derivative at the sphere boundaries):

$$A_L^\alpha = (-1)^{\ell+1} \kappa b_\alpha^2 \left[i_\ell(\kappa b_\alpha), R_\ell^\alpha(E, b_\alpha) \right] C_L^\alpha \tag{1.16}$$

$$(E < \bar{V}_{II},\ \alpha \neq \text{outer sph.})$$

$$A_L^\alpha = (-1)^{\ell+1} \kappa b_\alpha^2 \left[R_\ell^\alpha(E, b_\alpha), k_\ell^{(1)}(\kappa b_\alpha) \right] C_L^\alpha \tag{1.17}$$

$$(E < \bar{V}_{II},\ \alpha = \text{outer sph.})$$

$$A_L^\alpha = \kappa b_\alpha^2 \left[j_\ell(\kappa b_\alpha), R_\ell^\alpha(E, b_\alpha) \right] C_L^\alpha \tag{1.18}$$

$$(E > \bar{V}_{II},\ \alpha \neq \text{outer sph.})$$

$$A_L^\alpha = \kappa b_\alpha^2 \left[R_\ell^\alpha(E, b_\alpha), n_\ell(\kappa b_\alpha) \right] C_L^\alpha \tag{1.19}$$

$$(E > \bar{V}_{II},\ \alpha = \text{outer sph.})$$

Once all the wavefunctions for the occupied states of the molecule are obtained they are normalized and used to create a new

potential. To create the new potential, the charge density is first spherically averaged in the atomic spheres and volume averaged in the interatomic region (region II). Using this averaged charge density, potentials are calculated which are then spherically averaged in the atomic spheres and volume averaged in the inter-atomic region. This new potential is used to find a new set of one-electron eigenstates for the molecule; the entire process is repeated until self-consistency is achieved.

Molecular Partitioning Theory

Kjellander [12-15] made two related suggestions for further development of the Xα-SW method: the partitioning of the molecule or cluster into sub-clusters, and the approximation of the interaction between sub-clusters. The partitioning into sub-clusters is described in this section; the approximate coupling techniques are described in Chapter Three.

Often a molecule or a cluster can be divided into groups of atoms which can be enclosed by spheres. An example of this is shown in Fig. 1.2 for the molecule methanol. This method of partitioning space is used to define a new model potential, allowing a different intersphere potential to be defined for each of the spheres shown in Fig. 1.2. The intersphere potential for sphere 1 refers to the constant potential of the region inside sphere 1 but outside spheres 2 and 3. The intersphere potential for sphere 2 (or 3) refers to the constant potential of the region inside sphere 2 (or 3) but excluding the regions contained in the atomic spheres. In the partitioned model, the electron waves will be scattered from the sphere surfaces as well as from the atomic surfaces. For example, an outgoing wave from an atom inside sphere 2 strikes the surface of sphere 2, part of it will be reflected back into the interior of sphere 2 and the rest will be transmitted to the rest of the molecule outside of sphere 2.

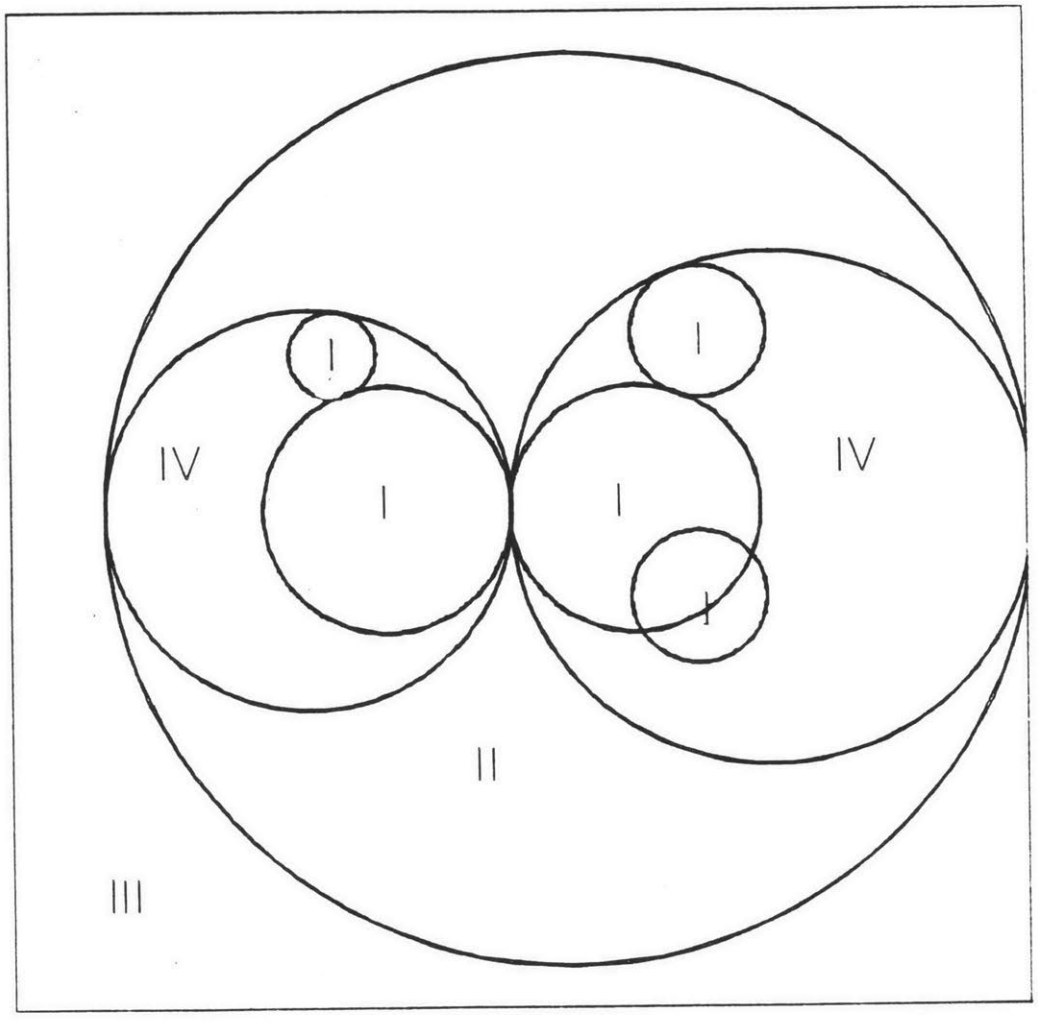

Figure 2 - Division of methanol molcule into two sub-clusters.

The basic motivation for partitioning the cluster into spherical regions as opposed to some other shape is that the calculation of the scattering matrix is particularly simple for a spherical surface. Scattering from an arbitrarily shaped surface can be mathematically formulated, but has been found to be computationally impractical [9].

The introduction of the sub-cluster spheres should improve the accuracy of the self consistent calculations in two ways. First, the flexibility of having regions of different intersphere potential should lead to electronic states which are closer to the hypothetical electronic states of the "true" potential, the molecular potential without any spherical or volume averaging. Of course, if the electronic states of the "true" potential could be calculated, the types of averages and approximations described here would be unnecessary. Second, the sub-cluster spheres allow the intersphere charge associated with each electronic state to be divided among the various spheres, rather than averaged throughout the entire interatomic region as is done in the standard SCF-Xα-SW method. The divided charge will then be volume averaged within the individual intersphere regions of the sub-clusters. The resultant charge distribution is more realistic than that of the standard SCF-Xα-SW procedure, and should lead to more accurate potentials in the atomic regions as well as the various intersphere regions.

The representation of the wavefunction in the partitioned system is somewhat more involved than in the standard Xα-SW case, because there are more types of regions. In what follows, the region numbers refer to types of regions (Roman numerals in Fig. 1.2) and should not be confused with the numbering of the partitioning spheres. The

mathematical notation will use the convention of numbering the partitioning spheres with the letters i,j,k,..., while the atomic spheres will be denoted by the Greek letters α, β, γ . An atomic sphere will be uniquely specified by the ordered pair (i, α), where σ i is the partitioning sphere containing atom α .

Region I refers to space inside an atomic sphere.

$$\Psi_I^{i\alpha}(\vec{r}) = \sum_L C_L^{i\alpha} R_\ell^{i\alpha}(E, r_{i\alpha}) Y_L(\hat{r}_{i\alpha}) \qquad (1.20)$$

where $C_L^{i\alpha}$ is the coefficient for atom alpha in sub-cluster i, $R_\ell^{i\alpha}$ is the corresponding radial function, and $r_{i\alpha} = |\vec{r} - \vec{R}_{i\alpha}|$, where $\vec{R}_{i\alpha}$ is the location of the center of atom α in sub-cluster i.

Region II refers to the space inside the outer sphere of the entire molecule (which shall be called the "system outer sphere") but outside of the sub-clusters.

$$\Psi_{II}(\vec{r}) = \sum_i \sum_L A_L'^i \phi_\ell(k_o r_i) Y_L(\hat{r}_i) + \sum_L A_L'^o \chi_\ell(k_o r_o) Y_L(\hat{r}_o) \qquad (1.21)$$

where $A_L'^o$ is a coefficient for the system outer sphere, $A_L'^i$ is a coefficient for sub-cluster i, $k_o = |E - \overline{V}_{II}|^{1/2}$, where $\overline{V}_{II}$ is the constant potential in Region II, and $r_i = |\vec{r} - \vec{R}_i|$,where $\vec{R}_i$ is the location of the center of sub-cluster i.

Region III refers to space outside the system outer sphere in which the potential is spherically averaged.

$$\Psi_{III}(\vec{r}) = \sum_L C^{\circ}_L R^{\circ}_\ell(E, r_o) Y_L(\hat{r}_o) \qquad (1.22)$$

where R°_ℓ refers to the radial function outside of the system outer sphere, and C°_ℓ are the coefficients for those functions.

Region IV refers to the various intersphere regions within the sub-clusters, but outside of the atoms of those sub-clusters.

$$\Psi^i_{IV}(\vec{r}) = \sum_{\alpha \in \sigma_i} \sum_L A^{i\alpha}_L \phi_\ell(\kappa_i r_{i\alpha}) Y_L(\hat{r}_{i\alpha}) + \sum_L A^i_L \chi_\ell(\kappa_i r_i) Y_L(\hat{r}_i) \qquad (1.23)$$

where $A^{i\alpha}_L$ is a coefficient for atom alpha in sub-cluster i, and A^i_L is a coefficient for the sphere surrounding that sub-cluster. The notation $\alpha \in \sigma_i$ denotes all atoms α contained in partitioning sphere σ_i.

A system of equations for the coefficients of the Region II wavefunction can now be written by adapting (1.11) of the previous section:

$$\sum_i \sum_{L'} \left\{ \left[\tilde{\tau}^i(E) \right]^{-1}_{LL'} \delta_{ij} - G^{ij}_{LL'}(E) \right\} A^{j}_{L'} = 0 \qquad (1.24)$$

where the matrix $\tilde{T}(E)^i$ represents the scattering of waves from the outside of sphere i; its elements are yet to be determined. The summation over j includes j=0, the system outer sphere. Note that because partitioning sphere i may contain several atomic spheres, it is not, in general, spherically symmetric; thus, $\tilde{T}(E)^i$ is not necessarily diagonal in the angular momentum indices.

In order to find $\tilde{T}(E)^i$, the relationship between A'^j_L and A^j_L is examined for a given sphere. In the spirit of the discussion of (1.4), A'^j_L is the coefficient for the scattered wave outside of sphere j (traveling outward away from the surface of sphere j), while A^j_L is the coefficient for the scattered wave inside of sphere j (traveling inward away from the surface of sphere j). Introducing the coefficient B'^j_L for the incoming wave outside of sphere j (traveling inward towards the surface of sphere j), the wavefunction just outside the surface of sphere j can be represented as

$$\Psi(\vec{r}) = \sum_L \left\{ A'^j_L \jmath_\ell(\kappa_0 r_j) + B'^j_L \chi_\ell(\kappa_0 r_j) \right\} Y_L(\hat{r}_j) \qquad (1.25)$$

Introducing the coefficient B^j_L for the incoming wave inside of sphere j (traveling outward towards the surface of sphere j), the wavefunction just inside the surface of sphere j can be represented as

$$\Psi(\vec{r}) = \sum_L \left\{ B_L^j \phi_\ell(k_j r_j) + A_L^j \chi_\ell(k_j r_j) \right\} Y_L(\hat{r}_j) \qquad (1.26)$$

By equating the wavefunction and its first derivative across the sphere boundary, the following relationships are obtained:

$$B_L'^j = M_\ell'^j A_L'^j + N_\ell'^j A_L^j \qquad (1.27)$$

$$B_L^j = M_\ell^j A_L^j + N_\ell^j A_L'^j \qquad (1.28)$$

where

$$M_\ell^j = -\left[\chi_\ell(\kappa_0 b_j), \chi_\ell(\kappa_j b_j)\right] \Big/ D_\ell^j \tag{1.29}$$

$$N_\ell^j = \left[\chi_\ell(\kappa_0 b_j), \phi_\ell(\kappa_0 b_j)\right] \Big/ D_\ell^j \tag{1.30}$$

$$M'^j_\ell = -\left[\phi_\ell(\kappa_0 b_j), \phi_\ell(\kappa_j b_j)\right] \Big/ D_\ell^j \tag{1.31}$$

$$N'^j_\ell = \left[\chi_\ell(\kappa_j b_j), \phi_\ell(\kappa_j b_j)\right] \Big/ D_\ell^j \tag{1.32}$$

$$D_\ell^j = \left[\chi_\ell(\kappa_0 b_j), \phi_\ell(\kappa_j b_j)\right] \tag{1.33}$$

Here b_j is the radius of partitioning sphere j. Other expressions for B_L^j and B'^j_L can be found by using (1.7):

$$B_L^j = \sum_{\alpha \in \sigma_j} G_{LL'}^{j_0, j\alpha}(E)\, A_{L'}^{j\alpha} \tag{1.34}$$

$$B'^{j}_{L} = \sum_{i \neq j} \sum_{L'} G^{ji}_{LL'}(E)\, A'^{i}_{L'} \qquad (1.35)$$

where the summation over i includes the system outer sphere (i=0). The Green's function matrix elements in the above equations are defined in (1.8) and (1.9), with the differences that $\kappa = \kappa_j$ for $G^{j\sigma,j\alpha}_{LL'}$ and $\kappa = \kappa_0$ for $G^{ji}_{LL'}$.

Substituting the above expressions for B and B′ in (1.27) and (1.28),

$$M^{j}_{\ell} A^{j}_{L} + N^{j}_{\ell} A'^{j}_{L} - \sum_{\alpha \in \sigma_j} \sum_{L'} G^{j\sigma,j\alpha}_{LL'}(E)\, A^{j\alpha}_{L'} = 0 \qquad (1.36)$$

$$M'^{j}_{\ell} A'^{j}_{L} + N'^{j}_{\ell} A^{j}_{L} - \sum_{i \neq j} \sum_{L'} G^{ji}_{LL'}(E) A'^{i}_{L'} = 0 \qquad (1.37)$$

(for all j except the system outer sphere (j=0); summation over i includes the system outer sphere). The equations (1.36) and (1.37) would be enough to determine A'^{j}_{L} and A^{j}_{L} if the atomic coefficients $A^{j\alpha}_{L}$ were known. An expression for the $A^{j\alpha}_{L}$ is found by adopting (1.12):

$$\sum_{\beta} \sum_{L'} \left\{ \left[t^{j\alpha}(E) \right]^{-1}_{\ell} \delta_{LL'} \delta_{\alpha\beta} - G^{j\alpha,j\beta}_{LL'}(E) \right\} A^{j\beta}_{L'} - \sum_{L'} G^{j\alpha,j\sigma}_{LL'} A^{j}_{L'} = 0 \qquad (1.38)$$

An expression for A°_{L} is found in a similar way:

$$\sum_{i}\sum_{L'}\left\{\left[t^{\circ}(E)\right]^{-1}_{\ell}\delta_{LL'}\delta_{\alpha\beta}-G^{\circ i}_{LL'}(E)\right\}A^{'i}_{L'}=0 \qquad (1.39)$$

where $\left[t^{j\alpha}(E)\right]^{-1}_{\ell}$ and $\left[t^{\circ}(E)\right]^{-1}_{\ell}$ are defined in (1.13) and (1.14), but with K_j and K_o replacing K. Equations (1.36), (1.37), (1.38), and (1.39) constitute a complete linear system for the coefficients A^{j}_{L}, $A^{'j}_{L}$, and $A^{j\beta}_{L}$. Now, define T^{j} as the scattering matrix for the atoms in sub-cluster j (excluding the scattering from the sphere surrounding sub-cluster j) so that

$$\left[T^{j}(E)\right]^{-1}_{\alpha\beta,LL'}=\left[t^{j\alpha}(E)\right]^{-1}_{\ell}\delta_{\alpha\beta}\,\delta_{LL'}-G^{j\alpha,j\beta}_{LL'}(E) \qquad (1.40)$$

With the aid of this definition, the linear system can be put in a matrix form which displays the physical meaning of the various matrix elements. For a system with two partitioning spheres and a system

outer sphere, the secular matrix is

$$\begin{bmatrix} t_0^{-1} & -G^{01} & -G^{02} \\ -G^{10} & \begin{matrix} M'^1 & N'^1 \\ N^1 & M^1 - G^{10,12} \end{matrix} & -G^{12} \\ -G^{20} & -G^{21} & \begin{matrix} M'^2 & N'^2 \\ N^2 & M^2 - G^{20,22} \end{matrix} \\ & -G^{12,10}[T^1]^{-1} & -G^{22,20}[T^2]^{-1} \end{bmatrix} \begin{bmatrix} A'^0 \\ A'^1 \\ A^1 \\ A^{12} \\ A'^2 \\ A^2 \\ A^{22} \end{bmatrix} = 0 \tag{1.41}$$

Here $G^{j\alpha,j\alpha}$ stands for a matrix composed of the elements $G^{j\alpha,j\alpha}_{LL'}$; analogous conventions apply of the other matrix symbols. $A^{i\alpha}$ stands for the column vector composed of the elements $A^{i\beta}_L$ $(\beta \epsilon \sigma_i)$; the other A symbols follow analogous conventions.

Note that the matrix is nearly in block diagonal form. Each

partitioned sphere has its own sub-matrix, and the sub-matrices are coupled together with the Green's function matrices G^{ij}. The M, M', N, and N' matrices serve as transmission and reflection coefficients at the partitioning sphere boundaries. The T matrices are scattering matrices for the clusters of atoms within the partitioning spheres.

Bound states are found in the same way as in the standard SCF-X -SW method: the energy is varied until a zero is found in the determinant of (1.41); the wavefunctions are then normalized. When all the molecular orbitals have been found, their charge densities are used to create a new potential. New bound states are then obtained using a mixture of the old and new molecular potentials. The process is repeated until self-consistency is attained.

A series of test calculations of the methanol molecule using this procedure are described in Chapter 2. Applications of this procedure to a chemisorption problem is presented in Chapter 4.

REFERENCES

1. K.H. Johnson, J. Chem. Phys. 45, 3085 (1966).

2. K.H. Johnson, Int. J. Quantum Chem. 1S, 361 (1967).

3. K.H. Johnson, Adv. Quantum Chem. 7, 143 (1973).

4. F. Herman, A.R. Williams, and K.H. Johnson, J. Chem. Phys. 61, 3508 (1974).

5. D.R. Salahub, R.P. Messmer, and K.H. Johnson, Molecular Physics 31, 529 (1976).

6. R.P. Messmer and S.H. Lamson, Chem. Phys. Letters 90, 31 (1982).

7. K.H. Johnson, Int. J. Quantum Chem. 4, 153 (1971).

8. V.C. Rakhecha and N.S. Satya Murthy, J. Phys. C 14, 1809 (1981).

9. A.R. Williams, Int. J. of Quan. Chem. Symp. No.8, 89 (1974).

10. P. Lloyd, Adv. Phys. (GB) 20, 69 (1972).

11. J. Siegel, D. Dill, and J.L. Dehmer, J. Chem. Phys. 64, 3204 (1976).

12. R. Kjellander, Chem. Phys. Letters 29, 280 (1974).

13. R. Kjellander, Chem. Phys. 12, 469, (1976).

14. R. Kjellander, Chem. Phys. 20, 153 (1977).

15. K.H. Johnson, F. Herman, and R. Kjellander, in Electronic Structure of Polymers and Molecular Crystals, edited by J.-M. Andre and J. Ladik (Plenum, New York, 1975).

CHAPTER 2 - MOLECULAR PARTITIONING APPLIED TO THE METHANOL MOLECULE

The modification of the standard SCF-Xα-SW potentials to include the partitioning spheres described in the previous chapter should provide a more realistic description of the electronic structure of a molecule or cluster of atoms. Observables, such as ionization energies, obtained from Xα-SW calculations using the partitioning spheres should be closer to experimental quantities than those obtained from Xα-SW calculations not using the spheres. To test this assumption, a series of calculations of the electronic structure of the methanol molecule have been performed and compared to published experimental observations. Methanol was chosen as a test case because it is an organic molecule with a relatively open structure. As discussed in Chapter 1, the large amount of intersphere volume associated with such open structures is considered an important source of inaccuracies; it is inaccuracies of this sort that the partitioning spheres should counteract. Because methanol is well characterized experimentally and theoretically [1-8], there should be little ambiguity in interpreting the results of the calculations. As an organic molecule, methanol can be considered representative of other types of systems of current interest which are not so well understood, such as polymers and biological molecules. If the partitioning method improves the results for methanol, these other larger systems should benefit from its use as well.

It has long been recognized that the large intersphere volume of

certain systems, such as organic molecules, presented difficulties to the standard SCF-Xα-SW method [9-11]. The most successful technique for dealing with this problem has been to increase the atomic radii, thus allowing the spherical atomic regions to overlap. Because the potential in the spherically averaged atomic regions is more realistic than the volume averaged potential in the intersphere region, increasing the volume in the atomic regions at the expense of the intersphere volume should improve the results. Of course, errors will be introduced if no corrections are made to the scattering equations to take account of the overlap. Although these corrections are well known [12], the general practice is for overlapping sphere calculations to be performed with the same formalism and computer codes developed for the tangent sphere case. Numerical tests have shown that for modest amounts of overlap, the introduced errors are small, and are generally far outweighed by the improvements in the potential. There is no a priori way to decide what the optimal amount of sphere overlap should be; by trial and error it has been found that an overlap of approximately twenty per cent (i.e., a 20% increase of the radii of the tangent atomic spheres) usually gives the best results. Typically, even when overlapping atomic spheres are used, the radius of the outer sphere is chosen so that there is no overlap between the outer sphere and any of the atomic spheres.

The introduction of partitioning spheres raises a number of questions concerning sphere radii and placement. How should the molecule or cluster be partitioned? Should partitioning spheres be allowed to overlap other partitioning spheres? Should they be allowed to overlap atomic spheres? Should they be allowed to overlap the

system outer sphere? As in the problem of deciding the optimal amount of atomic sphere overlap, there seems to be no a priori way to answer these questions; actual numerical tests are required. To this end, calculations of the methanol molecule using three different types of partitioning have been performed and are described in this chapter.

The first question to be addressed is the placement of the partitioning spheres. Consider the methanol molecule, shown in Fig. 2.1 with tangent, non-overlapping atomic spheres and in Fig. 2.2 with overlapping spheres. There are two non-equivalent ways to divide the molecule. First, it may be divided into a methyl (CH_3) fragment and an OH fragment. This division is appropriate if these fragments are considered as "building blocks" of the methanol molecule. Alternatively, the molecule may be divided into a CO fragment inside a single partitioning sphere with the the four hydrogen atoms outside this partitioning sphere but inside the system outer sphere. This division is appropriate if the CO bond is considered the most important in the molecule. The first approach is shown in Fig. 2.3 and 2.4, while the second is shown in Fig. 2.5.

The second question to be addressed is whether the partitioning spheres should be allowed to overlap. The case of tangent and overlapping partitioning spheres are shown in Fig. 2.3 and 2.4 respectively. As there is only one partitioning sphere in Fig. 2.5, this question does not arise; on the other hand, the partitioning in Fig. 2.5 does overlap several atomic spheres. Consideration of the geometric structure of methanol quickly reveals that this overlap cannot be avoided if tangent atomic spheres are used. The atomic sphere-partitioning sphere overlap could be eliminated if the atomic

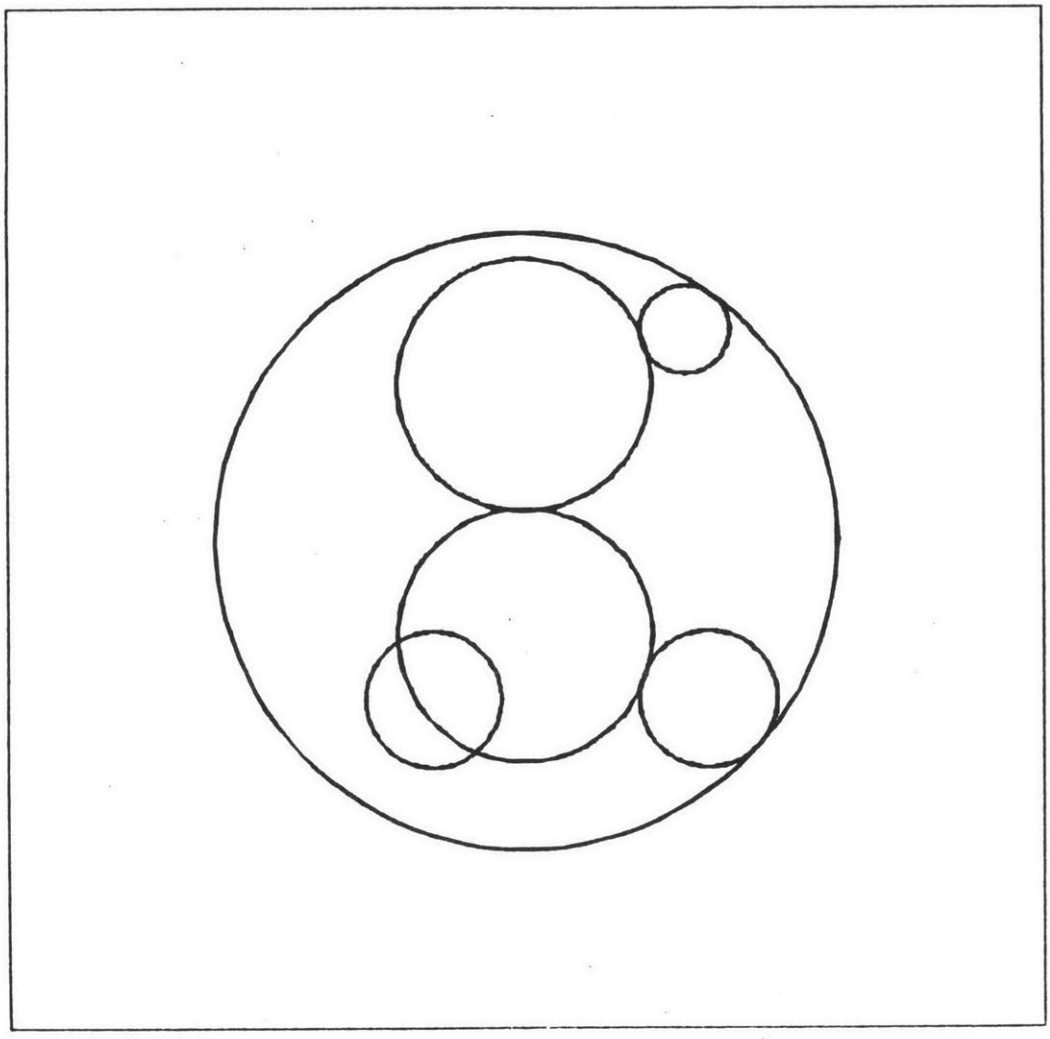

Fig. 2.1. Schematic diagram showing sphere sizes used in standard SCF-X -SW calculation of methanol with tangent atomic spheres. The diagram is a projection of the molecule onto a single plane.

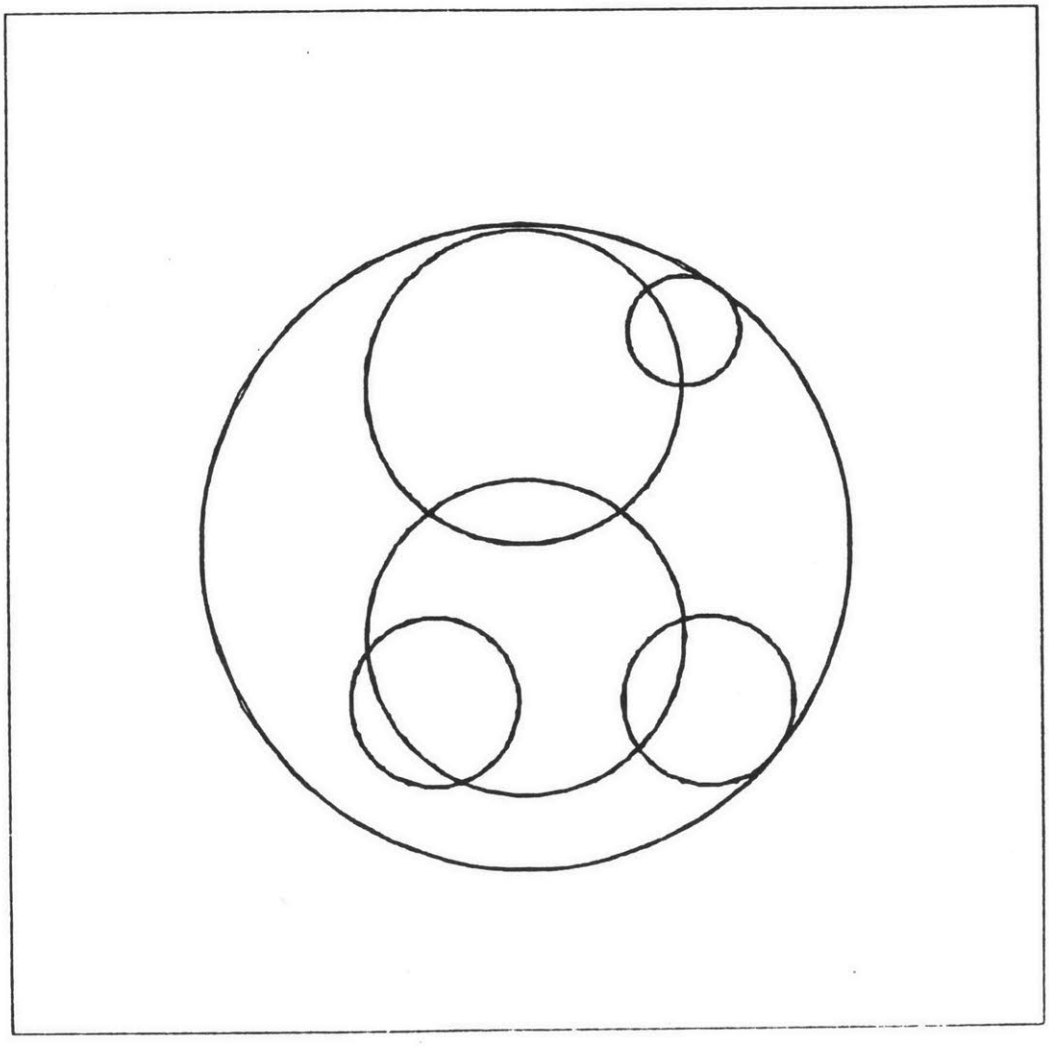

Fig. 2.2. Schematic diagram showing sphere sizes used in standard SCF-Xα-SW calculation of methanol with overlapping atomic spheres.

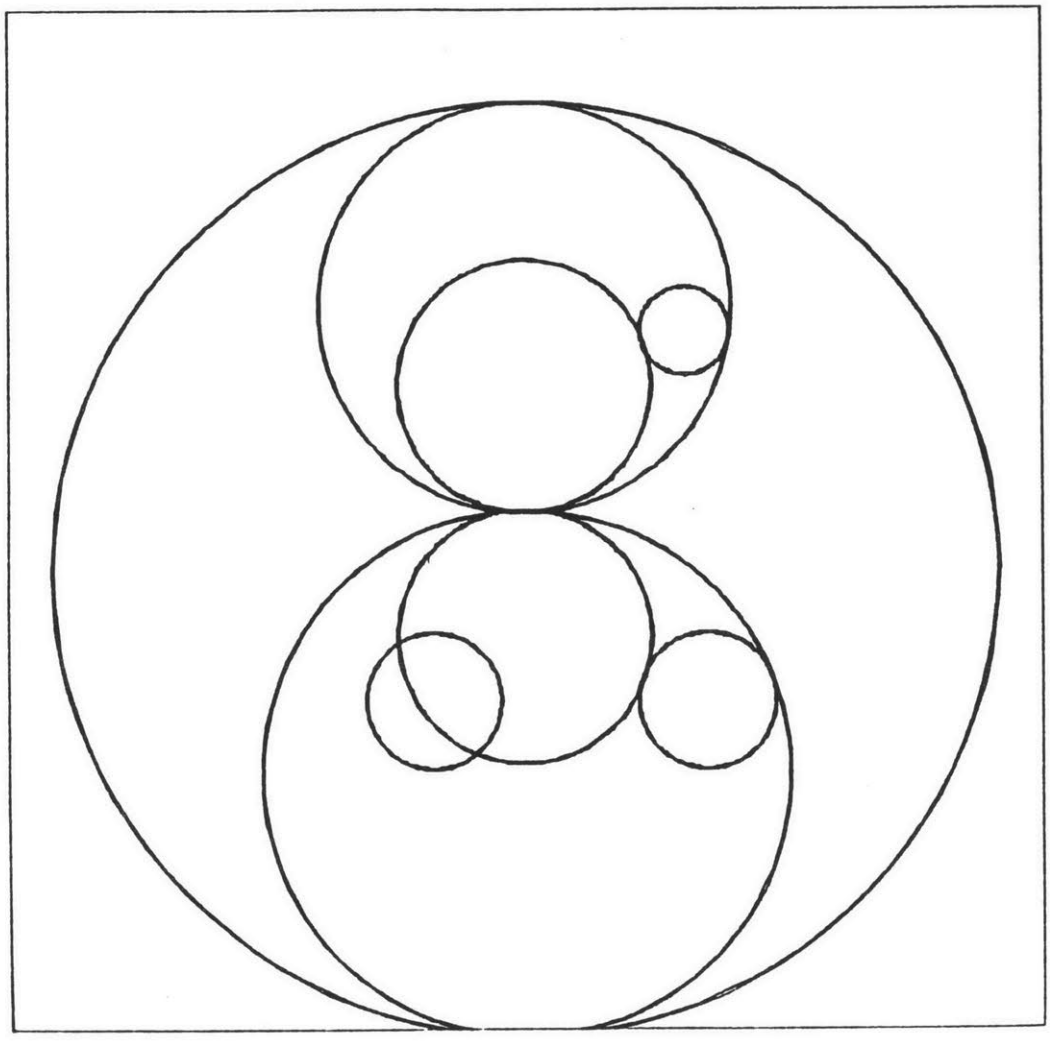

Fig. 2.3. Diagram of Model I partitioning of methanol, showing tangent partitioning spheres.

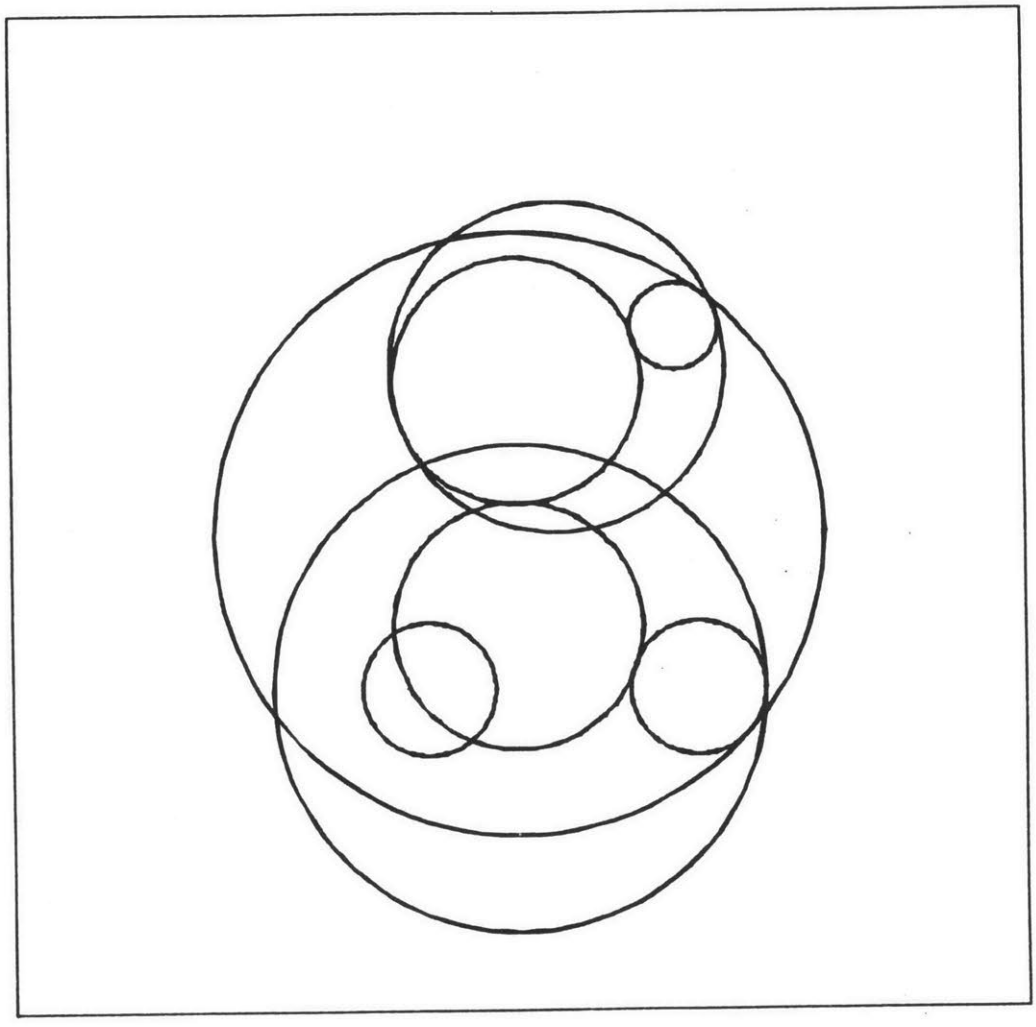

Fig. 2.4. Diagram of Model II partitioning of methanol, showing overlapping partitioning spheres.

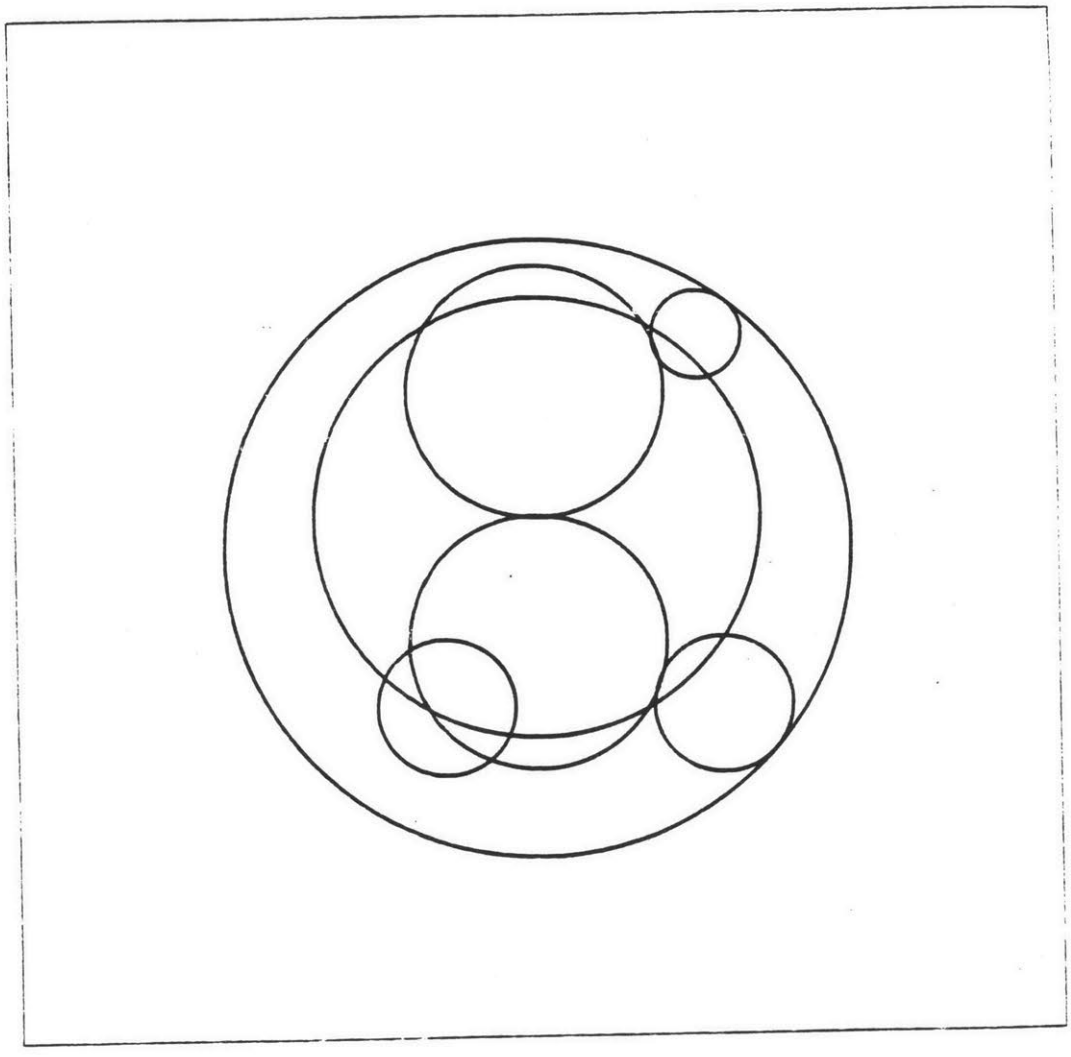

Fig. 2.5. Diagram of Model III partitioning of methanol, in which a single partitioning sphere surrounds the carbon and oxygen atoms.

sphere radii were drasticly reduced; however, the same considerations that make overlapping spheres an improvement over tangent spheres imply that the use of atomic radii smaller than tangent sphere radii would lead to decidedly inferior results. Note that all the partitioned calculations in this chapter have tangent rather than overlapping atomic spheres. The coordinates and radii of the atomic and partitioning spheres used in the different models are given in Table 2.1 [8].

Comparing the first partitioning scheme in Fig. 2.3 (Model I) with the second and third in Figs. 2.4 and 2.5 (Models II and III), it is clear that the requirement that the partitioning spheres do not overlap any other type of sphere is a severe restriction that results in large partitioning spheres as well as a large system outer sphere. This defeats the purpose of the partitioning method, which aims at reducing the effects of the volume averaged regions; yet, for the first partitioning scheme the overall intersphere volume is markedly increased. This problem is more general than this single example might suggest. Many molecules and clusters are not easily divisible into spherical regions unless these regions are allowed to overlap each other or with the smaller atomic regions. Thus, in order for the partitioning method to have the widest application, successful calculations with overlapping partitioning spheres should be possible.

Before comparing the detailed results of the various partitioning schemes, it might be useful first to review the electronic structure of methanol using the standard SCF-Xα-SW method with tangent spheres. The one electron energy levels of this calculation are shown in Fig. 2.6, with the omission of the C 1s and O 1s core levels. One standard

TABLE 2.1

ATOMIC COORDINATES FOR METHANOL

Atom	X	Y	Z	Radius	Alpha
out. sph.	0.0	0.0	0.0	3.483	0.75805
C	0.0	0.0	-1.267	1.349	0.75928
O	0.0	0.0	1.431	1.349	0.74447
H	0.0	1.951	-1.956	0.720	0.77720
H	0.0	1.715	2.022	0.720	0.77720
H	1.690	-0.976	-1.956	0.720	0.77720
H	-1.690	-0.976	-1.956	0.720	0.77720

PARTITIONING SPHERE COORDINATES

Model I:

Sphere No.	X	Y	Z	Radius	Alpha
1	0.0	0.0	-0.542	5.023	0.75805
2	0.0	0.0	2.282	2.200	0.74915
3	0.0	0.0	-2.742	2.823	0.76696

Model II:

Sphere No.	X	Y	Z	Radius	Alpha
1	0.0	0.0	0.0	3.483	0.75805
2	0.0	0.440	1.583	1.814	0.74915
3	0.0	0.0	-1.956	2.671	0.76696

Model III:

Sphere No.	X	Y	Z	Radius	Alpha
1	0.0	0.0	0.0	3.483	0.77720
2	0.0	0.0	0.082	2.357	0.75039

"textbook" description [7] of these levels is as follows:

1a' O 2s (weakly bonding)

2a' C 2s (weakly bonding)

3a' O 2p + C 2p + H 1s (HOC bonding)

1a" C 2p + H 1s (CH_3 bonding)

4a' C 2p + H 1s (CH_3 bonding)

5a' O 2p (HOC angle determining)

2a" O 2p (O lone pair)

The SCF-Xα-SW calculations support some of these descriptions, but reveal the situation as being more complicated. The molecular orbital calculations show more interaction between the carbon and oxygen (both bonding and antibonding) than the intuitive description suggests. The 1a" and 4a' levels, described as localized on the methyl group, have substantial amounts of oxygen character (21% and 52% respectively, compared to 47% and 38% for carbon). (1) The 4a' state should definitely be considered a carbon-oxygen sigma-bonding level, while the 1a" might be considered a carbon-oxygen pi bonding level. Similarly, the 5a' and 2a" states have a substantial amount of carbon character (27% and 16% respectively, compared to 50% and 70% for oxygen). The 5a' state should probably be considered an antibonding C-O sigma level, while the characterization of the 2a" as an oxygen

(1) Throughout this work, all references to percentage charge of a molecular orbital on a given atom assumes that the intersphere charge has been divided among the various atoms in proportion to the valence charge contained in the atomic spheres.

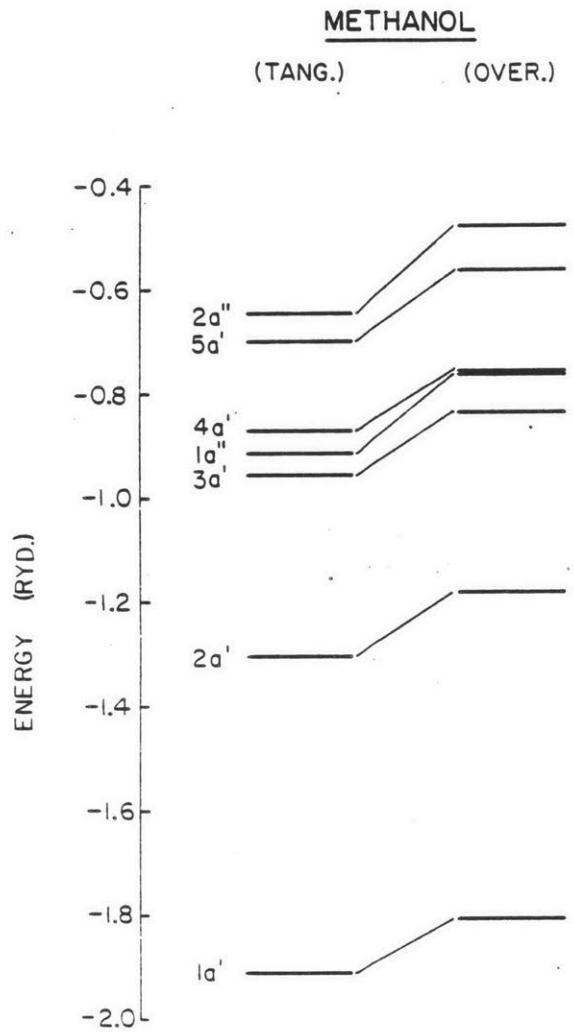

Fig. 2.6. Comparison of methanol energy levels found with standard SCF-Xα-SW method using tangent and overlapping atomic spheres.

lone pair seems correct, although it may be considered weakly antibonding. The strongest contribution from the hydrogen of the OH group is from the 3a' state, as expected, but this hydrogen also appears with bonding character in the 1a', 2a' and 5a' states as well. The hydrogen atoms in the methyl group have substantial bonding character in all of the valence orbitals except the 1a' level. The 1a" and 4a' levels are not exceptional in this regard, and it is erroneous to characterize only them as CH_3 bonding levels. Based on the standard Xα-SW calculations, a revised description of the methanol molecular orbitals may be as follows:

OH bonding	1a'	O 2s (weakly bonding)	
	2a'	C 2s (weakly bonding)	
	3a'	O 2p + C 2p + H 1s (HOC bonding)	
	1a"	O 2p + C 2p (pi bonding)	CH_3 bonding
	4a'	O 2p + C 2p (weakly sigma bonding)	
	5a'	O 2p + C 2p (pi antibonding)	
	2a"	O 2p (lone pair or weakly antibonding)	

Plots of the wavefunctions of these levels are shown in Figs. 2.7 - 2.13. These plots reinforce the description given above of substantial C-O interaction in all levels except the 1a' and 2a". These plots are are presented here as a reference for comparison with the partitioned calculations discussed later.

Also shown in Fig. 2.6 are the energy levels of a standard SCF-Xα-SW calculation with overlapping spheres. The energy level

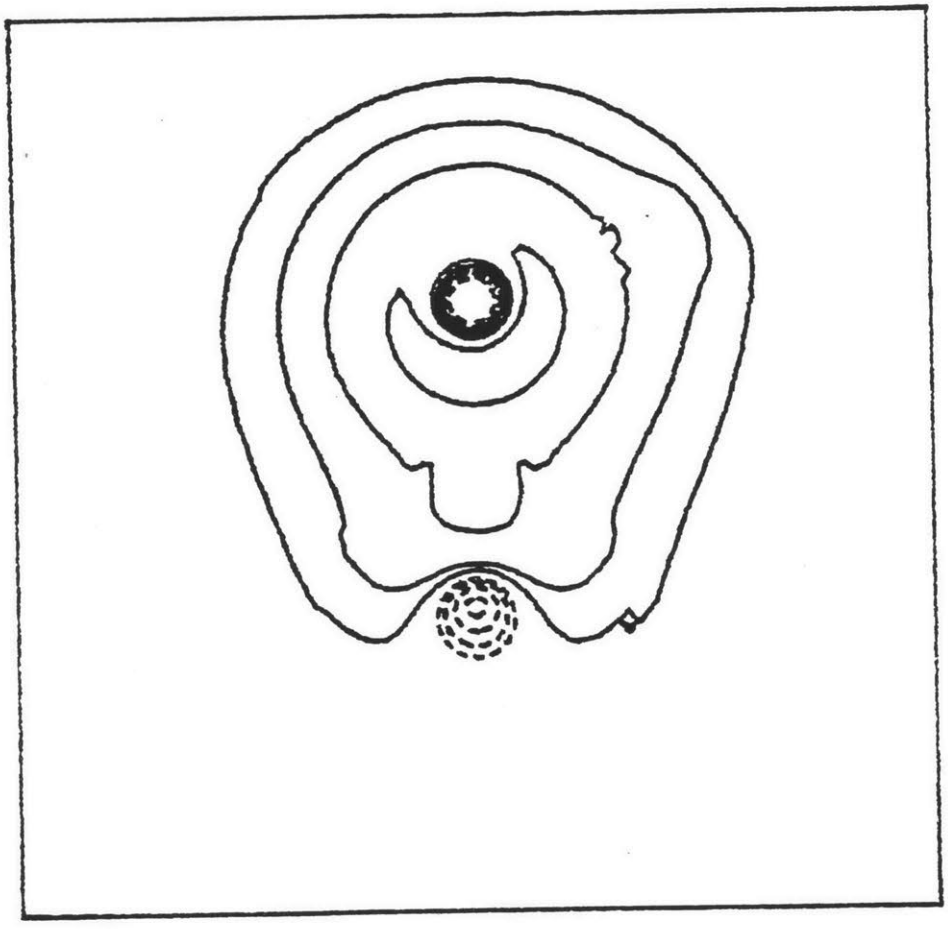

Fig. 2.7. Plot of the wavefunction of the methanol 1a′ orbital, found using standard SCF-Xα-SW method with tangent atomic spheres.

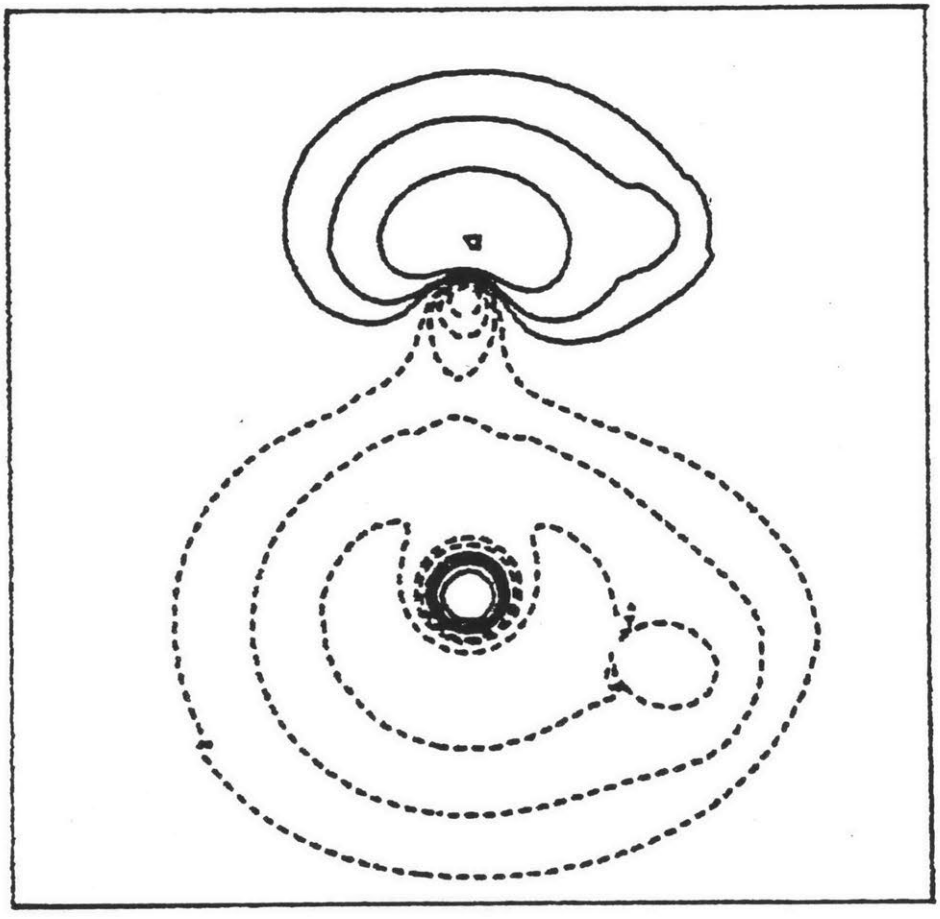

Fig. 2.8. Plot of the wavefunction of the methanol 2a′ orbital, found using standard SCF-Xα-SW method with tangent atomic spheres.

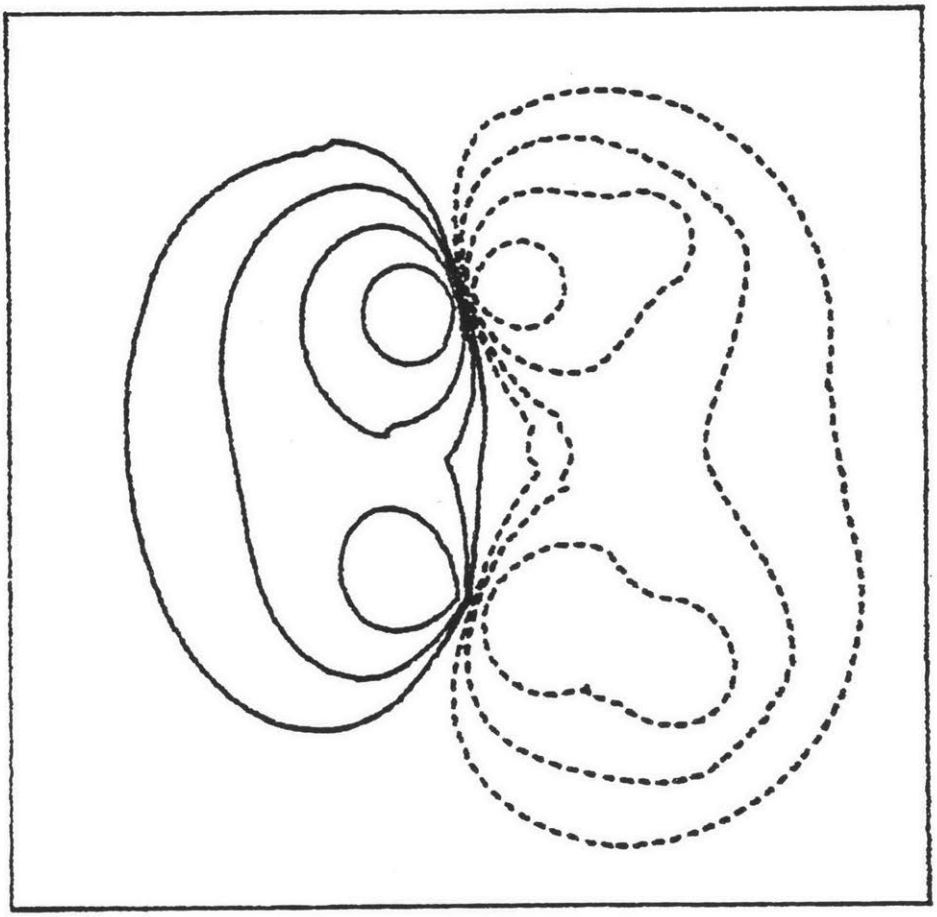

Fig. 2.9. Plot of the wavefunction of the methanol 3a′ orbital, found using standard SCF-Xα-SW method with tangent atomic spheres.

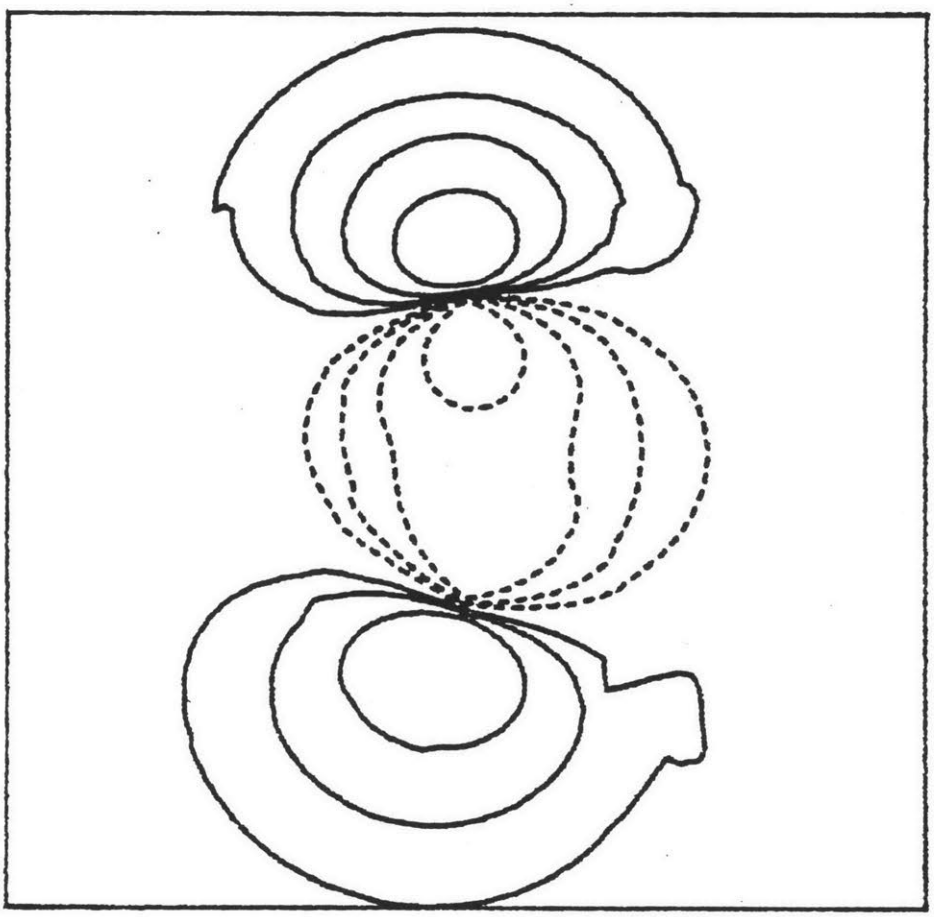

Fig. 2.10. Plot of the wavefunction of the methanol 4a′ orbital, found using standard SCF-Xα-SW method with tangent atomic spheres.

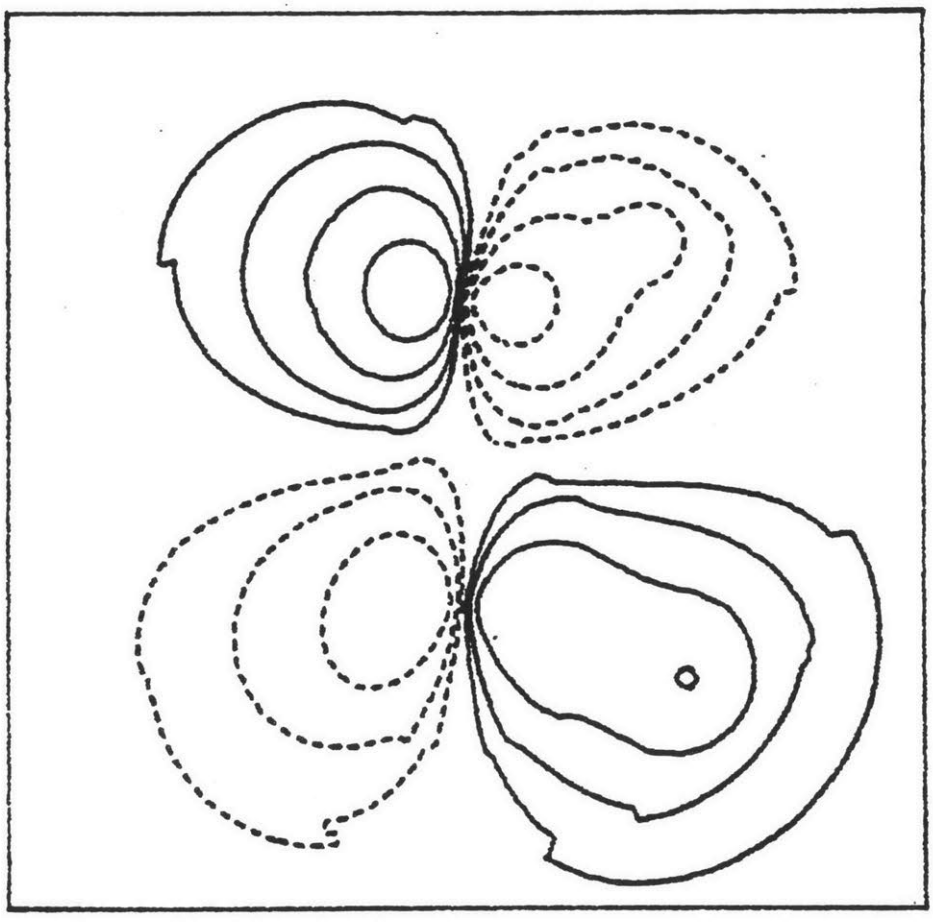

Fig. 2.11. Plot of the wavefunction of the methanol 5a′ orbital, found using standard SCF-Xα-SW method with tangent atomic spheres.

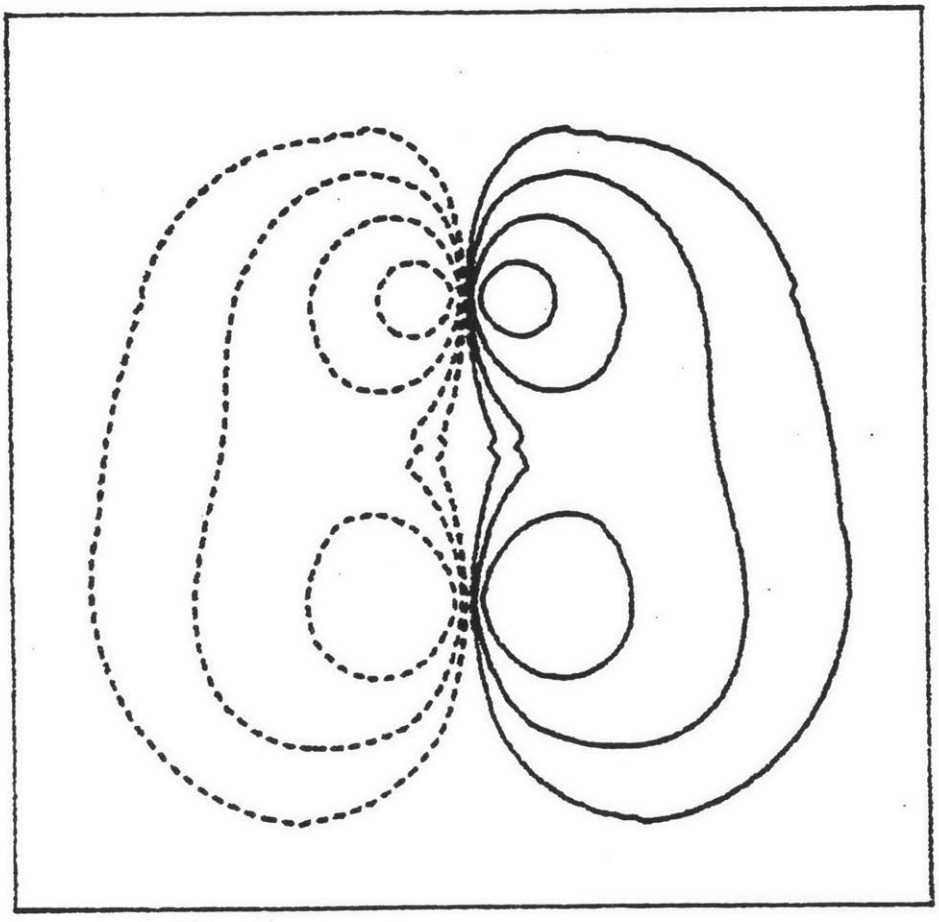

Fig. 2.12. Plot of the wavefunction of the methanol 1a'' orbital, found using standard SCF-Xα-SW method with tangent atomic spheres.

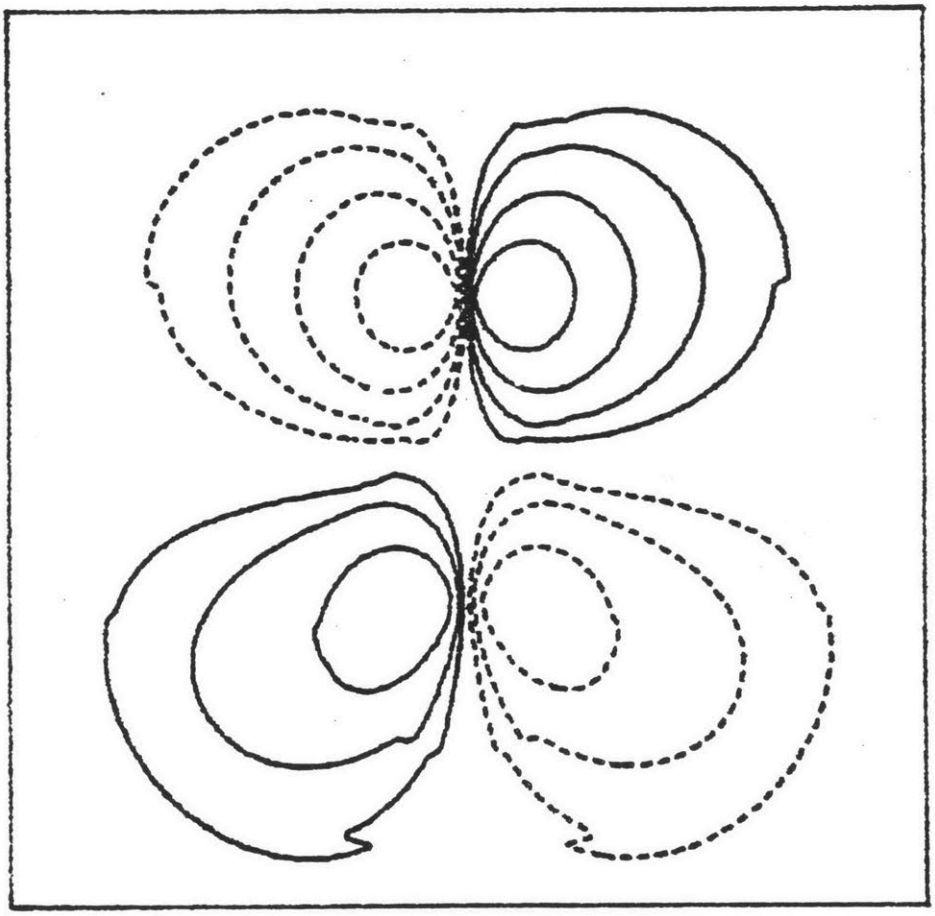

Fig. 2.13. Plot of the wavefunction of the methanol 2a'' orbital, found using standard SCF-Xα-SW method with tangent atomic spheres.

structure is similar to that of the tangent sphere case, except that the levels are all shifted higher and the 4a′ and 1a" levels are nearly degenerate. In general practice, the methanol calculation would be done with overlapping spheres in order to minimize the interatomic volume. Overlapping atomic spheres are not used in any of the partitioned calculations so that the effect of the partitioning spheres can be distinguished from the effects of the atomic sphere overlap.

Model I Partitioning

As mentioned above, the partitioning spheres in the Model I calculation are non-overlapping. Furthermore, the system outer sphere is tangent to the two partitioning spheres. Compared to the standard SCF-Xα-SW tangent sphere case (STAN-I), the total intersphere volume (i.e., inside the system outer sphere but outside the atomic spheres) has increased by 400%. However, if the total intersphere volume of the STAN-I calculation is compared to just the intersphere volume inside the partitioning spheres of Model-I, there is a 10% decrease. Nevertheless, because of the enormous system outer sphere, this partitioned calculation should not be expected to give better results than the STAN-I results. Still, the calculation is useful because it allows a direct examination of the effects of partitioning without the added complications of overlapping partitioning spheres.

A difficulty arises when comparing the Model I calculation with the STAN-I results: The STAN-I calculation uses a substantially smaller outer sphere radius than the Model I calculation, for reasons just mentioned. However, changing the size of the outer sphere radius by itself can affect the results of a calculation. Thus, differences between STAN-I and Model I can be due either to the outer sphere size or to the presence of the partitioning spheres. To isolate the effects of the partitioning spheres alone, another standard Xα-SW calculation has been performed (STAN-II) which is identical to STAN-I except that its outer sphere radius is equal to that of the Model I calculation. The one electron energies of STAN-II and the Model I calculation are

shown in Fig. 2.14.

In comparing the energy level diagrams of STAN-II and Model I to that of STAN-I in Fig. 2.14, two basic differences are noticeable. First, the energy levels of both STAN-II and Model I are lower (i.e., more deeply bound) than those of STAN-I. Second, the ordering of 4a' and 1a" levels is reversed in both STAN-II and Model I with respect to the ordering of STAN-I. Because these differences are found in both the STAN-II and Model I calculations, they must be due to the larger outer sphere.

To understand these energy shifts, ignore for the time being the effects of the partitioning spheres and consider the changes in the potentials caused just by increasing the outer sphere size; that is, consider the differences between the STAN-I and STAN-II calculations. To do this, the steps of charge averaging and potential averaging in the intersphere region must be considered separately. When the intersphere charge is volume averaged over a larger intersphere region, the charge that is normally close to the atomic nuclei is moved further away. The electronic charge is therefore less effective in screening the nuclear charge, and the potentials in the atomic and intersphere regions are therefore lowered (become more negative). However, the subsequent volume averaging of the intersphere potential has the effect of raising the average intersphere potential, because the larger intersphere volume now includes more space at large distances from the atomic nuclei. Thus, the charge averaging and potential averaging have opposite effects on the average intersphere potential; the potential generally has the greater effect, so that the average intersphere potential increases as the outer sphere radius is

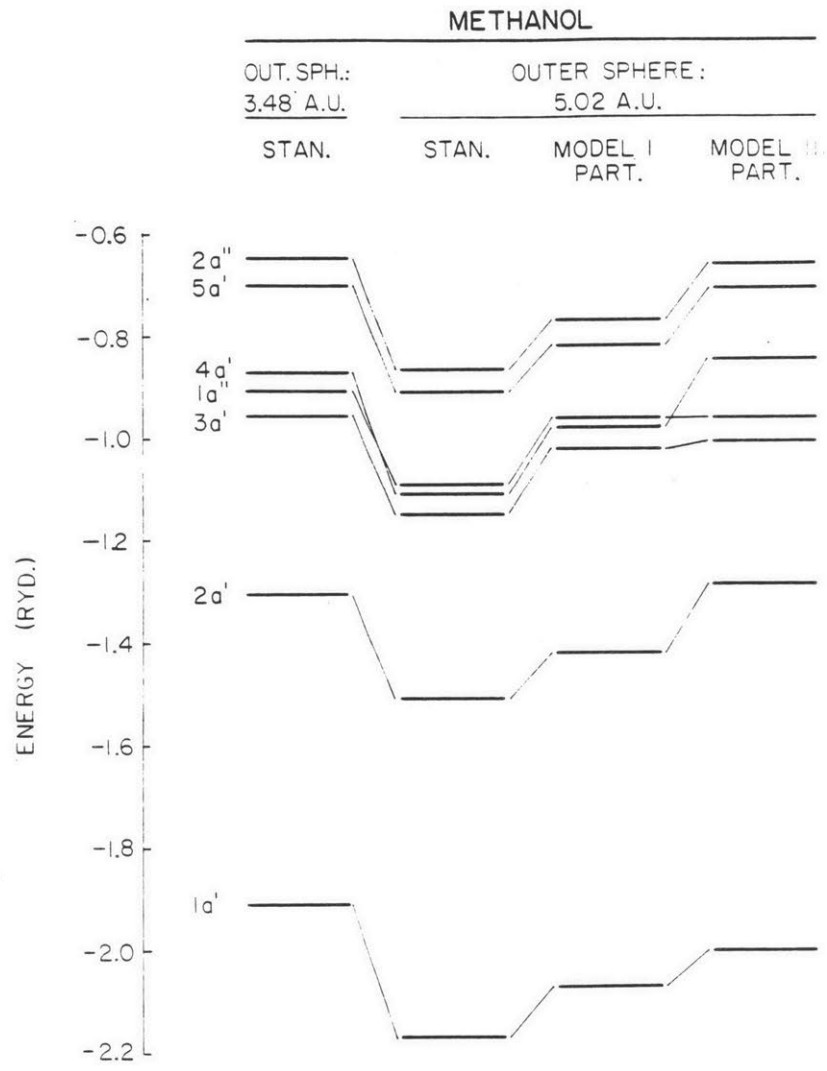

Fig. 2.14. Comparison of energy level diagrams for several methanol calculations. The first column is a standard SCF-Xα-SW calculation with an outer sphere radius of 3.48 bohrs. The second column is also a standard SCF-Xα-SW calculation, but with an outer sphere radius of 5.02 bohrs. The third column uses Model I partitioning, and the fourth column uses Model III partitioning modified with a larger outer sphere. Note that for the second and third columns the order of the 4a' and 1a'' levels are reversed. All calculations used tangent atomic spheres.

increased. Of course, the volume averaging of the intersphere potential has no effect on the atomic potentials, so the atomic potentials are always lowered with increasing outer sphere radius. From the results of self-consistent calculations of methanol, the effect of increasing the outer sphere radius from 3.31 bohrs to 5.02 bohrs is to raise the average intersphere potential from -1.018 to -0.946 rydbergs; the atomic potentials are lowered by roughly 0.30 to 0.60 rydbergs. The change in the atomic potentials dominates the effect on the one electron energy levels, which are lowered by roughly 0.1 rydbergs.

The change in the ordering of the 4a′ and 1a" levels is also explained by these potential shifts. The 1a" level is pi-bonding between the carbon and oxygen atoms, whils the 4a′ level is sigma-bonding. Because more of the pi wavefunction is in the intersphere region than the sigma wavefunction, the pi levels are more sensitive to the intersphere potential than sigma levels. Thus although all the energy levels are lowered by increasing the outer sphere radius, the 1a" is lowered less than the 4a′ level, due to the former's greater sensitivity to the intersphere potential.

The main effect of the addition of the partitioning spheres is to raise the energy levels, as seen in Fig. 2.14. This can be understood by examining the electrostatic effects of the additional spheres. Because the charge is volume averaged separately in each partitioning sphere, the electronic charge remains closer to the atomic nuclei than in the same case without the partitioning spheres (i.e., the STAN-II calculation). This results in more effective screening of the nuclear charge and a consequent rise in the atomic and intersphere potentials.

The step of volume averaging the intersphere potential has different effects in the regions inside the partitioning spheres and the region outside (between) the two partitioning spheres. Because the potential averaging inside the partitioning spheres is performed over a region closer to the atomic nuclei than in the case without the partitioning spheres, these average potentials should decrease. On the other hand, the averaging process should increase the average potential between the partitioning spheres because the regions near the atomic nuclei are now excluded. For the methanol case, the average potential in the intersphere region exterior to the partitioning spheres increases from the intersphere potential without the partitioning spheres (-0.653 compared to -0.946 rydbergs without the additional spheres), while the average potentials inside the sub-spheres decreases (-1.204 rydbergs for the OH sub-cluster and -1.112 rydbergs for the CH_3 sub-cluster). The atomic potentials are roughly 0.2 to 0.3 rydbergs higher with the partitioning spheres.

The net effect of the various shifts in the potentials is an overall rise in the one electron energy levels of roughly 0.05 to 0.06 rydbergs; otherwise the two calculations (STAN-II and Model I) give remarkably similar results. The ordering of ordering of the levels is identical and the spacing between the levels is qualitatively the same. The charge distributions of the levels are similar and plots of their wavefunctions show no important differences.

In principle, the one electron energy levels obtained from any method using the $X\alpha$ approximation for the exchange interaction can not be directly related to experimental values (such as ionization energies) because the $X\alpha$ energies are defined as the derivative of the

energy with respect to occupation number. This situation differs from the Hartree-Fock case, where Koopman's theorem states that one electron energies correspond directly to ionization energies [13]. In order to find ionization energies in the Xα method, Slater's concept of a transition state is used [14]. In a transition state calculation, the energy of a one electron excitation is found by reducing the occupation number of the initial state by 0.5 and increasing the occupation number of the final state by 0.5. After iterating to self-consistency with the changed occupation numbers, the excitation energy is found by taking the difference between the final and initial one electron energies.

Transition state calculations have been performed with the two methods (STAN-II and Model I) to obtain ionization energies; these energies are plotted in Fig. 2.15 along with published results of photoemission experiments of the free methanol molecule (hν=21.2 eV). As with the one electron energies, the main difference in the ionization energies obtained from the calculation using the partitioning spheres is that they are uniformly higher (less tightly bound) than those obtained without the partitioning spheres. The partitioning method does give better agreement with experiment; however, the ordering of the 1a" and 4a' orbitals is still reversed. It should be noted that the symmetry assignments given the experimental values are confirmed by several Hartree-Fock calculations.

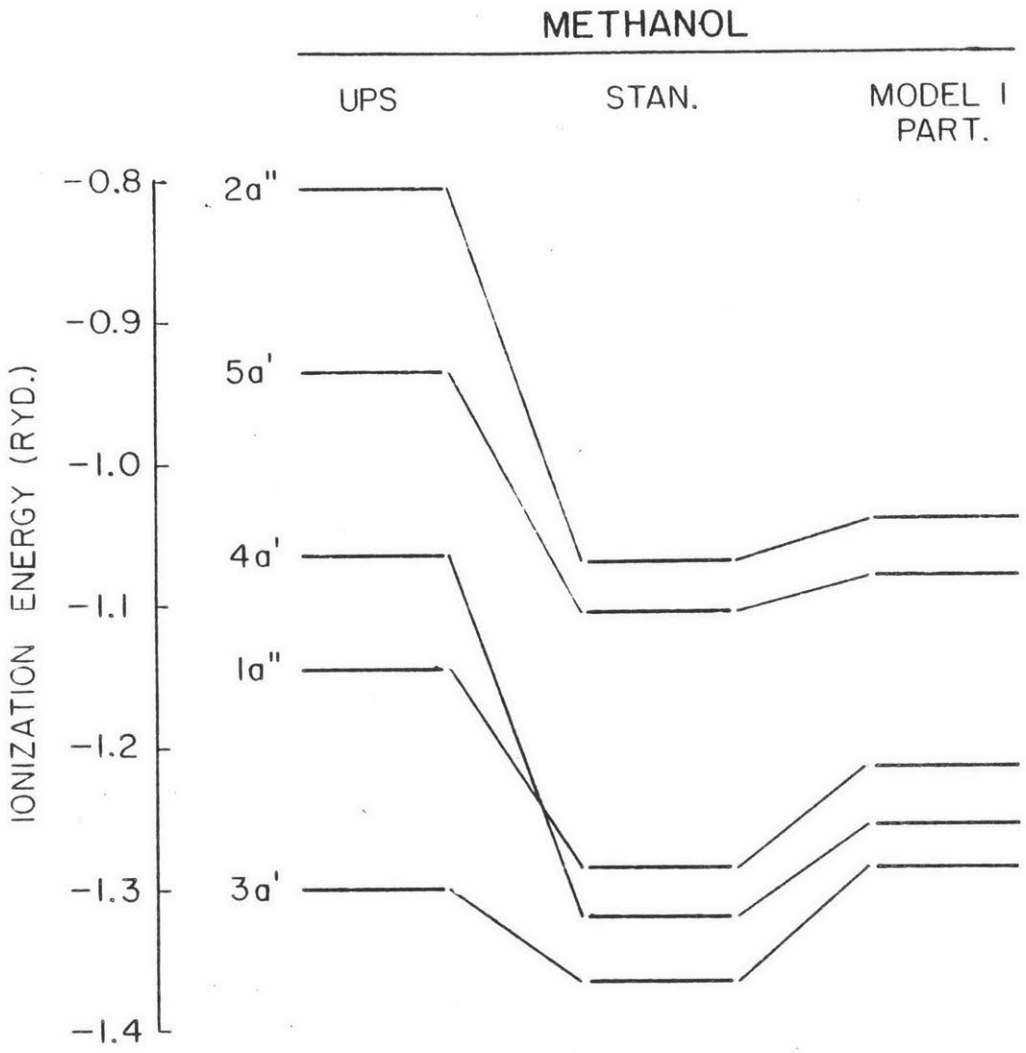

Fig. 2.15. Comparison of experimental photoemission data from methanol (see Ref. [1]) with two transition state ionization energy calculations. The first calculation uses the standard SCF-Xα-SW method with tangent atomic spheres and an oversized outer sphere of radius of 5.02 bohrs. The larger outer sphere matches that of the Model I partitioning case, which is shown in the third column. The Model I type of partitioning uses tangent partitioning spheres. Note that both calculations have the ordering of the 1a" and 4a' levels reversed.

Model II Partitioning

The restriction that the partitioning spheres must not overlap is a severe one for the case of methanol; it leads to very large outer sphere sizes, and, therefore, more regions of constant potential. This is ironic, in that the partitioning spheres were introduced in part to correct for errors caused by the intersphere regions. Thus, it is important to discover whether or not this restriction can be relaxed. To this end, a calculation with overlapping partitioning spheres having the geometry shown in Fig. 2.4 has been performed.

The partitioning spheres for this calculation have been chosen so that they do not overlap any atomic spheres, although partitioning spheres were allowed to overlap each other without restriction. The sphere centers were chosen so as to minimize the sphere volume. The resulting construction yields partitioning spheres with 26% overlap. (1) This is a large percentage which is near the upper limit of overlap that has been found feasible for atomic sphere overlap in previous studies. In addition, both partitioning spheres protrude significantly from the system outer sphere, which is the same size as that of the standard SCF-Xα-SW calculation (STAN-I). As before, none of the atomic spheres overlap.

---

(1) The overlap of two spheres is found in the following manner: Maintaining the ratio of the two radii constant, the radii are reduced until the spheres are tangent. The fractional increase of the reduced radii necessary to attain the original size is defined as the overlap. This definition corresponds to one used in earlier studies of overlapping atomic spheres.

The X one electron energy levels are shown in Fig. 2.16, along with those of the STAN-I. There are two noticeable differences in the spectra. First, the levels of the partitioned calculation (with the exception of the 1a' and 4a') are somewhat higher in energy. This agrees with the general expectation that the nuclear charges are more effectively screened in partitioned calculations due to the electronic charge being contained to a greater degree inside the partitioning spheres. Second, the ordering of the 4a' and 1a" are reversed in comparison to the standard SCF-Xα-SW calculation. Unlike the previous case of the tangent partitioning spheres in which the incorrect ordering was caused by the large outer sphere, this misordering must be caused by the partitioning spheres themselves. Still, the same type of arguments that explained the previous misordering probably apply to this case as well. The 1a" state, being a C-O pi orbital, has more of its wavefunction outside of the two partitioning spheres than the 4a' state (a C-O sigma orbital). The former state is therefore more sensitive to the constant potential in this region, which is considerably higher than the overall constant potential for the non-partitioned case (-0.76 versus -1.06 rydbergs respectively). The other constant potentials for the partitioned calculation were -1.64 rydbergs for the OH sub-cluster and -1.19 rydbergs for the CH_3 sub-cluster.

The results for the transition state calculations for this type of partitioning are shown in Figure 2.17. Although the misordering of

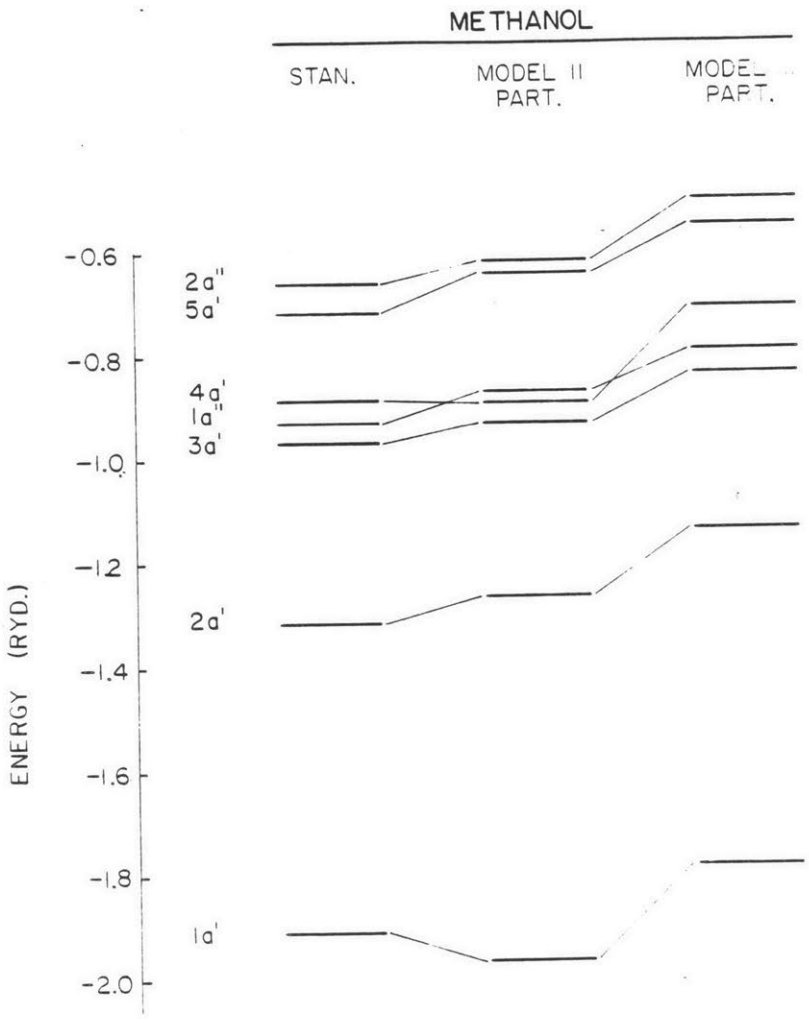

Fig. 2.16. Comparison of methanol energy level diagram for the standard SCF-Xα-SW case (outer sphere radius of 3.48 bohrs, tnagent atomic spheres) with those of the Model II and Model III partitioning cases. Note that the order of the 1a'' and 4a' levels is reversed for Model II, but is correctly found with Model III.

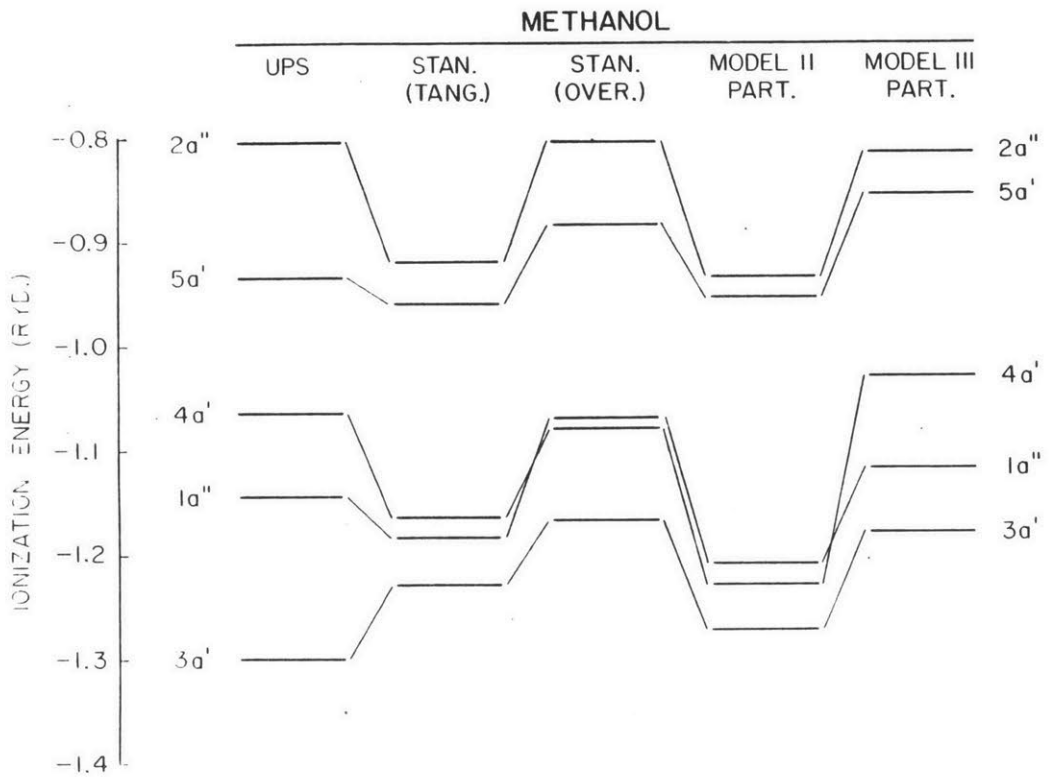

Fig. 2.17. Comparison of experimental photoemission data from methanol (see Ref. [1]) with several transition state ionization energy calculations. All of the calculations used an outer sphere of radius 3.48 bohrs. The first two calculations used the standard SCF-Xα-SW method with tangent and overlapping atomic spheres, respectively. The last two calculations used Model II and Model III partitioning. Note that the order of the 1a" and 4a' levels are reversed for the standard overlapping case and for the Model II partitioning case.

the 4a' and 1a'' levels persists, in other respects the ionization energies do not compare unfavorably with the standard SCF-Xα-SW results (also shown in Figure 2.17).

The arguments given above may not be the complete explanation for the misordering of the levels; it is possible that errors introduced by the large amount of partitioning sphere overlap may play a role. Studies of errors introduced by the overlap of atomic spheres in the standard SCF-Xα-SW method have identified two types of error: errors introduced during the solution of Schrodinger's equation, and errors introduced during the solution of Poisson's equation (creation of the potential) [10]. In general practice, no explicit corrections for the overlap are added to the formalism of the tangent atomic sphere case. Similarly, in the present case no corrections are included to account for overlap of the partitioning spheres. It is possible that both types of errors occur with this calculation, for although similar percentages of atomic sphere overlap have been shown to give reasonable results, the absolute amount of overlap of the partitioning spheres is much greater (due to the larger radii). Nevertheless, the wavefunctions obtained from this calculation show no gross discontinuities at the partitioning sphere boundaries, indicating that the solution to Schrodinger's equation is performed accurately. Unfortuanately, there is no simple analogous check on the solution of Poisson's equation.

Thus, the interpretation of the Model IL partitioning results is somewhat ambiguous. The misordering of the energy levels could be caused by overlap errors or by a poor choice of partitioning spheres. This ambiguity can be resolved only by further calculations with

overlapping partitioning spheres.

Model III Partitioning

The partitioning spheres in the first two calculations in this chapter divided the methanol molecule into OH and methyl fragments. This division seems reasonable if these two sub-units are considered as the fundamental building blocks from which the molecule is constructed, i.e., if the molecular orbitals of methanol can be described as orbitals obtained by relatively weak interactions between the molecular orbitals of OH and CH_3. However, another viewpoint would hold that the C-O bond is the most fundamental sub-unit in the molecule, and that the carbon and oxygen atoms should be within a single sub-sphere rather than split between two spheres. From this perspective, methanol could be understood as a carbon monoxide molecule plus four additional hydrogen atoms. Support for this view is given by the discussion earlier in this chapter of the standard $X\alpha$-SW results for methanol; there it was seen that there is much more C-O interaction than is typically assumed.

These considerations emphasize the point that the choice of how a given system is partitioned will affect the results of that calculation. In general, interactions between atoms inside a given partitioning sphere will be enhanced, while interactions between atoms in different partitioning spheres will be attenuated. To see why this is so, it is necessary to note that the constant potentials inside the partitioning spheres are generally lower than the constant potentials in the region outside the partitioning spheres (the reasons for this

tendency were discussed in the previous two sections). The Green's function matrix elements which describe the propagation of the electron in the intersphere region decay rapidly with increasing intersphere potential. For molecular orbital energies below that of a given constant potential, this decay is roughly proportional to

$$\exp(-\kappa R) \qquad (2.1)$$

where $\kappa = |E - \bar{V}|^{\frac{1}{2}}$ and R is the distance between the two scattering centers [15]. For propagation between two partitioning spheres, V for region (II) is used in this expression; because it is generally higher than the constant potential within the partitioning spheres (Region IV), the interaction between atoms in different partitioning spheres is correspondingly reduced. Therefore it would be logical to place the partitioning spheres such that the strong chemical interactions take place between the atoms belonging to the same sphere and the weaker ones occur between atoms in different spheres. In this way, the theoretical description would more nearly match the chemical reality.

Fig. 2.5 shows the sphere placement of a calculation in which the carbon and oxygen atoms have been placed in a single partitioning sphere. Because of the geometry of the methanol molecule, the partitioning sphere must overlap several atomic spheres. The partitioning sphere radius was chosen by minimizing the volume of the overlap region while simultaneously insisting that no atom be overlapped by more than 25% of its atomic sphere radius. This percentage is consistent with the most severe atom-atom overlaps used

in standard SCF-Xα-SW calculations.

The general features of the one-electron energy levels (shown in Fig. 2.16) are similar to those of the corresponding standard SCF-Xα-SW calculation, except for a slight upward shift of from 0.5 to 1.0 eV. This upward shift is consistent with the increased screening of the nuclear charges, as dicussed in previous sections. Note that the ordering of the 1a" and 4a' levels are correct in this calculation. An examination of the wavefunctions and charge distributions of the various molecular orbitals show no significant differences between the results of the standard SCF-Xα-SW and the partitioned calculations (see Figs. 2.18 - 2.22). In particular, there are no severe discontinuities of the wavefunction in the overlap region, which implies that the amount of overlap used here is quite reasonable.

The transition state ionization energies, shown in Fig. 2.17, are in respectable agreement with experiment. Overall, they are somewhat too weakly bound in comparison to experimental values, while the standard SCF-Xα-SW ionization energies are too strongly bound. The spacing of the levels is more realsitic than the standard SCF-Xα-SW calculation. Furthermore, there is no ambiguity in the ordering of the troublesome 1a" and 4a' levels.

Also shown in Fig. 2.17 are the transition state ionization energies for the standard SCF-Xα-SW calculation with overlapping spheres. The one electron energies (shown in Fig. 2.14) had the correct ordering, although the 1a" and 4a' levels were nearly degenerate. Here it is seen that the ionization energies are incorrectly ordered.

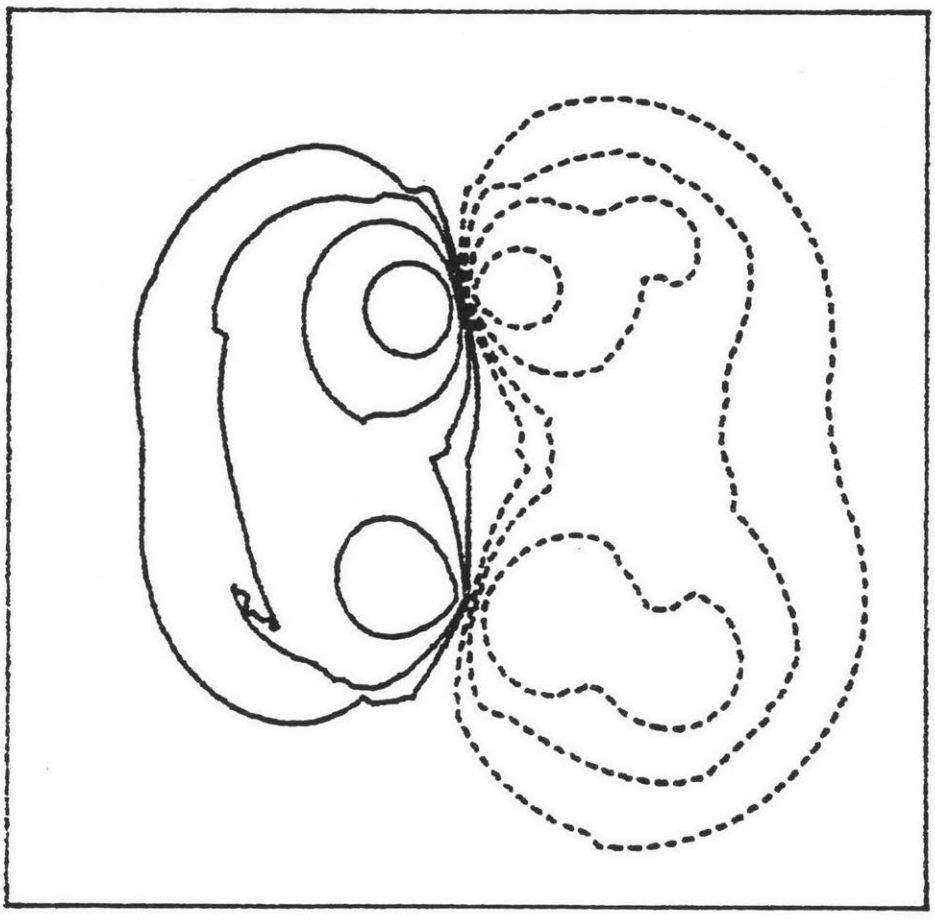

Fig. 2.18. A plot of the wavefunction of the 3a' methanol orbital found using Model III partitioning.

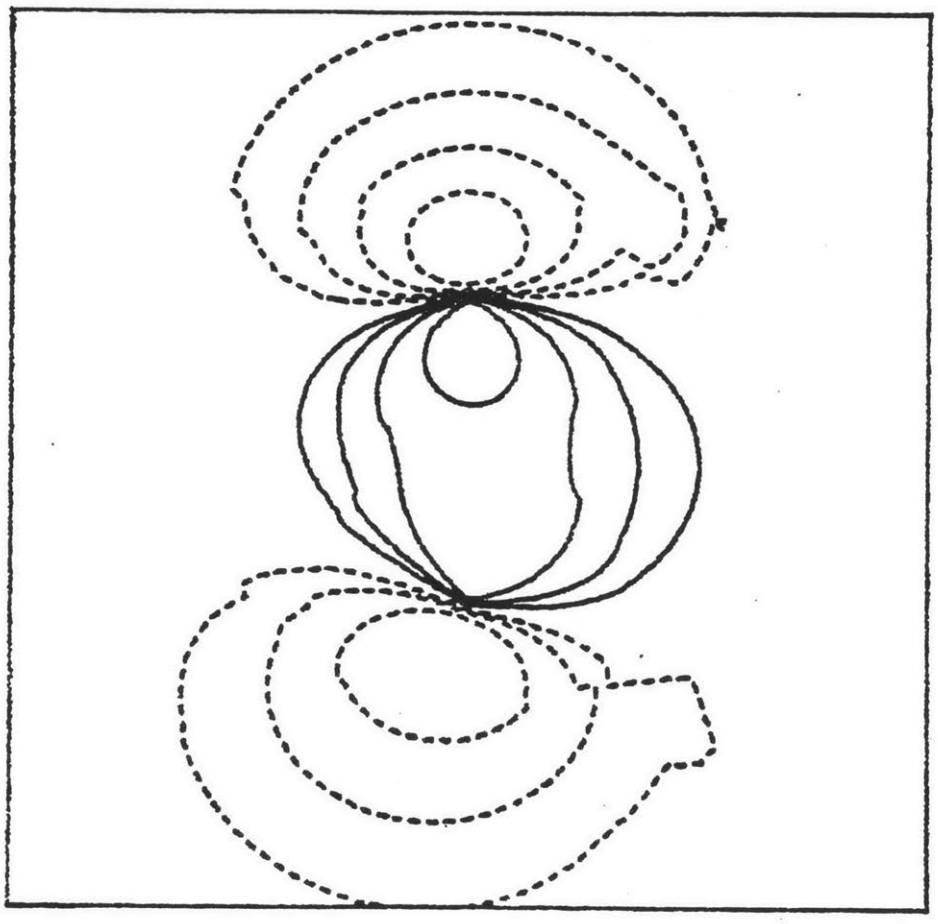

Fig. 2.19. A plot of the wavefunction of the 4a' methanol orbital found using Model III partitioning.

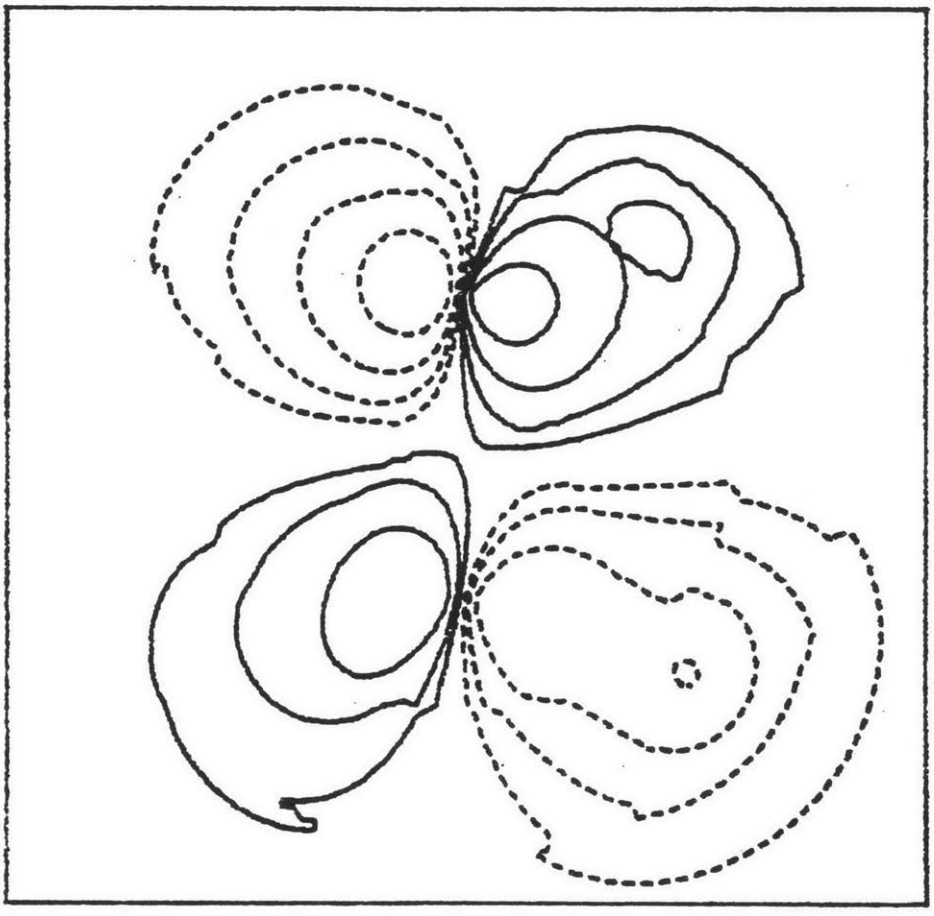

Fig. 2.20. A plot of the wavefunction of the 5a' methanol orbital found using Model III partitioning.

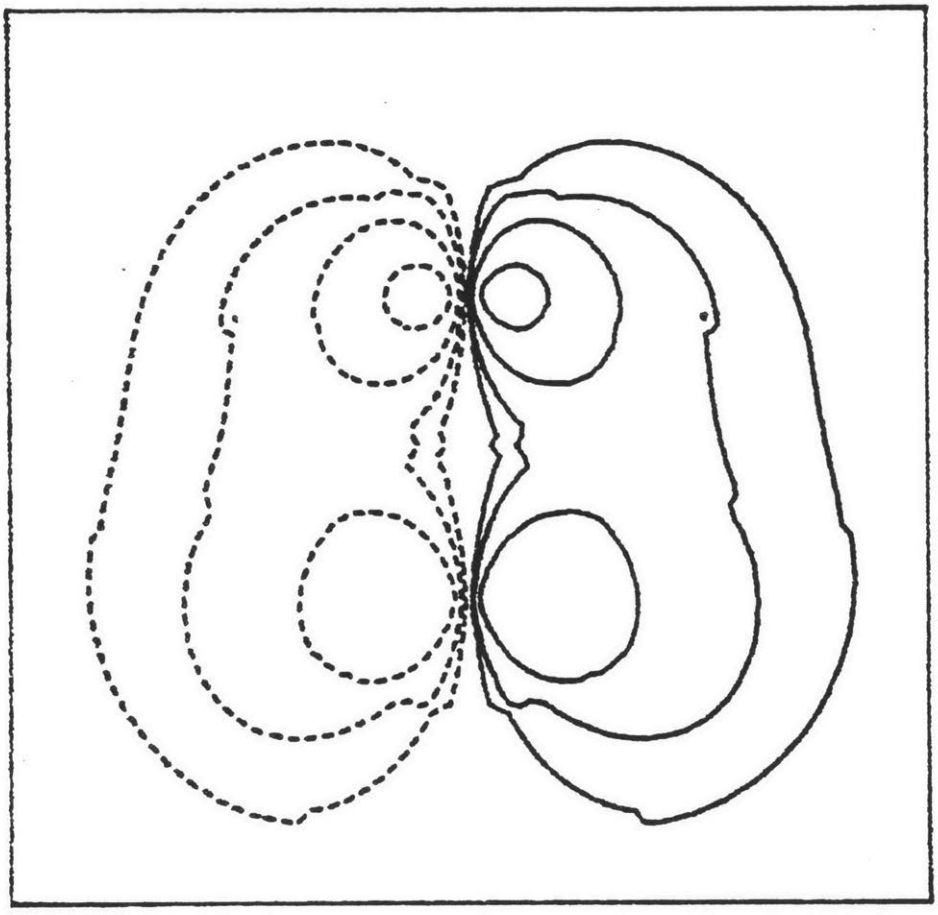

Fig. 2.21. A plot of the wavefunction of the 1a'' methanol orbital found using Model III partitioning.

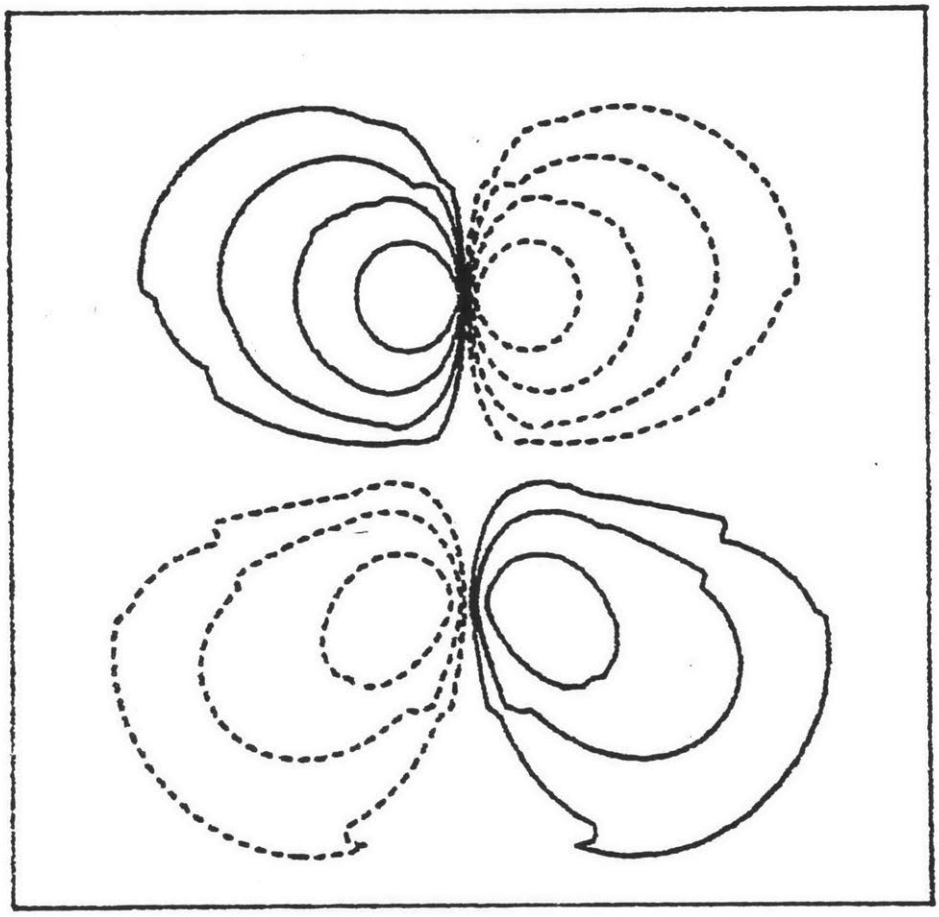

Fig. 2.22. A plot of the wavefunction of the 2a'' methanol orbital found using Model III partitioning.

The generally favorable results of the Model III partitioning are encouraging. Because of this, one further methanol calculation was done using this type of partitioning, but with the system outer sphere having a radius equal to that of the Model I type of partitioning (5.02 bohrs). In that previous calculation, it was found that the size of the outer sphere led to a misordering of the 4a′ and 1a" levels. The point of the present calculation is to see if the Model III type of partitioning will correct this misordering even with the large outer sphere. Of course, this is not a realistic calculation, because there is no reason to use such a large outer sphere in this case. However, the results of this calculation may be applicable to other molecules for which the outer sphere must be rather large.

The energy levels of this second Model III partitioning calculation are shown in Figure 2.14, along with the other calculations using the larger outer spheres. The 1a" and 4a′ levels do, in fact, have the correct ordering; furthermore, the downward shift of energy levels of the standard SCF-Xα-SW (STAN-II) and Model I partitioning (with respect to the standard SCF-Xα-SW calculation with outer sphere radius equal to 3.48 bohrs) is substantially reduced.

To repeat, this is not a realistic calculation. However, it does simulate a calculation which must use a very large outer sphere. Previous standard SCF-Xα-SW studies of benzene and other relatively large organic molecules have encountered problems with the relative ordering of σ and π levels [11]. The use of partitioning spheres may be a way to prevent such difficulties.

SUMMARY

It has been demonstrated that the Model III type of partitioning does give improved agreement with experiment. In the standard SCF-Xα-SW calculations, the 4a' and 1a" levels are either nearly degenerate or incorrectly ordered. Even the standard SCF-Xα-SW case using overlapping atomic spheres, which would be expected to give the best results, yields an incorrect ordering of the ionization energies. Using the Model III type of partitioning there is no ambiguity in the ordering of these levels even with the oversized outer sphere. Still, the importance of this result is not so much the specific application to methanol, but the potential of applying the partitioning method to larger molecules. Methanol, with only six atoms, is a rather small molecule with a reasonably sized outer sphere. With larger molecules, the partitioning method's effectiveness should increase as the size of the outer sphere increases. This has been demonstrated, albeit in a somewhat artificial manner, with the methanol studies using large outer spheres.

Aside from demonstrating that the partitioning method can give improved results, the studies reported in this chapter give guidelines on how partitioning calculations should be done. First, and most important, is the use of careful judgment with regard to the placement of the partitioning spheres. It seems that the most important chemical interactions of the molecule or cluster should take place within a

single partitioning sphere. For the case of methanol, splitting the central C-O bond into two sub-clusters gives inferior results. A second guideline is that the use of a partitioning scheme which necessitates a large system outer sphere may be counter-productive. The drawbacks associated with a large outer sphere may overwhelm the benefits of the partitioning spheres. Finally, it appears feasible to use partitioning spheres with modest amounts of overlap. However, because of the uncertainty in the interpretation of the Model II calculations, this final point should be confirmed with further tests.

Thus, the partitioning method has been shown to be a useful improvement on the standard SCF-Xα-SW method. A further application of this method to a chemisorption problem is described in Chapter 4; additional applications to a wide variety of other areas are part of an ongoing research program.

REFERENCES

1. L. Karlsson, R. Jadry, L. Mattsson, F.T. Chau, and K. Siegbahn, Physica Scripta 16, 225 (1977).

2. K. Siegbahn, C. Nordling, G. Johansson, J. Hedman, P.-F. Heden, K. Hamrin, V. Gelius, T. Bergmark, L.-O. Werme, R. Manne, and Y.B. Baer, ESCA Applied to Free Molecules (North Holland Publ. Co., Amsterdam, 1969).

3. M.B. Robin and N.A. Kuebler, J. Electron Spectrosc. 1, 13 (1972).

4. L.C. Snyder and H. Basch, Mol. Wave Fcs. and Properties (John Wiley, New York, 1972).

5. W.L. Jorgensen and L. Salem, The Organic Chemist's Book of Orbitals (Academic Press, New York, 1973).

6. D. Betteridge in Molecular Spectroscopy 1971, edited by P. Hepple (Inst. of Petroleum, London, 1972).

7. J.H.D. Eland, Photoelectron Spectroscopy (John Wiley, New York, 1974).

8. K. Kimura and M. Kubo, J. Chem. Phys. 30, 151 (1959).

9. D.R. Salahub, R.P. Messmer, and K.H. Johnson, Molecular Physics 31, 529 (1976).

10. F. Herman, A.R. Williams, and K.H. Johnson, J. Chem. Phys. 61, 3508 (1974).

11. D.A. Case, M. Cook, and M. Karplus, J. Chem. Phys. 73, 3294 (1980).

12. A.R. Williams, Int. J. of Quan. Chem. Symp. No. 8, 89 (1974).

13. C. Kittel, Quantum Theory of Solids (John Wiley, New York, 1974).

14. J.C. Slater, The Self-Consistent Field for Molecules and Solids, Vol. 4 (McGraw-Hill, New York, 1974).

15. R. Kjellander, Chem. Phys. 12, 469 (1976).

CHAPTER 3 - APPROXIMATE COUPLING THEORY AND APPLICATIONS TO METHANOL

There are a wide variety of interesting electronic structure problems that involve a number of atoms greater than that which is practical or possible with standard SCF-Xα-SW methods. Examples are biological molecules, in which the sub-unit of interest may contain tens or hundreds of atoms [1-4]; polymers, in which a series of identical sub-units may interact with each other [5-8]; and a whole class of problems in which a cluster of atoms is used to represent a localized portion of a solid [9-11]. The use of clusters to represent solids has had much success, but questions remain regarding the effects of using a small number of atoms as a substitute for a macroscopic object [12]. Studying larger clusters may resolve some of these uncertainties.

Often the constituents of these large clusters or molecules can be divided into two groups of atoms: one having the most scientific interest, and the other acting as an environment for the first, modifying its electronic properties in some manner. For example, a biological molecule may have an active enzymatic site consisting of a transition metal and its nearest neighbors. The enzymatic properties of this site may be modified by other sub-groups which are physically more distant. If the electronic coupling between these groups is weak, it may be appropriate to treat their interaction in some approximate way. Such approximations may allow calculations to be performed which would otherwise be impossible. In the following two sections, techniques for performing such approximate calculations will

be discussed.

Molecular Field Approximation

One approach to approximating the partitioned scattered wave equations can be understood by examining the matrix of (1.41) (the full partitioned matrix). The matrix is almost in block diagonal form, with the three sub-matrices corresponding to the scattering matrices of the system outer sphere and the two sub-clusters. The deviation from block diagonal form is caused by the Green's function matrix elements which couple the two sub-clusters with each other and with the system outer sphere.

If we assume that these inter-cluster Green's function elements are zero (with the Green's function elements coupling atoms within a given sub-cluster remaining non-zero), the secular matrix divides into three block diagonal matrices. The linear systems represented by these matrices can be solved independently. This level of approximation may be called the "molecular field" approximation, because although we are ignoring any coupling between the sub-clusters of the molecule, the potentials for each sub-cluster include the electrostatic effects of the neighboring sub-clusters. Thus, even this lowest order approximation will give energy levels and wavefunctions that differ considerably from those of an isolated sub-cluster.

From (1.41), it is seen that the matrix corresponding to one of

the sub-clusters has the form

$$\begin{bmatrix} M'^{i} & N'^{i} & \\ N^{i} & M^{i} & -G^{io,i\alpha} \\ & -G^{i\alpha,io} & [T^{i}]^{-1} \end{bmatrix} \tag{3.1}$$

However, this matrix must be modified; the boundary conditions at infinity must be determined for the molecular field approximation. The sub-cluster under consideration is viewed as isolated in the constant potential of the inter-cluster region, and it is assumed that this constant potential stretches to infinity. There will be no scattering from infinity, which imposes the following boundary condition: all spherical waves exterior to the sphere surrounding sub-cluster σ_i will be "out-going" waves, that is n_ℓ or h_ℓ. This is equivalent to demanding that all B'^{i}_{L} vanish, where B'^{i}_{L} are the coefficients of the "incoming" waves exterior to the sub-cluster. Setting B'_L equal to zero in (1.27),

$$A'^{i}_{L} = -\frac{N'^{i}_{\ell}}{M'^{i}_{\ell}} A^{i}_{L} \tag{3.2}$$

and are no longer linearly independent, so is eliminated from (3.1) to obtain

$$\begin{bmatrix} -\frac{N^i N'^i}{M'^i} + M^i & -G^{io,i\alpha} \\ -G^{i\alpha,io} & [T^i]^{-1} \end{bmatrix} \tag{3.3}$$

Using the definitions of N , N' , M and M' in (1.29) through (1.33) and some algebra,

$$M^i_\ell - \frac{N^i_\ell N'^i_\ell}{M'^i_\ell} = [\chi_\ell(\kappa_i b_i), \phi_\ell(\kappa_o b_i)] \Big/ [\phi_\ell(\kappa_o b_i), \phi_\ell(\kappa_i b_i)]$$

$$\equiv [\tau^i]^{-1}_\ell \tag{3.4}$$

Here τ^i is the scattering matrix element corresponding to the change in constant potential upon going from the interior to the exterior of the sphere surrounding sub-cluster σ_i . Thus, the

secular matrix for the molecular field approximation is written

$$\begin{bmatrix} [\tau^i]^{-1} & -G^{io,i\alpha} \\ -G^{i\alpha,io} & [T^i]^{-1} \end{bmatrix} \begin{bmatrix} A^o \\ A^\alpha \end{bmatrix} = 0 \qquad (3.5)$$

This is not the only boundary condition that could used for a molecular field approximation. Alternatively, one could construct a model in which the potentials for all sub-clusters except sub-cluster a are replaced by the inter-cluster constant potential, while retaining the spherically averaged potential of the system outer

sphere. Such a model would have a secular matrix of the form

$$\begin{bmatrix} t_o^{-1} & -G^{oi} & & \\ -G^{io} & M'^{i} & N'^{i} & \\ & N^{i} & M^{i} & -G^{io,i\alpha} \\ & & -G^{io,i\alpha} & [T^{i}]^{-1} \end{bmatrix} \begin{bmatrix} A'^{o} \\ A'^{i} \\ A^{i} \\ A^{i\alpha} \end{bmatrix} = 0 \qquad (3.6)$$

This model may have the advantage of providing a better representation of eigenstates with energies greater than the inter-cluster constant potential. For (3.5), such eigenstates are technically resonances rather than bound states. Calculations using both forms of the molecular field approximation have been performed, and are reported later in this chapter.

Contraction Of The Secular matrix And The Approximate Coupling Method

In order to go beyond the molecular field approximation, the effects of electronic coupling between the sub-clusters must be considered as well as the electrostatic coupling. The method presented here, which has been created with the assumption of relatively weak electronic interaction, is called "approximate" or "iterative" coupling. There are two components of this approximation: first, contraction of the secular matrix; second, evaluation of the matrix elements of the environment only at certain specified trial energies (to be discussed further below).

Contraction of the secular matrix is accomplished using a simple property of linear algebra [15]. As an example, consider the following linear system:

$$\begin{bmatrix} \bar{\bar{T}}_a^{-1} & G_{ab} \\ G_{ba} & \bar{\bar{T}}_b^{-1} \end{bmatrix} \begin{bmatrix} A_a \\ A_b \end{bmatrix} = 0 \qquad (3.7)$$

Here $\bar{\bar{T}}_a^{-1}$, $\bar{\bar{T}}_b^{-1}$, G_{ab}, and G_{ba} are sub-matrices; A_a and A_b are column vectors. A solution to this linear system is possible only when the determinant of the entire matrix vanishes. However, this linear system can be re-written in a way that

eliminates the A_b coefficient. To see this, the matrix multiplication of the column vectors is explicitly written out to obtain the following two matrix equations:

$$\overline{T}_a^{-1} A_a + G_{ab} A_b = 0 \tag{3.8}$$

$$G_{ba} A_a + \overline{T}_b^{-1} A_b = 0 \tag{3.9}$$

Solving (3.9) for column vector A_b ,

$$A_b = -\overline{T}_b G_{ba} A_a \tag{3.10}$$

where $\overline{T}_b$ is the matrix inverse of $\overline{T}_b^{-1}$. Substituting (3.10) into (3.9)

$$\overline{T}_a^{-1} A_a - G_{ab} \overline{T}_b G_{ba} A_a = 0 \tag{3.11}$$

Here the order of the secular matrix has been reduced, i.e., the matrix has been "contracted"; solutions to the linear system of (3.11) are obtained only when the determinant of the following matrix vanishes:

$$\overline{\overline{T}}_a^{-1} - G_{ab}\overline{\overline{T}}_b G_{ba} \tag{3.12}$$

Once the column vector A_a has been obtained, A_b can be obtained using (3.10). Thus, solution of the reduced linear system of (3.11) is equivalent to solution of (3.7), with the exception of cases in which the matrix inverse of $\overline{\overline{T}}_b^{-1}$ does not exist (i.e., when $\det(\overline{\overline{T}}_b^{-1})$ vanishes).

Taking the deteminant of the smaller matrix of (3.11) is certainly computationally more efficient than calculating the determinant of the larger matrix of (3.7); however, (3.11) was obtained by taking the matrix inverse of $\overline{\overline{T}}_b^{-1}$, so it is not clear whether or not there is an overall computational advantage in following this procedure.

The above mathematical manipulations can be directly applied to electronic structure calculations using multiple scattering theory [13,14,16,17]. In the approximate coupling method, $\overline{\overline{T}}_a^{-1}$ and $\overline{\overline{T}}_b^{-1}$ are identified with the diagonal sub-matrices of (1.41), while G_{ab} and G_{ba} are identified with the off diagonal sub-matrices. The G_{ab} and G_{ba}, which represent the Green's functions connecting the individual sub-clusters, are assumed to be small in some sense. Suppose the energy eigenvalues of the sub-cluster corresponding to the sub-matrix $\overline{\overline{T}}_a^{-1}$ were found using the molecular field approximation; these energy eigenvalues should not differ greatly from those of (3.11), provided G_{ab} and G_{ba} are small. This suggests the following prescription for an approximate multiple scattering theory:

1) First, an energy eigenvalue (EO) is found from sub-matrix $\overline{T}_a^{-1}$ using the molecular field approximation.

2) The matrix elements of G_{ab}, $\overline{T}_b^{-1}$, and G_{ba} are calculated using EO as the energy; the matrix inverse of $\overline{T}_b^{-1}$ is taken.

3) Determinants of the matrix

$$\overline{T}_a^{-1}(E) - G_{ab}(EO)\,\overline{T}_b(EO)\,G_{ba}(EO) \tag{3.13}$$

are calculated at various values of E until a zero is found. This final value of E (call it E1) is assumed to be an approximate solution of (3.11).

Note that in the third step of this procedure, the matrix elements G_{ab}, $\overline{T}_b$, and G_{ba} are unchanged. This means that they must only be calculated once per eigenvalue. Similarly, the matrix inverse of $\overline{T}_b$ need be taken only once per eigenvalue. Thus, this procedure can lead to very substantial improvements in computational efficiency, particularly for large systems.

The crucial question, of course, is the accuracy of this approximation. How close is the energy E1 to the eigenvalue of (3.11)? In general, it can be said that E1 is a good approximation if G_{ab} and G_{ba} are small, and if G_{ab}, G_{ba}, and $\overline{T}_b$ are relatively slowly varying over the energy range of interest. If the molecular field eigenvalue EO differs greatly from the corresponding eigenvalue of (3.11), it may be safe to assume that the conditions for

weak coupling are not being met. However, even if the conditions of weak coupling are not met, an iterative scheme can be used to find an accurate energy. This iterative scheme is discussed in the next section of this chapter.

The precise form of the approximate scattered wave theory can be found by placing (1.41) in the form (3.13). Identifying $\overline{T}_a^{-1}$ with the sub-matrix of sphere 1 and $\overline{T}_b^{-1}$ with the sub-matrix of sphere 2 and that of the system outer sphere, one obtains:

$$\begin{bmatrix} M'^1 & N'^1 & \\ N^1 & M' & -G^{10,12} \\ & -G^{12,10} & [T^1]^{-1} \end{bmatrix}$$

$$- \begin{bmatrix} -G^{10} & -G^{12} & 0 & 0 \\ 0 & & & \\ 0 & & & \end{bmatrix} \begin{bmatrix} t_0^{-1} & & \\ & M'^2 \; N'^2 & \\ & N^2 \; M^2 - G^{20,22} & \\ & -G^{22,20} [T^2]^{-1} & \end{bmatrix}^{-1} \begin{bmatrix} -G^{01} & 0 & 0 \\ -G^{21} & & \\ 0 & & \\ 0 & & \end{bmatrix}$$

(3.14)

where the notation $[\ ]^{-1}$ denotes matrix inversion.

From the form of the second term of (3.14), it can be seen that only the M'^{1} sub-matrix of the first term is modified. If this modification is denoted $\overline{M}'(E)$, (3.14) can be re-written (with explicit energy dependence):

$$\begin{bmatrix} M'^{1}(E)-\overline{M}'(E0) & N'^{1}(E) \\ N^{1}(E) & M^{1}(E) - G^{10,12}(E) \\ & - G^{12,10}(E) \left[T^{1}(E)\right]^{-1} \end{bmatrix}$$

(3.15)

This matrix looks like an SCF-Xα-SW calculation for sub-cluster 1, but with modified boundary conditions at the surface of the partitioning sphere. The effects of scattering from sphere 2 and from the system outer sphere are entirely included in the term $\overline{M}'(E)$. With this division of the molecule, sphere 1 will be referred to as the "principal" sub-cluster, while sphere 2 and the system outer sphere will together be referred to as the "environment". This division is arbitrary; for this example, it is equally possible to treat sub-cluster 2 as the principal sub-cluster, with sub-cluster 1 and the system outer sphere constituting the environment.

To find an eigenstate using this approximation, the following procedure is used: first, the matrix elements of $\overline{M}'(E)$ are computed

with energy E_0, the molecular field energy level. Then E is varied until a zero of the determinant of (3.15) is found. Note that the matrix $\overline{M}'(E)$ is calculated only once per eigenvalue, leading to very substantial savings in computational effort.

Approximate Coupling Techniques Applied To Methanol

To see if the approximate coupling method gives reasonable results in practice, two test calculations have been performed on the methanol molecule. The two calculations use different methods of partitioning the atoms in the molecule, corresponding to Model I and Model III of Chapter 2. The discussion of the motivation for the different types of partitioning in Chapter 2 is applicable to the current case as well. If the CH_3 and OH fragments are considered the fundamental building blocks of the molecule, Model I is favored. If the CO bond is considered the fundamental unit, Model III is more appropriate. These distinctions are heightened by the use of the approximation method, which explicitly assumes weak coupling between the partitioned sub-clusters. Because the results of the fully coupled calculations of Chapter 2 show that there is substantial C-O interaction in most of the methanol orbitals, the approximate coupling method should be more appropriate for Model III type of partitioning, in which the carbon and oxygen atoms are in a single sub-cluster. Nevertheless, an approximate coupling calculation has also been performed for the Model I type of partitioning (in which the carbon and oxygen atoms are in separate sub-clusters) to see if the technique can be used in a situation that might more accurately be considered as "strong coupling."

Model III Approximate Coupling

In the Model III calculation, the partitioning sphere containing the carbon and oxygen atoms is treated as the principal sub-cluster, while the four hydrogen atoms and the system outer sphere are treated as the environment. The potentials for the approximate calculation were obtained from the converged, fully coupled Model III calculation described in Chapter 2; thus, the success of the approximate calculation can be judged by how closely it replicates the molecular orbital energies and wavefunctions of the previous calculation.

The second column of energy levels in Fig. 3.1 shows the results of the initial molecular field calculation for the CO sub-cluster. The formalism of (3.6) is used, so that scattering from the system outer sphere is included. All scattering from the four hydrogen atoms is, of course, neglected. Note that two pairs of levels are degenerate: the 1a", 3a' pair and the 2a", 5a' pair. This degeneracy is due to the fact the true symmetry of the CO sub-cluster is $C_{\infty v}$, so that the degenerate pairs correspond to π levels of an isolated molecule. Even though the potentials in the molecular field calculation include the electrostatic effects of the hydrogen atoms, the spherical averaging process in the C and O atomic spheres precludes any symmetry breaking.

For purposes of comparison, a standard SCF-Xα-SW calculation of an isolated CO molecule was performed using the C-O bond distance of methanol. The results are displayed in the first column of Fig. 3.1.

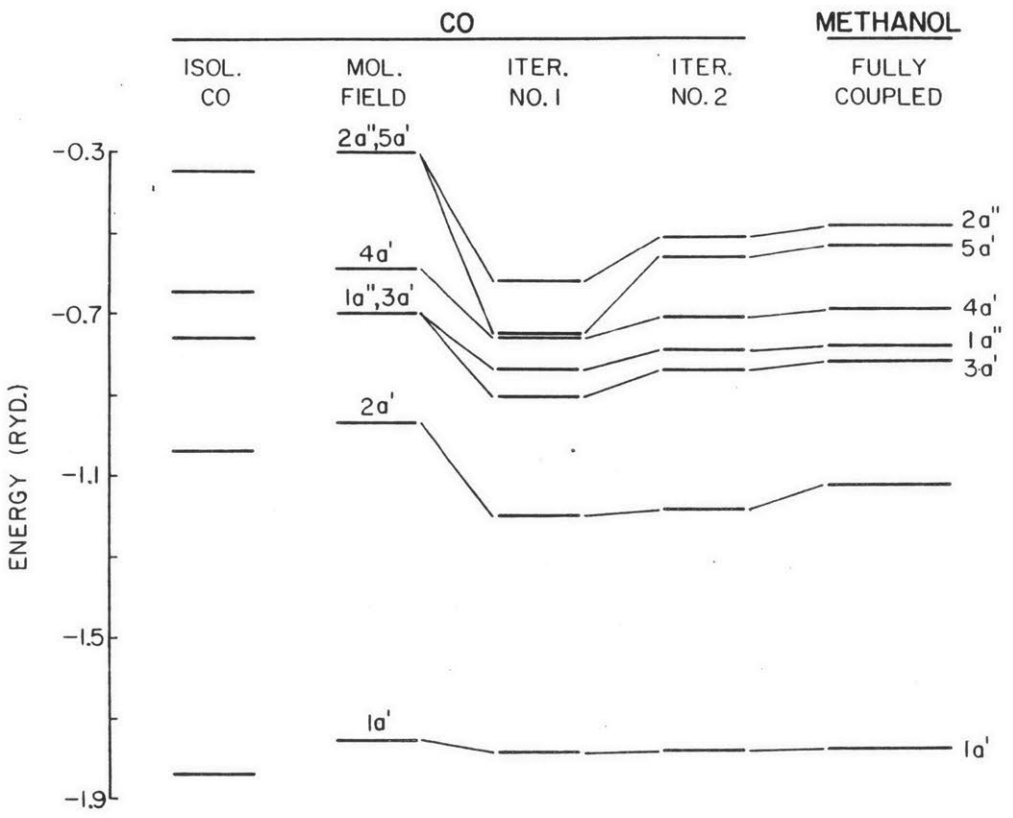

Fig. 3.1. Energy levels of approximate coupling calculations of methanol using Model III partitioning, compared with a standard SCF-Xα-SW calculation of an isolated CO molecule on the left and the "exact" Model III partitioning results from Chapter 2 on the right. The second column shows the molecular field energies found using the formalism of (3.6). The third and fourth columns show the first and second iteration approximate coupling results. The iteration scheme is described in the text.

The energy levels seem very similar to those of the molecular field calculation, except that they are shifted lower by about 0.5-0.6 rydbergs. This shift is explained by the donation of charge from the hydrogen to the carbon and oxygen atoms in the methanol molecule. Because this particular molecular field calculation uses a potential converged in a fully coupled calculation, the energy levels reflect the charge transfer but not the stabilization energy associated with the interaction with the hydrogen atoms. For an approximate calculation on a system too large for the fully coupled method, such converged potentials would not be available. In such a case, the initial potential would be obtained by superimposing potentials (or charge densities) of the various sub-clusters; the sub-cluster potentials would be obtained from standard $X\alpha$-SW calculations.

Column three of Fig. 3.1 shows the energy levels of the first iteration of the approximate coupling method. The initial environment energies (E_0 in (3.13)) were taken from the molecular field results. Comparing the approximately coupled results to the fully coupled results in the fifth column, it is seen that although the energy levels have the correct ordering, they have a tendency to "overshoot" the fully coupled values. To correct this, a simple iteration scheme was devised. In the fourth column of Fig. 3.1 are the energy levels of another approximate coupling calculation, but with initial energies obtained from the average of the molecular field energies and the first iteration approximately coupled energies (i.e., those of column three). The energy levels resulting from the second iteration are in remarkably good agreement with those of the fully coupled case.

Plots of wavefunctions from molecular field and the first iteration approximately coupled calculations are shown in Figs. 3.2 through 3.8. Wavefunctions from the second approximately coupled calculation are not shown because they are virtually identical with those from the fully coupled calculation of Chapter 2.

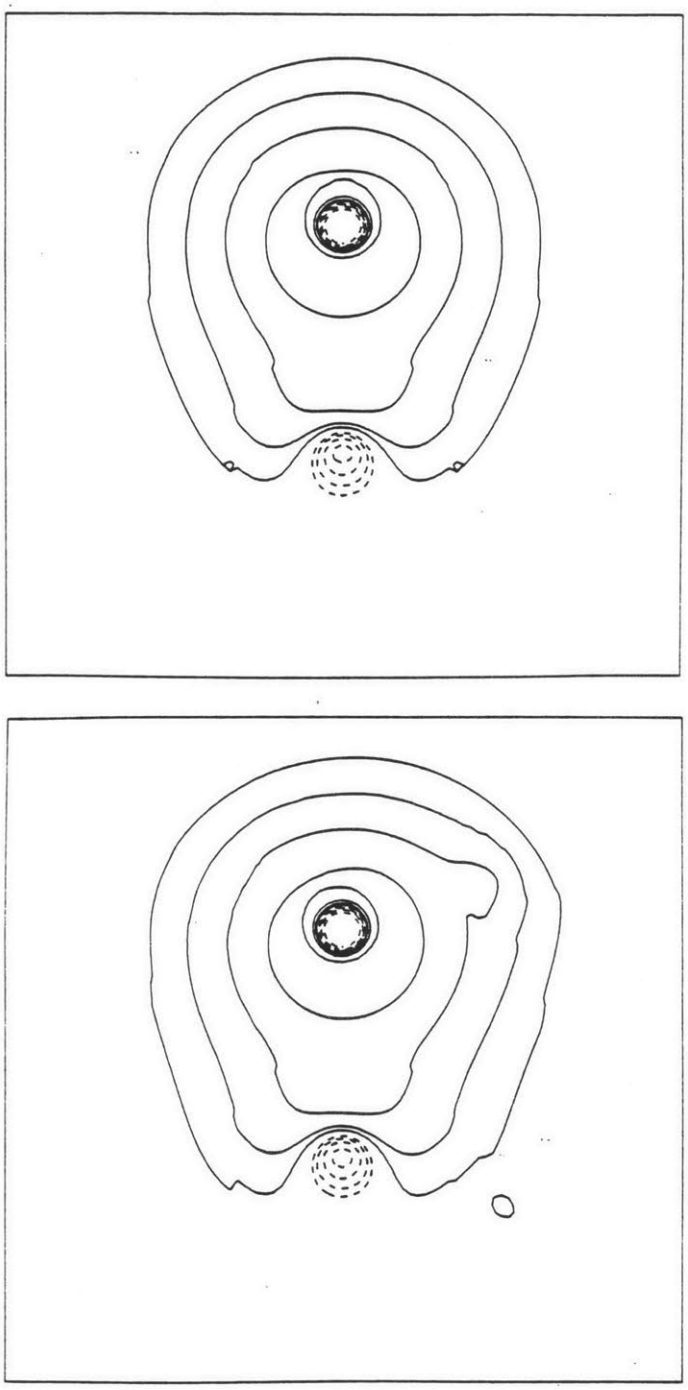

Fig. 3.2. Wavefunction plots of the molecular field (upper) and first iteration approximate coupling calculations (lower) of the 1a′ methanol orbital using Model III partitioning.

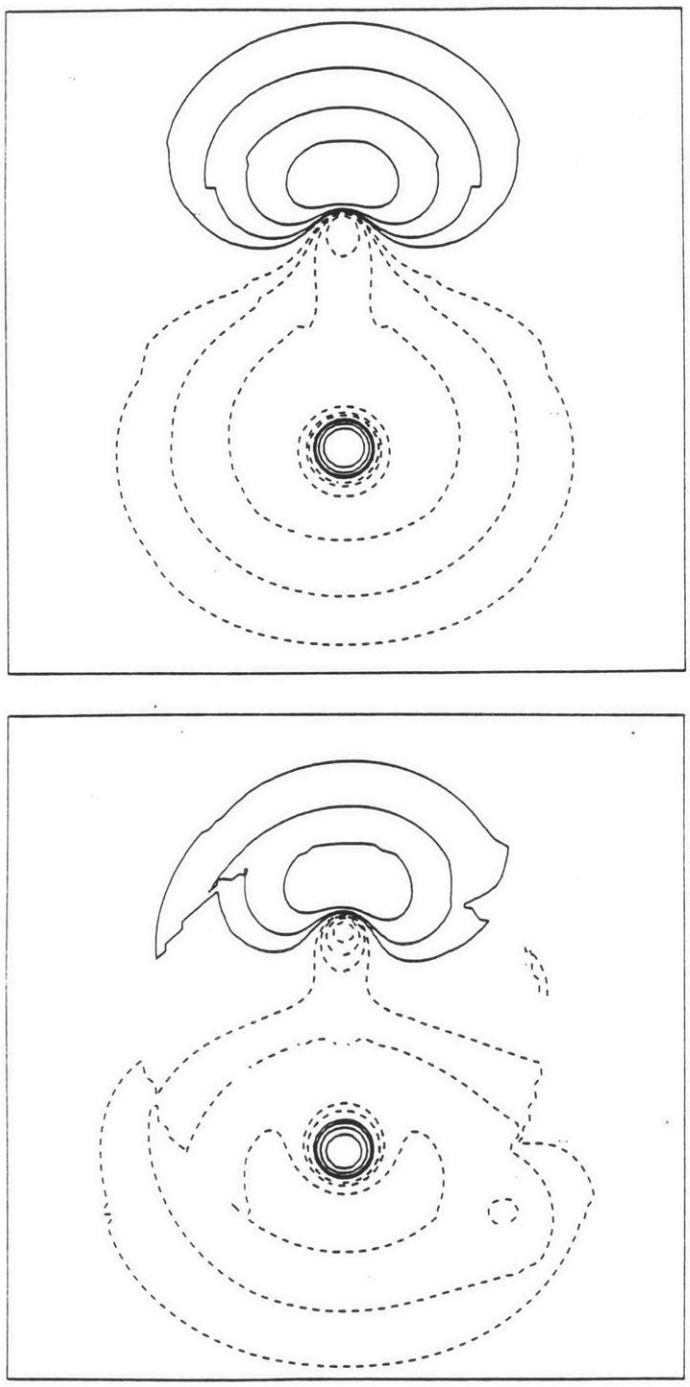

Fig. 3.3. Wavefunction plots of the molecular field (upper) and first iteration approximate coupling calculations (lower) of the 2a' methanol orbital using Model III partitioning.

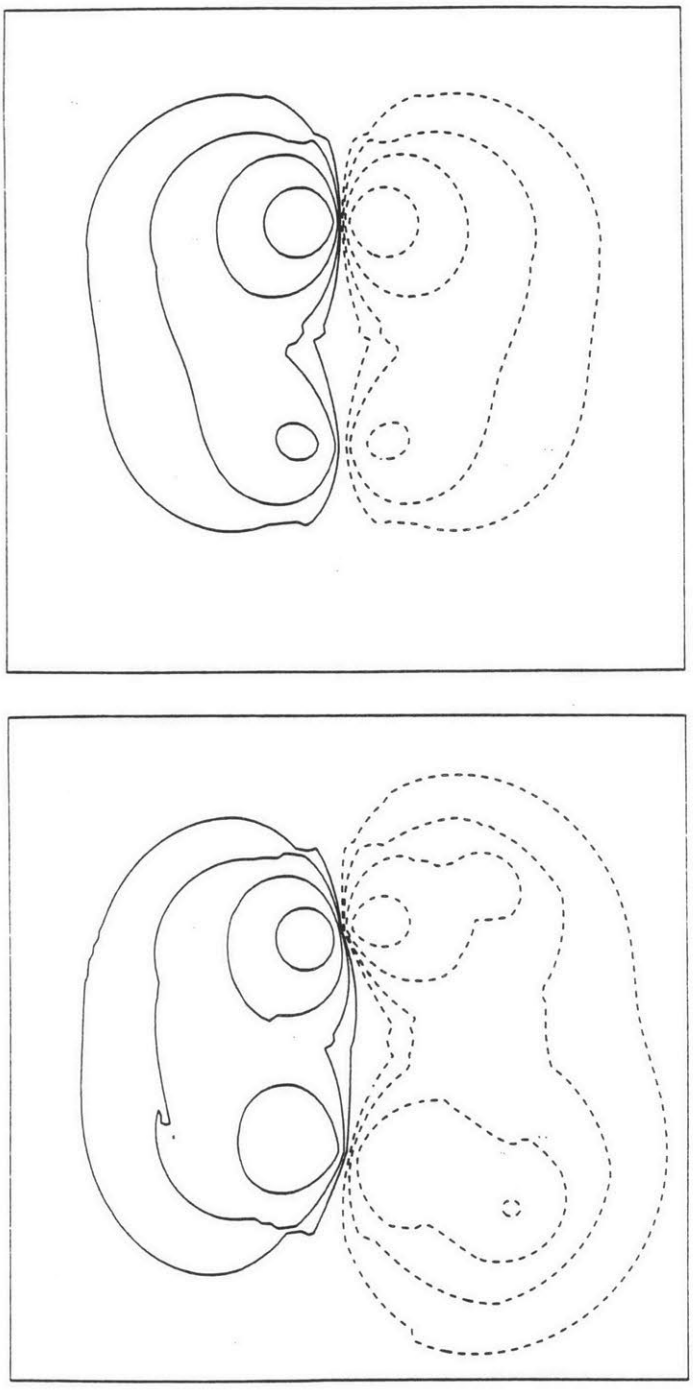

Fig. 3.4. Wavefunction plots of the molecular field (upper) and first iteration approximate coupling calculations (lower) of the 3a' methanol orbital using Model III partitioning.

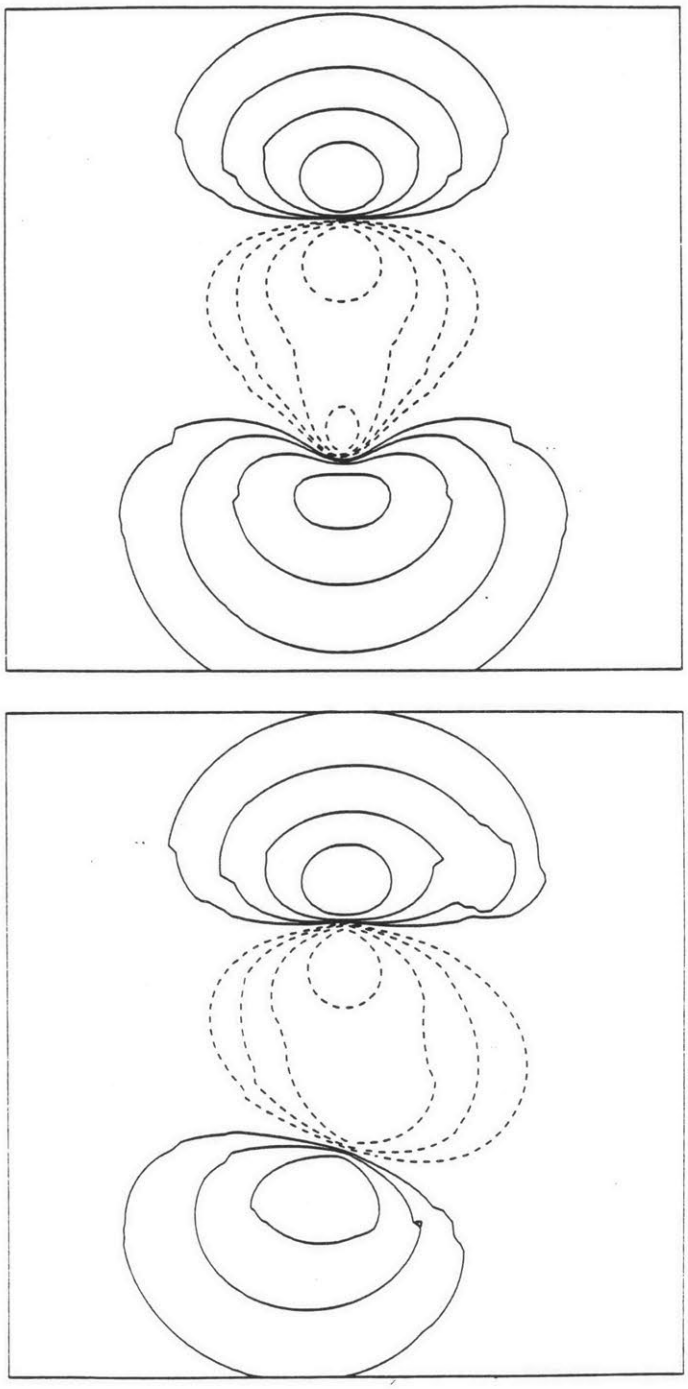

Fig. 3.5. Wavefunction plots of the molecular field (upper) and first iteration approximate coupling calculations (lower) of the 4a' methanol orbital using Model III partitioning.

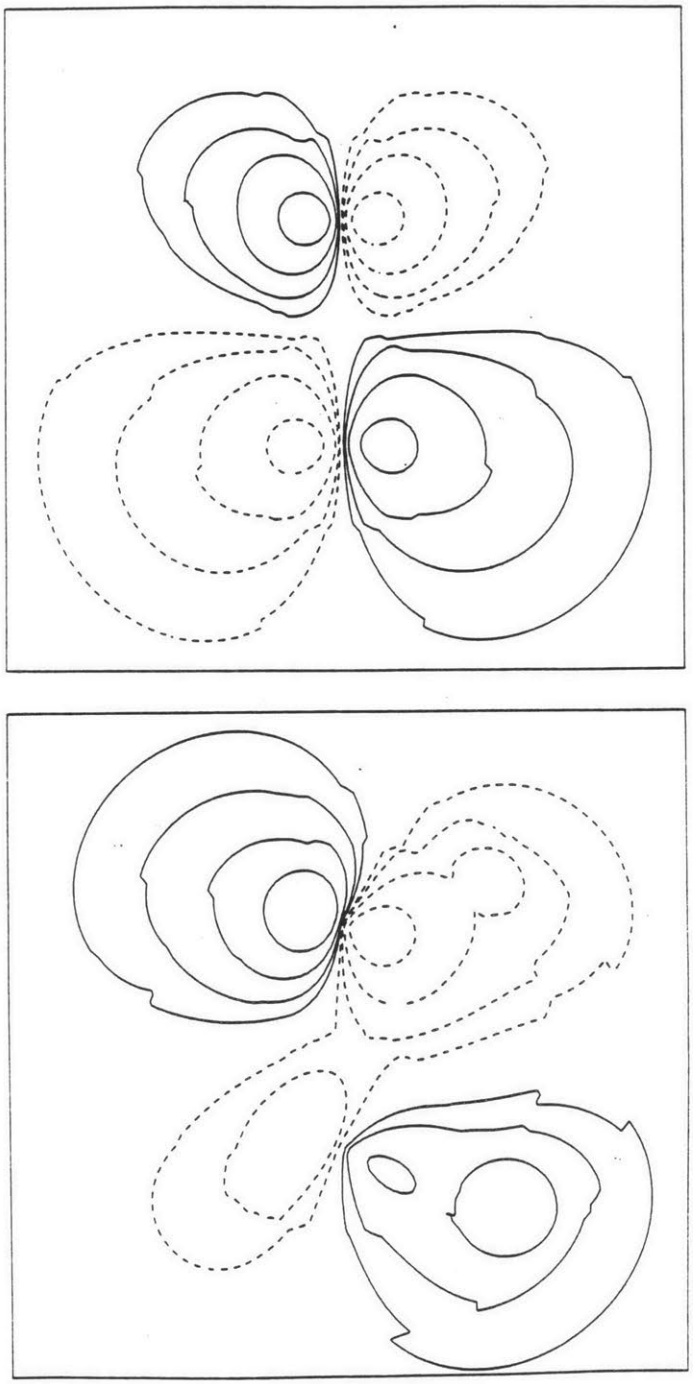

Fig. 3.6. Wavefunction plots of the molecular field (upper) and first iteration approximate coupling calculations (lower) of the 5a′ methanol orbital using Model III partitioning.

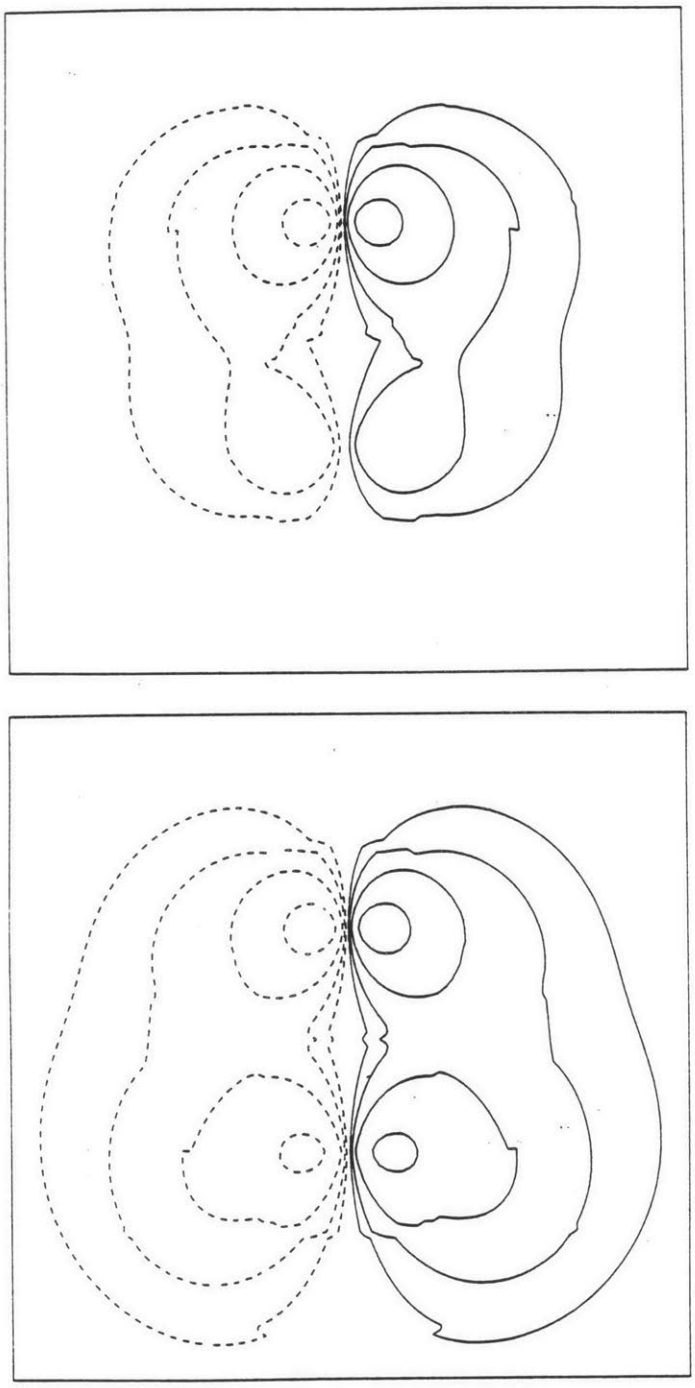

Fig. 3.7. Wavefunction plots of the molecular field (upper) and first iteration approximate coupling calculations (lower) of the 1a" methanol orbital using Model III partitioning.

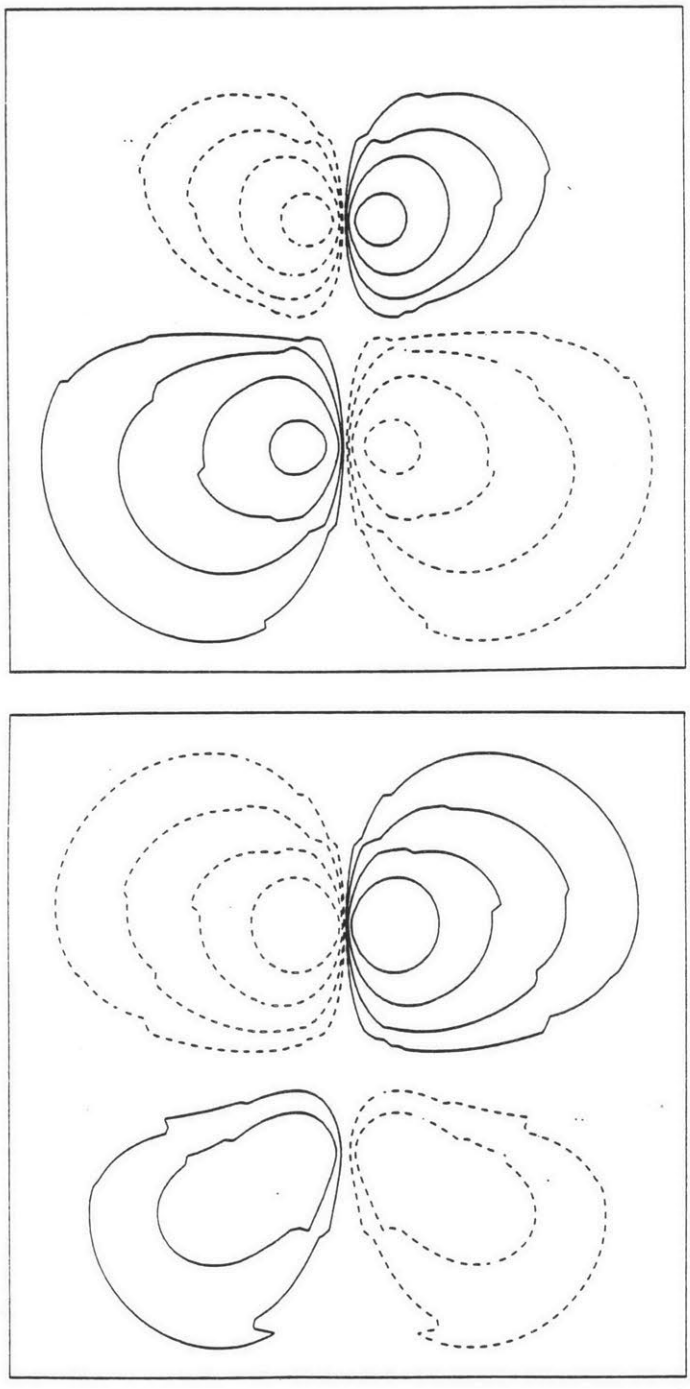

Fig. 3.8. Wavefunction plots of the molecular field (upper) and first iteration approximate coupling calculations (lower) of the 2a" methanol orbital using Model III partitioning.

Model I Approximate Coupling

The motivation of the approximate coupling calculation using Model I type of partitioning is to see if the method works in a situation in which the interaction between the principal sub-cluster and the environment might more accurately be considered "strong coupling". In Model I partitioning, a CH_3 fragment is in one sub-cluster, while an OH is in the other, thus separating the atoms that constitute the most important bond in the molecule.

To apply the approximate coupling method to this type of partitioning, two sets of calculations must be done: one set in which the methyl fragment is the principal sub-cluster (with the OH and system outer sphere as the environment) and another set with the OH fragment as the principal sub-cluster (with the CH_3 and system outer sphere as the environment). The results of these two sets of calculations are shown in Fig. 3.9, with the former set on the left and the latter on the right. Two iterations of the approximate coupling calculations are shown along with the molecular field results. The results of the fully coupled calculations from Chapter 2 are shown in the center column of the figure. Energy level diagrams of standard SCF-Xα-SW calculations of the isolated, neutral fragments are shown in Figs. 3.10 and 3.11. The standard SCF-Xα-SW calculations used the coordinates of the fragments as they exist in the methanol molecule; furthermore, the radii of the outer spheres were equal to the radii of the corresponding partitioning spheres of the Model I calculation. The molecular field calculation was performed using the formalism of (3.5), in which scattering from the system outer sphere

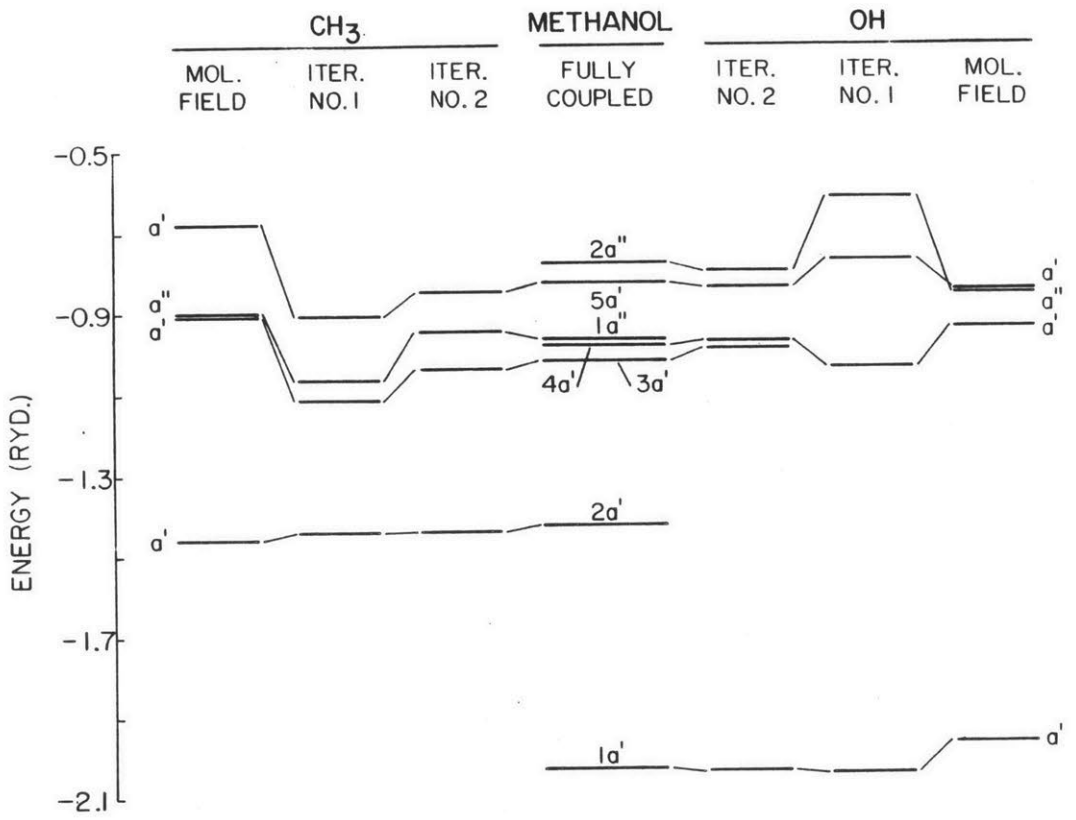

Fig. 3.9. Approximate coupling calculations of methanol with Model I partitioning compared with the "exact" results from Chapter 2 in the center column. The calculations on the left use the methyl fragment as the principal sub-cluster, while those on the right use the OH fragment as the principal sub-cluster.

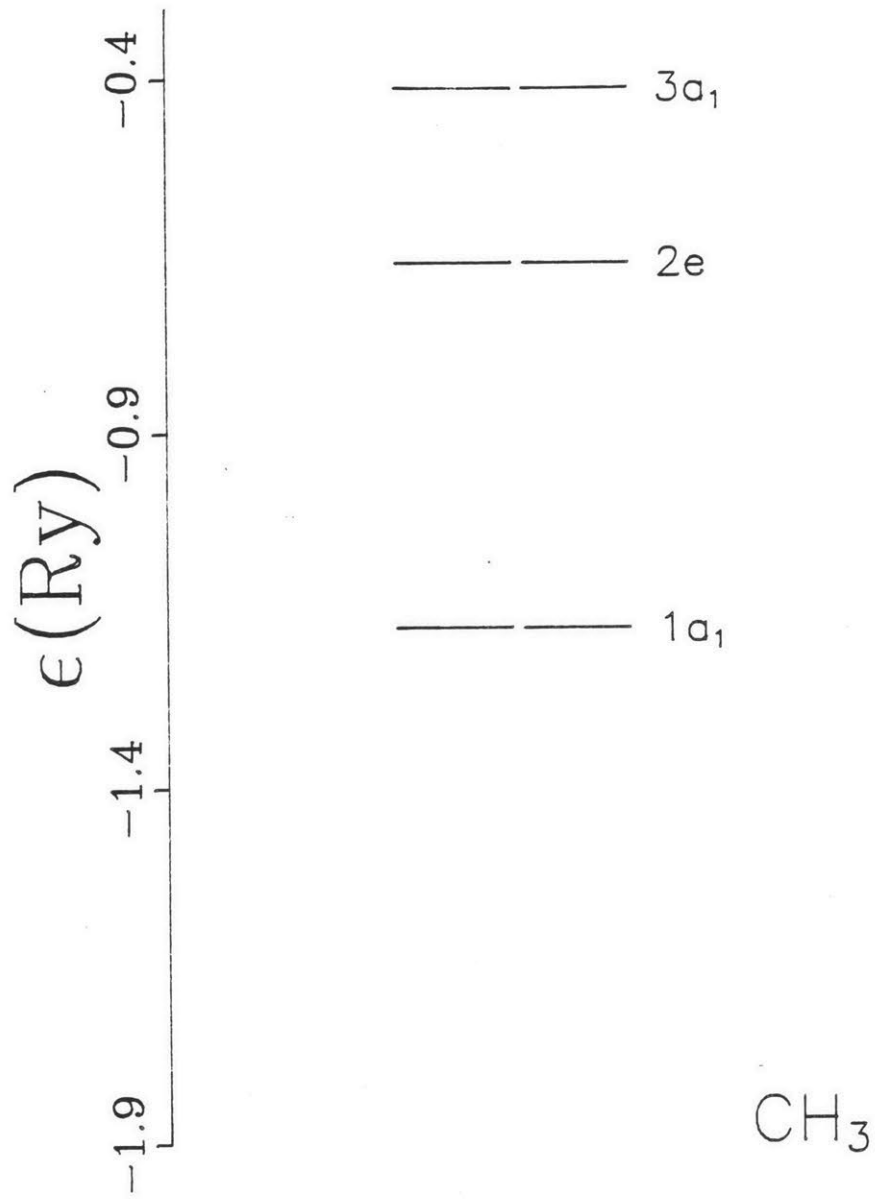

Fig. 3.10. Energy level diagram of an isolated methyl fragment found using the standard SCF-Xα-SW method. Interatomic distances of the methanol molecule were used in this calculation.

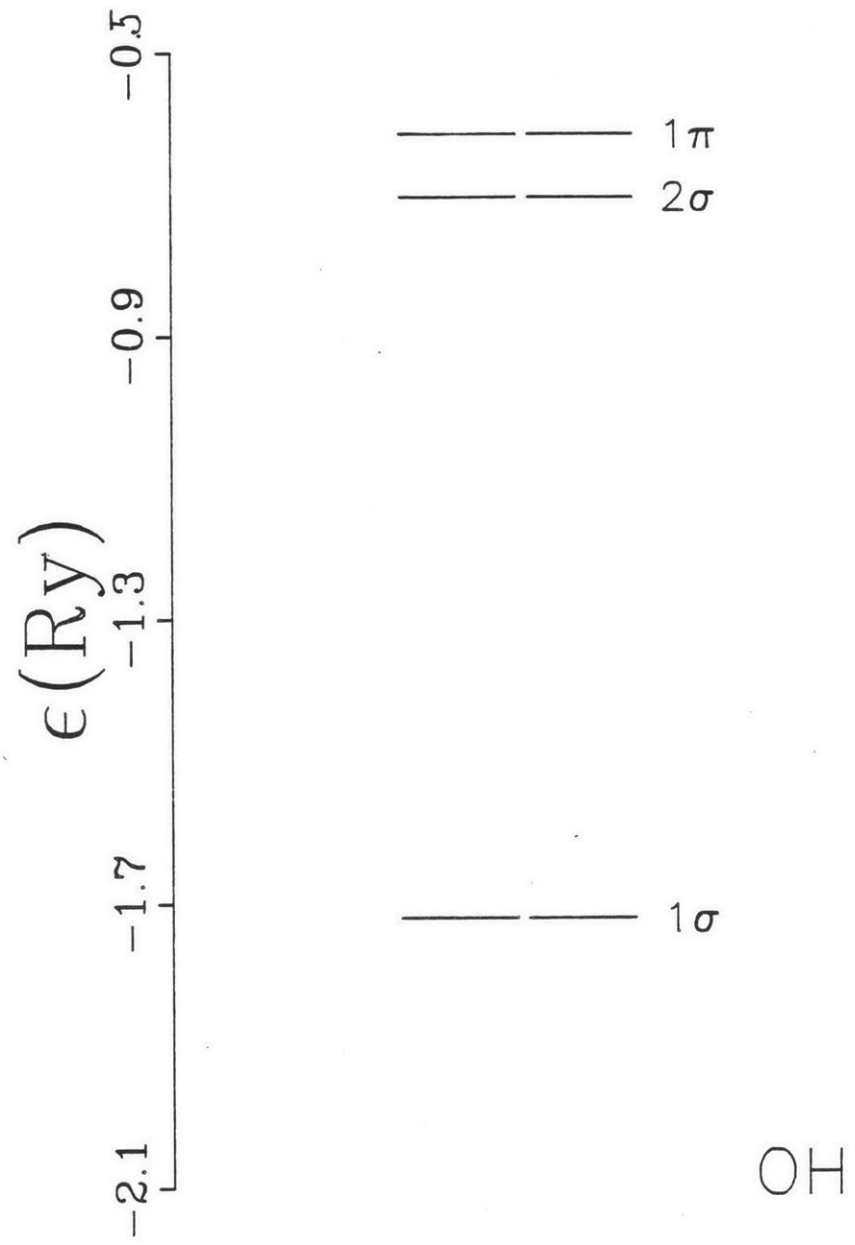

Fig. 3.11. Energy level diagram of an isolated OH fragment found using the standard SCF-Xα-SW method. Interatomic distances of the methanol molecule were used in this calculation.

is neglected. The iteration scheme used for the approximate coupling calculations was the same as that used in the previous section, in which the average of the initial and final energies of the first iteration is used as the initial environment energy of the second iteration.

The molecular field energies are shifted downward significantly from the energies of the standard SCF-Xα-SW calculations of the isolated fragments. This differs from the Model III situation, where the electron donation from the hydrogen atoms caused the molecular field energies to rise. In the present case, most of the electron transfer has occurred in the isolated fragments. The lowering of the energies is caused by bringing the carbon and oxygen nuclei closer together, as well as by the large system outer sphere (see Chapter 2 for a discussion of the effects of a large outer sphere).

It's interesting to note that not all of the methanol orbitals can be obtained from approximate coupling calculations using a single principal sub-cluster. For example, the CH_3OH 1a' level is found only when the OH fragment is chosen as the principal sub-cluster. This is explained by the character of the 1a' level, which is predominantly O 2s (91% oxygen versus 7% carbon). The reason that this orbital is localized on the oxygen atom is closely related to the large energy difference between it and the closest CH_3 molecular field level. The approximate coupling method can be considered as a modification of the boundary conditions of the partitioning sphere containing the principal sub-cluster (see (3.15)); however, in this case there are no nearby CH_3 energy levels to be so modified. Thus, it is not surprising that the methanol 1a' level cannot be found when the CH_3 fragment is

treated as the principal sub-cluster. Similar comments apply to the methanol 2a' orbital, which is primarily localized on the carbon atom (65% carbon versus 18% oxygen).

The situation becomes more complex with the higher lying valence levels (3a', 4a', 5a', 1a", and 2a"). The 3a' and 5a' orbitals can be found using either fragment as a starting point, while the 4a', 1a" and 2a" orbitals can not. An explanation of why a methanol level can be found from either sub-cluster lies in the nature of the levels, which share electronic charge more evenly between the carbon and oxygen atoms than the lower lying 1a' and 2a' levels. The 5a' orbital consists of 50% oxygen and 32% carbon, while the 3a' consists of 64% oxygen and 27% carbon. This delocalization is an expected result of the relatively close proximity in energy of the CH_3 and OH molecular field levels.

However, a relatively equal charge distribution does not ensure that an orbital can be derived from either sub-cluster. For example, the charge of the 1a" orbital is equally distributed between the carbon and oxygen atoms, yet this level cannot be found when the OH group is used as the principal sub-cluster. Apparently, this is due to the relatively large energy difference between the OH molecular field a" level and the methanol 1a" level. There seems to be a limit to the energy shift that the approximate coupling scheme can tolerate. This limit cannot be precisely specified, and, in fact, seems to vary from one case to the next.

The rather complicated interlacing of the two sets of molecular field levels to form the methanol spectrum emphasizes the point that the interaction between the two sub-clusters is strong rather than

weak. In fact, the structure of the upper valence levels of methanol bears little resemblance to the structures of the CH_3 and OH fragments. The five high lying methanol levels are divided into two groups, depending on whether the C-O interaction is bonding (3a', 4a', 1a") or antibonding (5a', 2a"). Within these two groups there are smaller energy splittings determined by the degree of hydrogen interaction or by whether the C-O bond is sigma-like or pi-like. By contrast, the energy splittings of the corresponding molecular field levels are entirely determined by the interaction with hydrogen. In the OH sub-cluster, the molecular field 2a' level (at E = -0.94 rydbergs) is sigma bonding between O and H, while the degenerate pair (3a',1a") is non-bonding (i.e., O p orbitals oriented perpendicular to the O-H axis). In the molecular field levels of the CH_3 sub-cluster, the degenerate pair at -0.90 rydbergs (2a',1a") are C p orbitals lying in the plane of three hydrogen atoms. The higher C p orbital (the a' at -0.675 rydbergs) is perpendicular to this plane, i.e., it lies along the C-O axis. Thus, the 3a' corresponds to a carbon p orbital that is non-bonding with respect to hydrogen, in contrast to the degenerate pair which is non-bonding.

Wavefunction plots of the molecular field and first iteration approximate coupling levels are shown in Fig. 3.12 - 3.17. The discontinuities in the wavefunctions at the partitioning sphere boundaries for the molecular field levels are due to the use of the formalism of (3.5). This can be contrasted with molecular field wavefunctions in the previous section which were found using (3.6); clearly, this latter technique gives more realistic wavefunctions.

Looking at the wavefunction plots, it is clear that there is

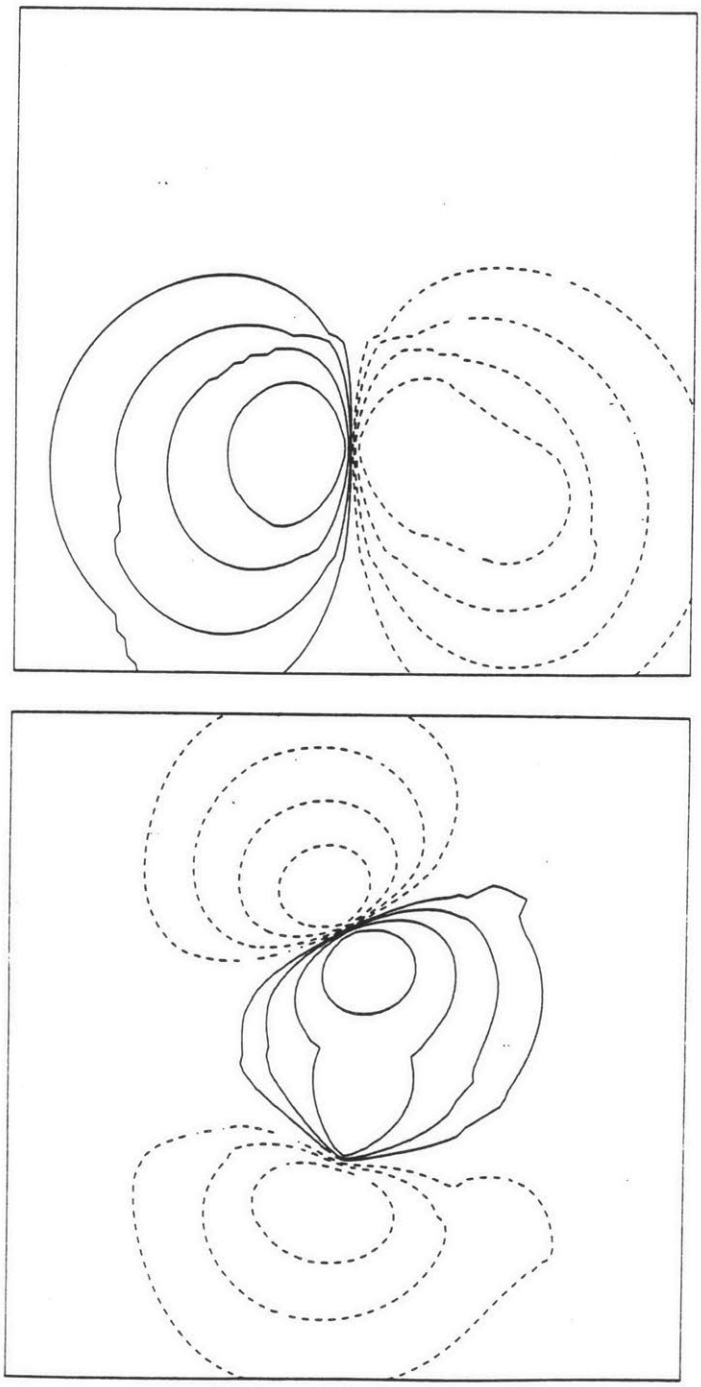

Fig. 3.12. Wavefunction plots of the molecular field (upper) and first iteration approximate coupling (lower) calculations of the 3a' methanol orbital using Model I partitioning. The methyl fragment is the principal sub-cluster.

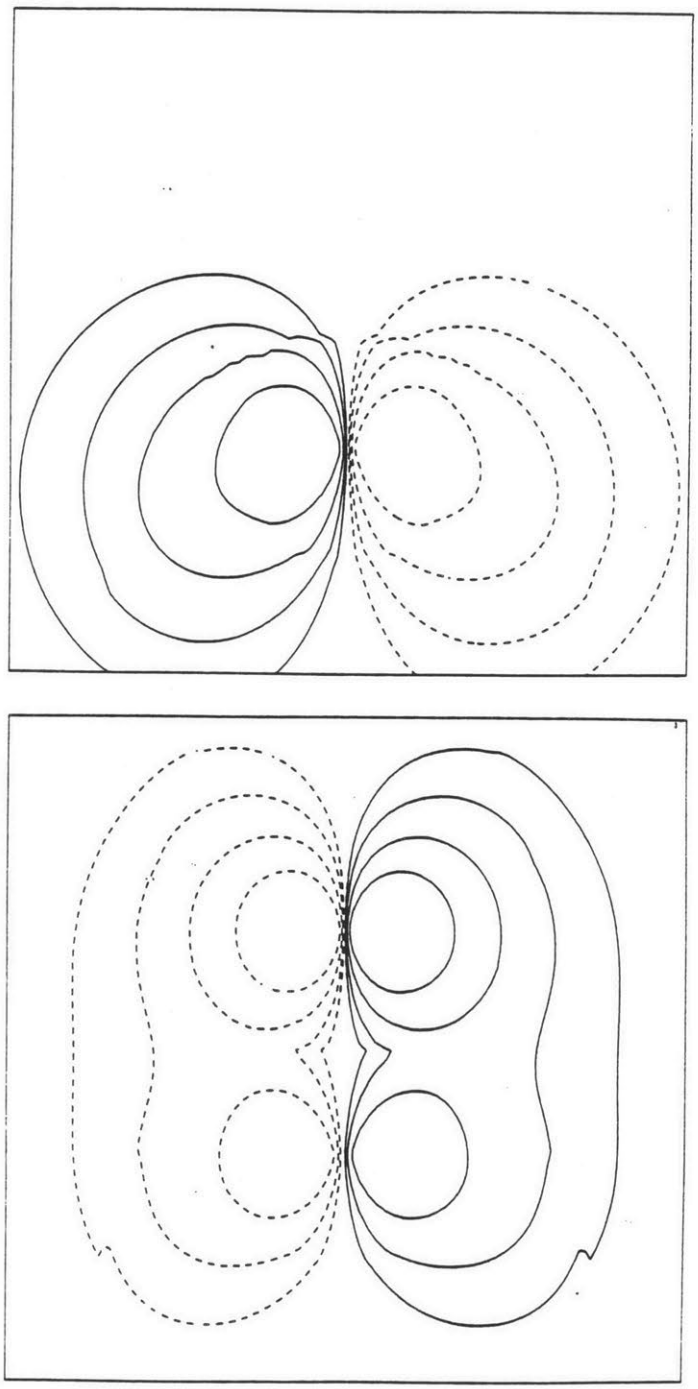

Fig. 3.13. Wavefunction plots of the molecular field (upper) and first iteration approximate coupling (lower) calculations of the 1a" methanol orbital using Model I partitioning. The methyl fragment is the principal sub-cluster.

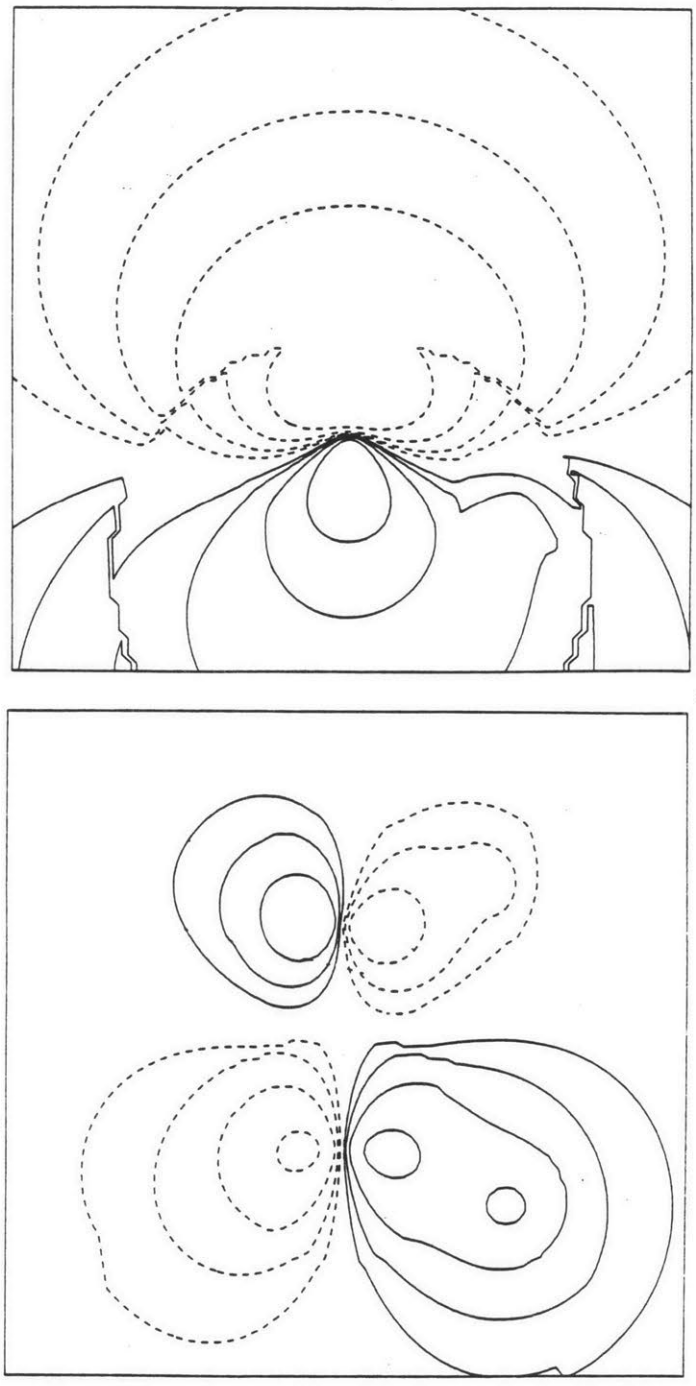

Fig. 3.14. Wavefunction plots of the molecular field (upper) and first iteration approximate coupling (lower) calculations of the 5a′ methanol orbital using Model I partitioning. The methyl fragment is the principal sub-cluster.

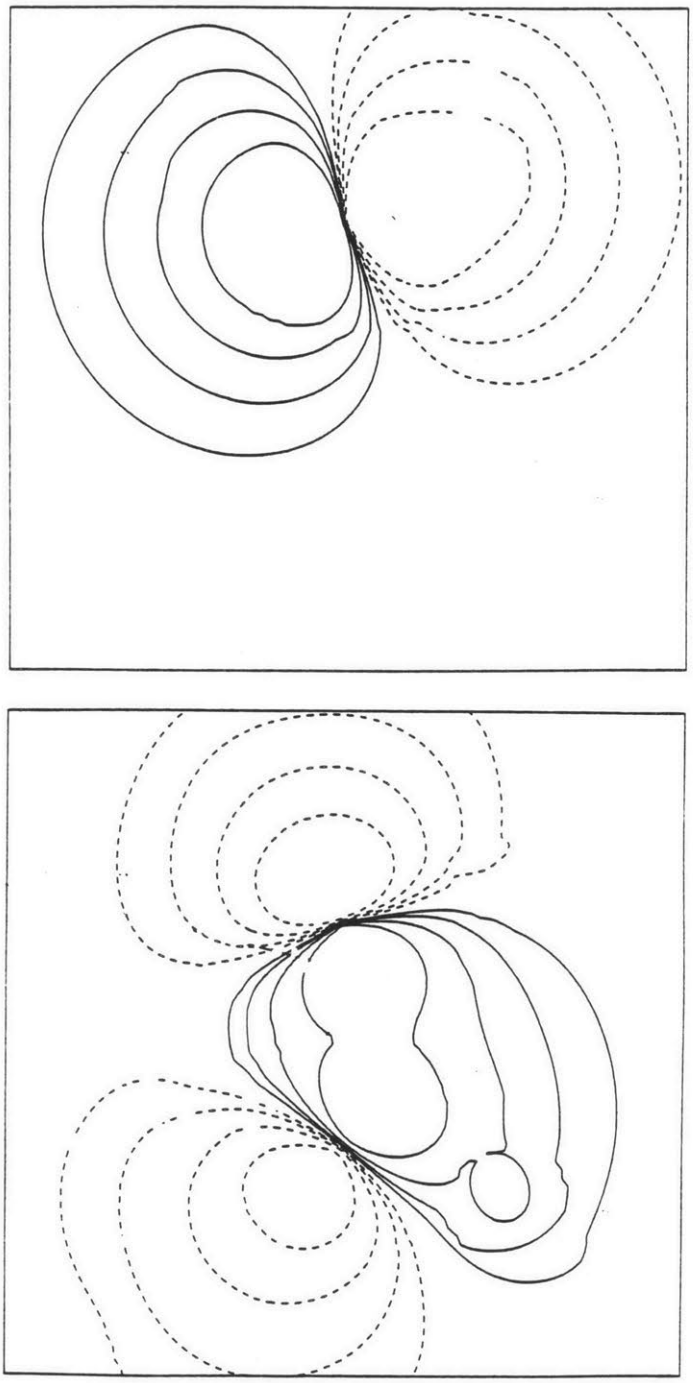

Fig. 3.15. Wavefunction plots of the molecular field (upper) and first iteration approximate coupling (lower) calculations of the 4a' methanol orbital using Model I partitioning. The OH fragment is the principal sub-cluster.

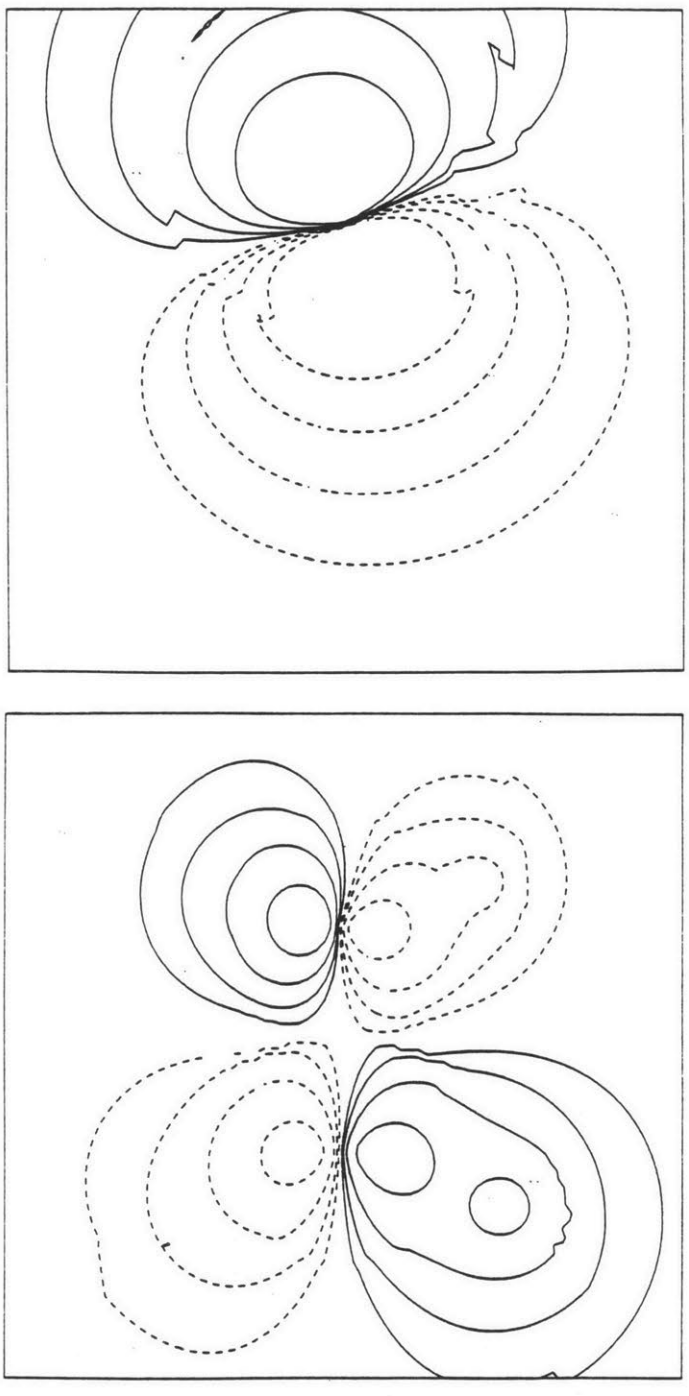

Fig. 3.16. Wavefunction plots of the molecular field (upper) and first iteration approximate coupling (lower) calculations of the 5a' methanol orbital using Model I partitioning. The OH fragment is the principal sub-cluster.

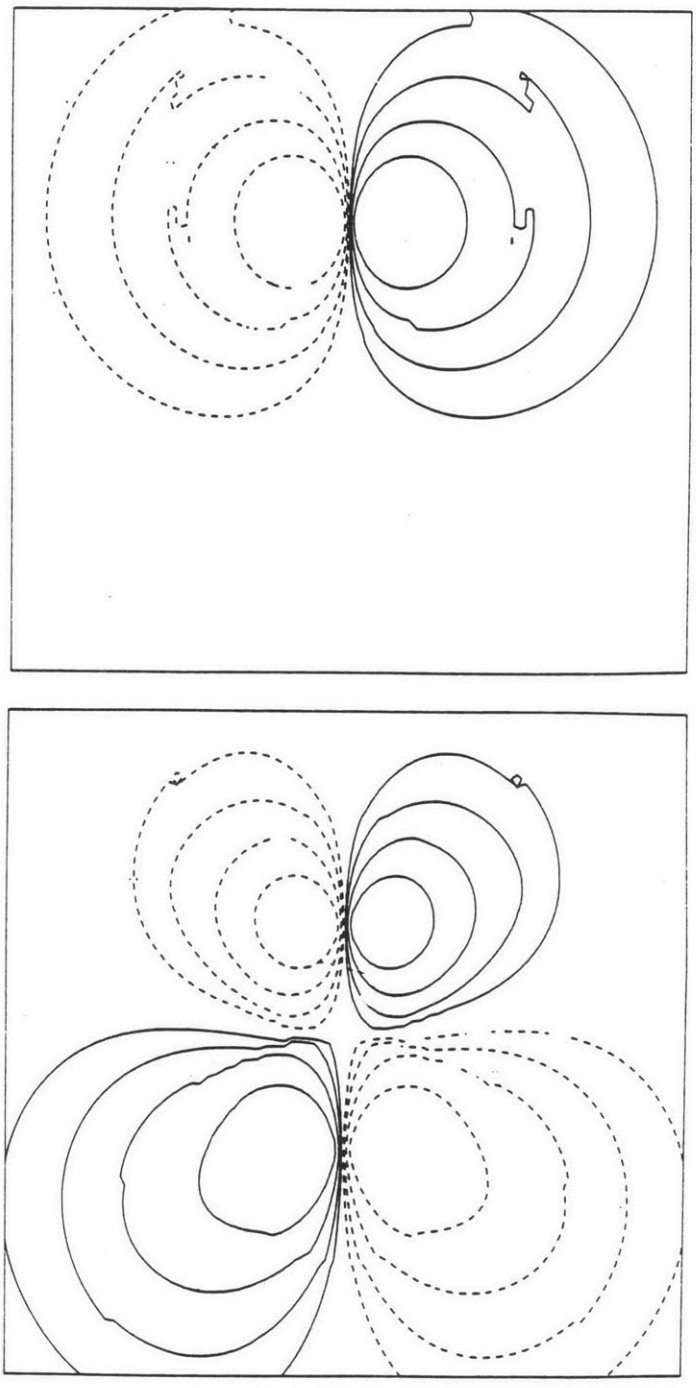

Fig. 3.17. Wavefunction plots of the molecular field (upper) and first iteration approximate coupling (lower) calculations of the 2a" methanol orbital using Model I partitioning. The OH fragment is the principal sub-cluster.

little relation between the orientation of the atomic p orbitals of the molecular field levels of a' symmetry and their orientation in the corresponding approximate coupling states. For example, in the OH molecular field level 3a', the O p orbital is nearly aligned with the C-O axis (see Fig. 3.15). However, the approximate coupling state derived from that level is a pi state, with the O p orbital perpendicular to the C-O axis. The changes in the other molecular field" states are no less drastic. Note that the symmetry restrictions of the a' states prevent similar changes.

This state of affairs, in which the electronic structures of the sub-units are unrecognizable in the structure of the whole system, differs significantly from the Model I calculations reported earlier in this chapter. In the previous case, it was clear that the approximate coupling wavefunctions had the same basic character as the molecular field wavefunctions. Because it involves relatively weak coupling between the principal sub-cluster and the environment, the Model III type of partitioning is more in the spirit of the approximate coupling calculations. That this method works in the current strongly coupled case is an encouraging indication that this a robust and perhaps widely applicable approximation.

Discussion

The most surprising outcome of these tests is how quickly the approximate coupling results converge to the "exact" fully coupled results. It's probably not possible to explain precisely why this happens. Perhaps one can only re-state what does happen: The electronic bound states of a sub-unit of a cluster are relatively insensitive to the "freezing" of the energy of the scattering matrix of that sub-unit's environment. This insensitivity extends even to the case in which the bound state is delocalized and has substantial charge density in the environment.

It has been that this technique works; but is it actually useful in practice? It is clearly a potentially powerful tool for calculating electronic states of systems much larger than is now practical. However, some of the potential difficulties have been hidden by the simple nature of the examples shown in this chapter. In a real application of this technique, the results of a fully coupled calculation would obviously not be available. It is possible that an orbital of the entire system which could be derived from either sub-cluster (as occurred in the Model I calculation) could be mistakenly counted as two different orbitals. This problem is unlikely to happen if the results are carefully examined, as the two orbitals would be seen as very close in energy and very similar in character. However, such a discrimination depends on the judgement of the investigator, and cannot be mechanically implemented in the computer codes.

Another possible problem is that of failing to find an energy level. This could conceivably happen in a "strong coupling" situation in which the molecular field energy is distant from the energy of the corresponding level of the whole system. Again, the judgment of the investigator must be relied upon. In such cases, it's possible to use a "best guess" for the initial environment energy, rather than the molecular field energy. Convergence to the true eigenstate should be rapid. It should be pointed out that this situation has not occurred in any test to date.

Neither of these problems are critical; at worst, they demand some human interaction in an otherwise automated procedure. In addition, such problems are minimized by the extent to which the sub-clusters can be described as weakly interacting. The partitioning of the system should be chosen with this in mind.

The starting potentials for the tests in this chapter were obtained from self-consistent calculations of the corresponding fully coupled system. In a real application, such potentials would not be available. A starting potential could be obtained by combining the potentials (or charge densities) from self-consistent standard SCF-Xα-SW calculations of the individual sub-clusters. The eigenstates for this potential would then be found using the approximate coupling techniques. Although the calculations described in this chapter were not done self-consistently, there is, in principle, no obstacle to doing so. In fact, it may be important to perform self-consistent calculations for cases in which significant charge transfer between clusters is expected.

The approximate coupling techniques described in this chapter

have been shown to work both in situations where the inter-cluster coupling could be described as "weak" and where it could be described as "strong". In both cases, the approximate method rapidly converged to the fully coupled (or "exact") results. However, the test clusters used were relatively small. A further test of this method on a larger, more realistic application is described in Chapter 4.

REFERENCES

1. H.B. Gray and E.I. Solomon, in Copper Proteins, edited by T.G. Spiro (John Wiley, New York, 1981).

2. E.I. Solomon, K.W. Penfield, and D.E. Wilcox, Structure and Bonding 53, 1 (1983).

3. C.Y. Yang, K.H. Johnson, R.H. Holm, and J.G. Norman, J. Am. Chem. Soc. 97, 6596 (1975).

4. K.H. Johnson, J.G. Norman, and J.W.D. Connolly in Computational Methods for Large Molecules and Localized States in Solids, edited by F. Herman, A.D. McLean, and R.K. Nesbet (Plenum, New York, 1973).

5. P.M. Grant and Inder P. Batra, Synthetic Metals 1, 193 (1979).

6. G.B. Street and T.C. Clarke, IBM J. Res. Develop. 25, 51 (1981).

7. C.B. Duke in Extended Linear Chain Compounds, Vol. 2, edited by J.S. Miller (Plenum, New York, 1982).

8. K.H. Johnson, F. Herman, and R. Kjellander, in Electronic Structure of Polymers and Molecular Crystals, edited by J.-M. Andre and J. Ladik

(Plenum, New York, 1975).

9. C.E. Van Dijkum, Ph.D. thesis, U. of Amsterdam, Amsterdam (1980).

10. R.P. Messmer, S.K. Knudson, K.H. Johnson, J.B. Diamond, and C.Y. Yang, Phys. Rev. B 13, 1396 (1976).

11. V.I. Anisimov, V.A. Gubanov, D.E. Ellis, and E.Z. Kurmaev, J. Phys. F: Metal Phys. 11, 405 (1981).

12. J.A. Appelbaum and D.R. Hamann, Rev. Mod. Phys. 48, 479 (1976).

13. R. Kjellander, Chem. Phys. Letters 29, 270 (1974).

14. R. Kjellander, Chem. Phys. 12, 469 (1976).

15. P.-O. Lowdin, J. Mol. Spectry. 14, 112 (1964).

16. R. Kjellander, Chem. Phys. 20, 153 (1977).

17. A.R. Williams, P.J. Feibelmann, and N.D. Lang, Phys. Rev. B 26, 5433 (1982).

CHAPTER 4 - CO CHEMISORPTION ON SUPPORTED RHODIUM CATALYSTS: APPLICATIONS OF MOLECULAR PARTITIONING AND APPROXIMATE COUPLING THEORY

The chemisorption of CO and other molecules on transition metal catalysts has received much attention. Because many practical applications involve supported catalysts [1], the interaction between the support material (typically alumina or silica) and the transition metal catalyst (typically a platinum group element) is of particular interest. In this chapter, molecular orbital calculations of clusters representing rhodium supported on alumina (both with and without chemisorbed CO) are presented and discussed. Aside from the intrinsic interest in the chemistry of this system, a primary purpose for this study is the opportunity it provides for a realistic application of the partitioning techniques discussed in Chapter Two and the approximate coupling techniques discussed in Chapter Three.

In the past, the SCF-Xα-SW method has been successfully applied to many types of catalytic problems [2-5]. For heterogeneous catalysts, small clusters of atoms are chosen to model the active catalytic surfaces. Many questions of theoretical interest, such as the nature of the "potential surface", cannot be answered with Xα-SW calculations (or with most other computational techniques); nevertheless, knowledge of the bonding and electronic interactions between the chemisorbed molecule and the surface can lead to a broader understanding of the catalytic process.

The chemisorption of CO on alumina supported rhodium has been extensively studied with infrared spectroscopy and NMR [6-8]. Although there is some disagreement in interpretation, these studies identify

at least three distinct types of rhodium binding sites. Species I consists of two CO molecules bound to a single isolated rhodium atom. Species II is a single CO bound to a rhodium atom which is part of a larger metallic "raft" of rhodium atoms, while species III is a CO bridged between two rhodium "raft" atoms. J.T. Yates and co-workers [9] claim that electron microscopy experiments have shown that species I is not atomically dispersed. In their view, species I atoms occur on the edges of the metallic rafts. However, the case for atomically dispersed rhodium has been made by C.A. Rice and co-workers [8] using infrared spectroscopy. Rice and other investigators also claim that there is evidence that the species I rhodium is in a +1 oxidation state. Other types of binding sites have been tentatively identified by Rice, including an isolated rhodium atom with a single CO.

In this study, two model clusters have been used to study the CO-rhodium-alumina chemisorption problem. The first consists of a single rhodium atom supported on a seven atom group representing alumina. The second ($CO/RhAlO_6$) is the same as the first but with a CO molecule attached carbon first to the rhodium atom. This second cluster can be considered to represent the single carbonyl isolated rhodium species identified by Rice et al; however, it is likely that this model will also give insight into the chemical bonding of the dicarbonyl rhodium (species I). The interatomic distances used to construct these clusters were obtained from Ref. [10]; they are displayed in Table 4.1. Schematic diagrams of the clusters are shown in Figs. 4.1 and 4.2.

The standard SCF-Xα-SW calculations of these two clusters are presented in the second section of this chapter. A partitioned

TABLE 4.1

Coordinates for $RhAlO_6$

Atom	X	Y	Z	Radius	Alpha
outer sph.	0.0	0.0	-1.052	6.419	0.73554
Al	0.0	0.0	-2.086	2.215	0.72853
O1	-2.947	0.0	2.827	2.539	0.70217
O1	1.474	-2.552	0.0	1.989	0.74447
O1	1.474	2.552	0.0	1.989	0.74447
O2	2.947	0.0	-4.170	2.129	0.74447
O2	-1.474	2.552	-4.170	2.129	0.74447
O2	-1.474	-2.552	-4.170	2.129	0.74447

Coordinates for $CO/RhAlO_6$

outer sph.	0.0	0.0	1.628	8.633	0.73896
C	0.0	0.0	6.701	1.417	0.75928
O	0.0	0.0	8.837	1.425	0.74447

Coordinates for Partitioning Spheres of $CO/RhAlO_6$

sph. 1	0.0	0.0	7.773	2.488	0.75039
sph. 2	0.0	0.0	-1.052	6.419	0.73554

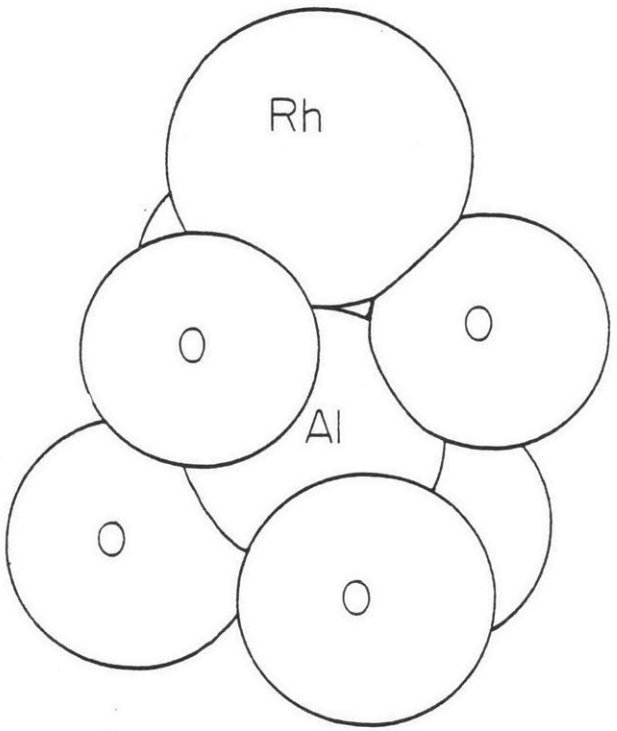

Fig. 4.1. Schematic drawing of $RhAlO_6$ cluster.

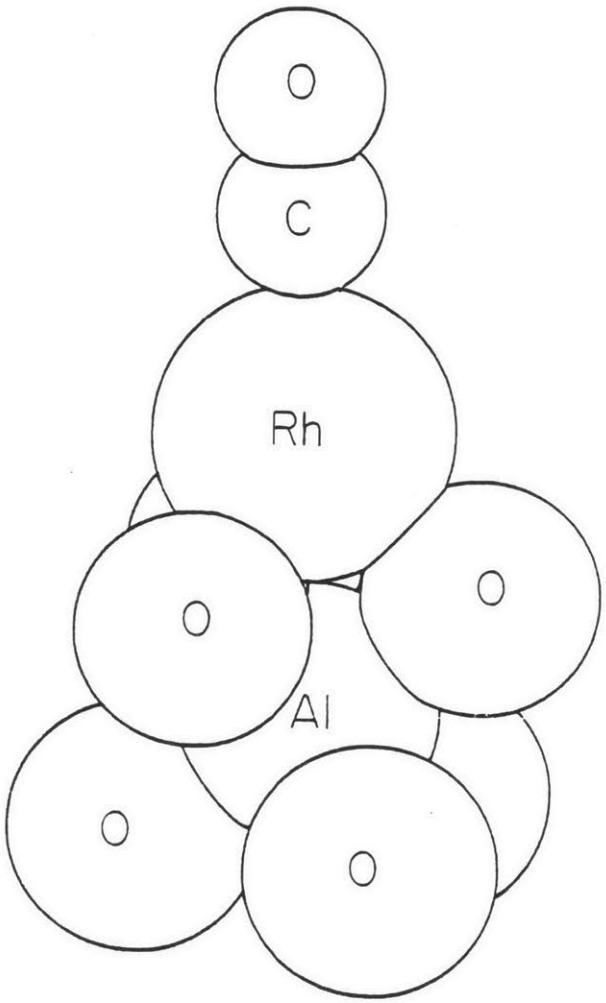

Fig. 4.2. Schematic drawing of $CO/RhAlO_6$ cluster.

calculation of the second cluster is described in the third section, and the approximate coupling treatment of the second cluster is described in the last section.

Standard SCF-Xα-SW Calculation of $RhAlO_6$ and $CO/RhAlO_6$

The electron energy levels for the $RhAlO_6$ and $CO/RhAlO_6$ clusters are shown in Fig. 4.3. Both of these calculations assumed a charge of -9 on each of the clusters; to stabilize the electronic charge, a Watson sphere of radius 6.4186 bohrs was used for the $RhAlO_6$ cluster, and a Watson sphere of radius 8.6328 bohrs was used for the $CO/RhAlO_6$ cluster. In addition, both clusters used an inner Watson sphere of radius 4.9131 bohrs.

For most catalytic systems, it is generally true that the molecular orbitals of greatest catalytic importance are those lying near the Fermi level. The three highest occupied levels of the $RhAlO_6$ cluster (e, a_1, and e) are primarily rhodium d orbitals (d-xz, d-z2, and dx2-y2 respectively, where the z axis points along the aluminum-rhodium axis). Plots of the wavefunctions of these orbitals are shown in Figs. 4.4-4.6. These rhodium levels are pushed to the top of the valence band by their antibonding interaction with the oxygen atoms of the alumina support. Similar effects have been seen in numerous other molecular orbital studies of transition metal- support or transition metal-ligand interactions.

Many other orbitals throughout the upper valence band (-1.1 to -0.5 rydbergs) have some rhodium d character. In the center of this band the rhodium is essentially non-bonding, while in the four lowest levels it is bonding. The a1 level at E= -1.03 rydbergs consists of rhodium d-z2 bonding with aluminum and oxygen, while the three next higher lying orbitals are rhodium-oxygen bonding levels.

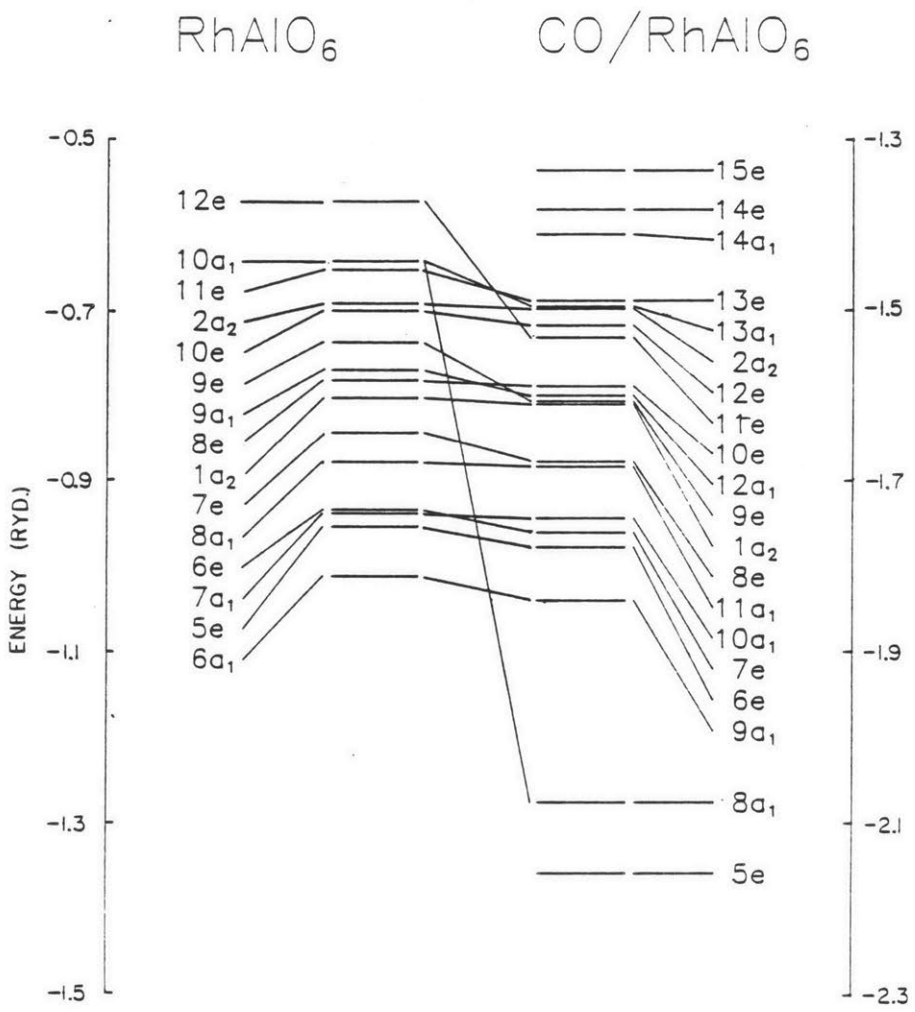

Fig. 4.3. Comparison of the energy level diagrams of the $RhAlO_6$ and $CO/RhAlO_6$ clusters. Both of these calculations were done with the standard SCF-Xα-SW method. The CO 4 sigma level interacts with the 10a1 orbital of the $RhAlO_6$ cluster to form the primary CO-rhodium bond (the 8a1 orbital). The CO pi antibonding orbital interacts with the 12e orbital of the $RhAlO_6$ cluster, leading to "back-donation." Note that the energy scales of the two calculations have been adjusted for purposes of comparison.

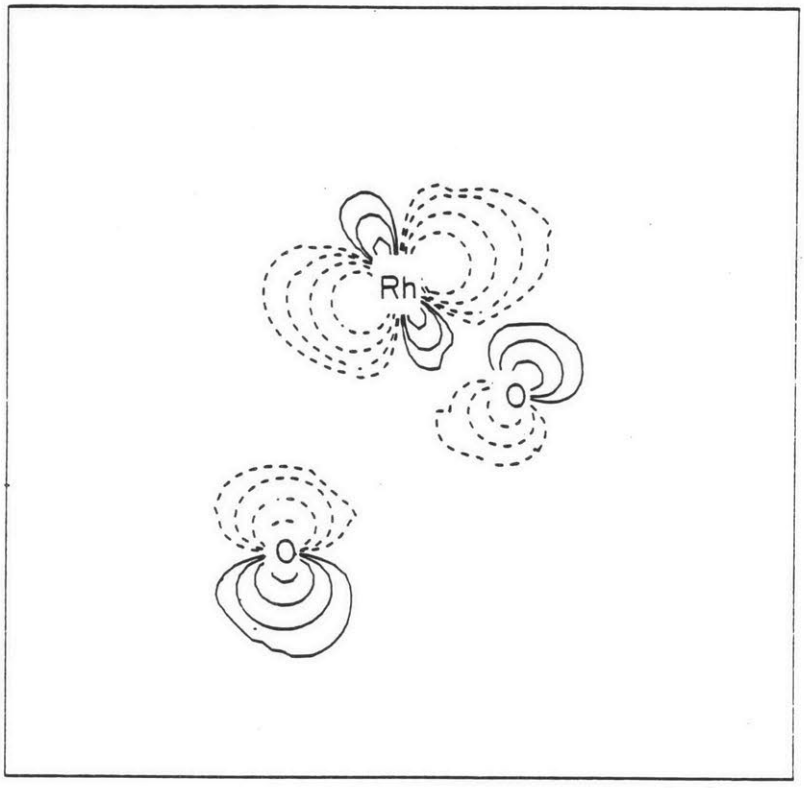

Fig. 4.4. A wavefunction plot of the 11e orbital of the $RhAlO_6$ cluster.

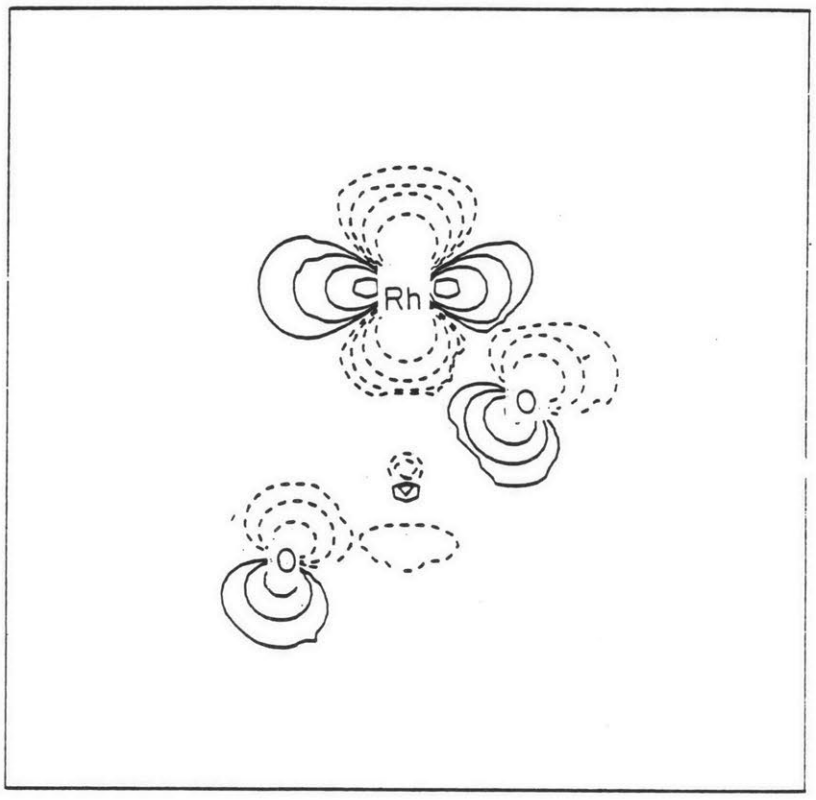

Fig. 4.5. A wavefunction plot of the 10a1 orbital of the $RhAlO_6$ cluster, showing the Rh d-z2 character; this orbital leads to the primary rhodium-CO bond in the $CO/RhAlO_6$ cluster (the 8a1 level).

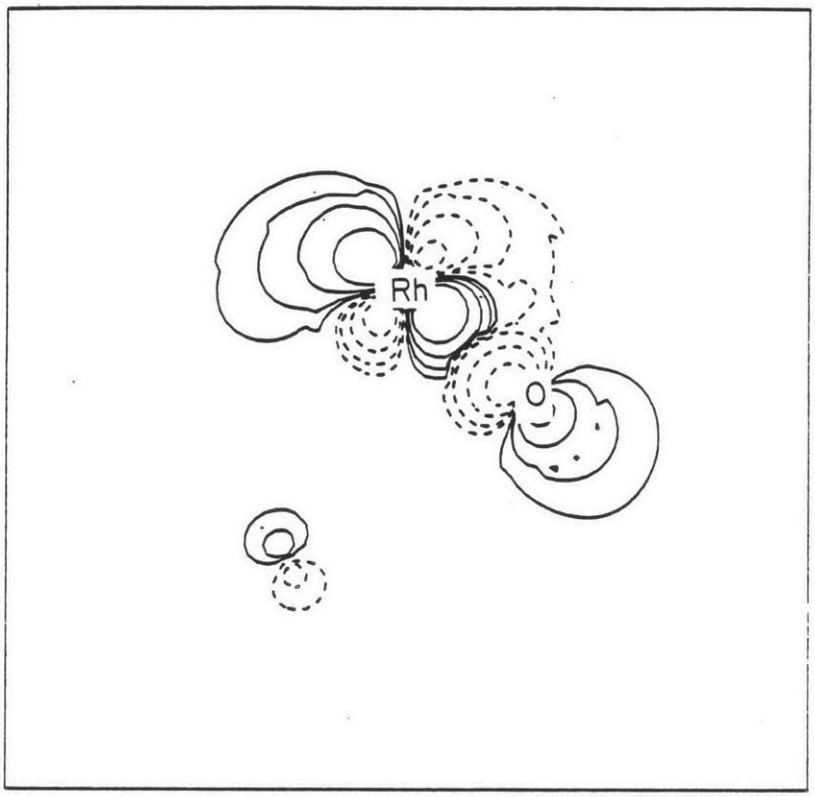

Fig. 4.6. A wavefunction plot of the 12e orbital of the $RhAlO_6$ cluster; this is the highest occupied molecular orbital.

The energy levels of the $CO/RhAlO_6$ cluster (in Fig. 4.3) have been shifted so that the levels can be easily compared with those of the $RhAlO_6$ cluster. It can be seen that the energy level structures are nearly identical. The significant differences arise from those orbitals having substantial CO-rhodium bonding interactions, namely the $8a_1$ and the 11e levels. The $8a_1$ level, whose wavefunction plot is shown in Fig. 4.7, consists of a strong CO-rhodium sigma bond, derived from the 5 sigma level of the isolated CO molecule. The 11e level, shown in Fig. 4.8, is the CO-rhodium "back-bond", consisting of a pi bonding interaction between the rhodium and the carbon atom, and a pi antibonding interaction between the carbon and the oxygen. This corresponds to the CO 2 pi level, which is unoccuppied in the isolated CO molecule. The back donation is relatively weak, as the carbon and oxygen atoms each have less than 6% of the charge in the e orbital. Note should be taken of the other two valence levels of CO: the e level at -2.16 rydbergs corresponds to the CO 1 pi, and the a_1 level at -2.53 rydbergs (not shown in Fig. 4.3) corresponds to the CO 4 sigma. Both of these orbitals are non-bonding with respect to the rhodium.

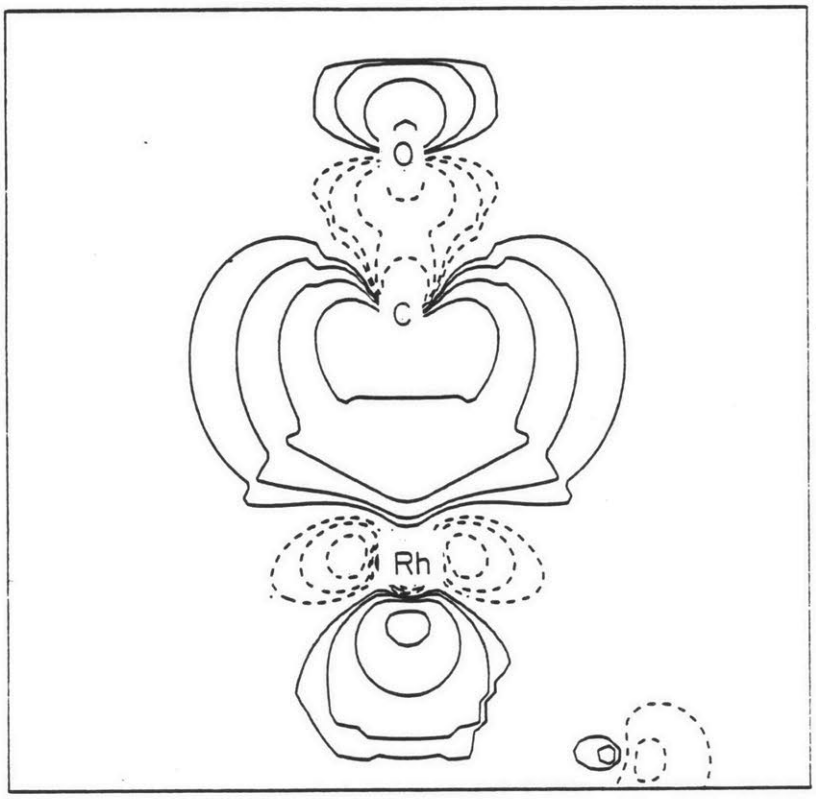

Fig. 4.7. A wavefunction plot of the 8a1 orbital of the $CO/RhAlO_6$ cluster, found using the standard SCF-Xα-SW method.

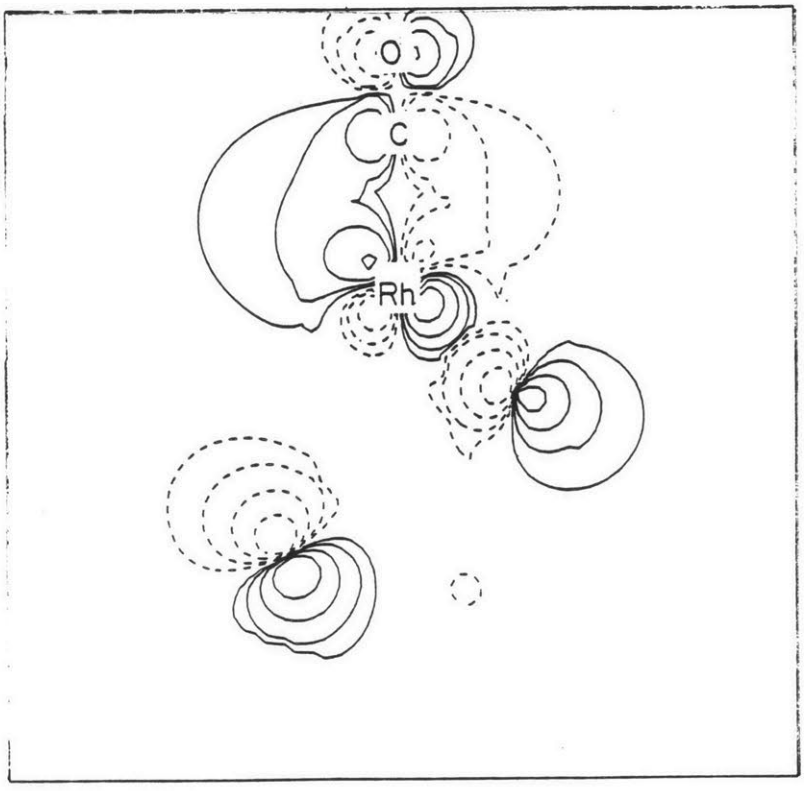

Fig. 4.8. A wavefunction plot of the 12e orbital of the $CO/RhAlO_6$ cluster, calculated using the standard SCF-Xα-SW method. This plot shows the "back-donation" of charge from the rhodium to the CO pi antibonding orbital.

Partitioned Calculation of $CO/RhAlO_6$

A cluster composed of a molecule chemisorbed on a surface presents a particularly appropriate application of the partitioning techniques described in Chapters 1 and 2. Such clusters are often characterized by a large outer sphere and by a great deal of "empty" interatomic space. The volume averaging of charge and potential over such a large interatomic region may lead to significant inaccuracies; these effects can be reduced by the inclusion of partitioning spheres. In addition, placing the surface sub-cluster and the adsorbed molecule in separate partitioning spheres appeals to physical intuition. The surface and adsorbate are chemically quite distinct; it is expected that the interactions within each sub-cluster will dominate those between the sub-clusters.

A schematic diagram of the partitioning spheres used in the $CO/RhAlO_6$ cluster is shown in Fig. 4.9. Note that the geometry of the cluster allowed tangent partitioning spheres to be used. Without the partitioning spheres, the volume of the interatomic region is 1523 cubic bohrs; the interatomic volume inside the two partitioning spheres is 814 cubic bohrs. Thus, the use of the partitioning spheres decreases what might be called the "effective" interatomic volume by nearly 50%.

The electron energy levels of the partitioned calculation are shown in Fig. 4.10, along with the standard SCF-Xα-SW results for the identical cluster. The partitioned calculation used the same Watson and inner Watson sphere as that used in the standard SCF-Xα-SW case. It can be seen that the primary result of using the partitioning

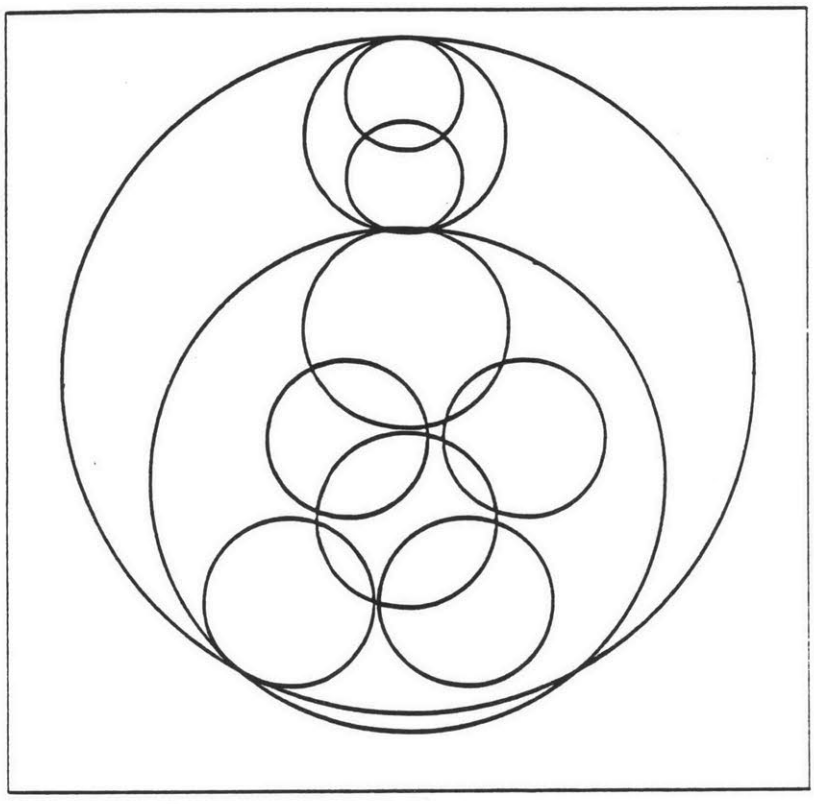

Fig. 4.9. Schematic drawing of the partitioning spheres used for the $CO/RhAlO_6$ cluster.

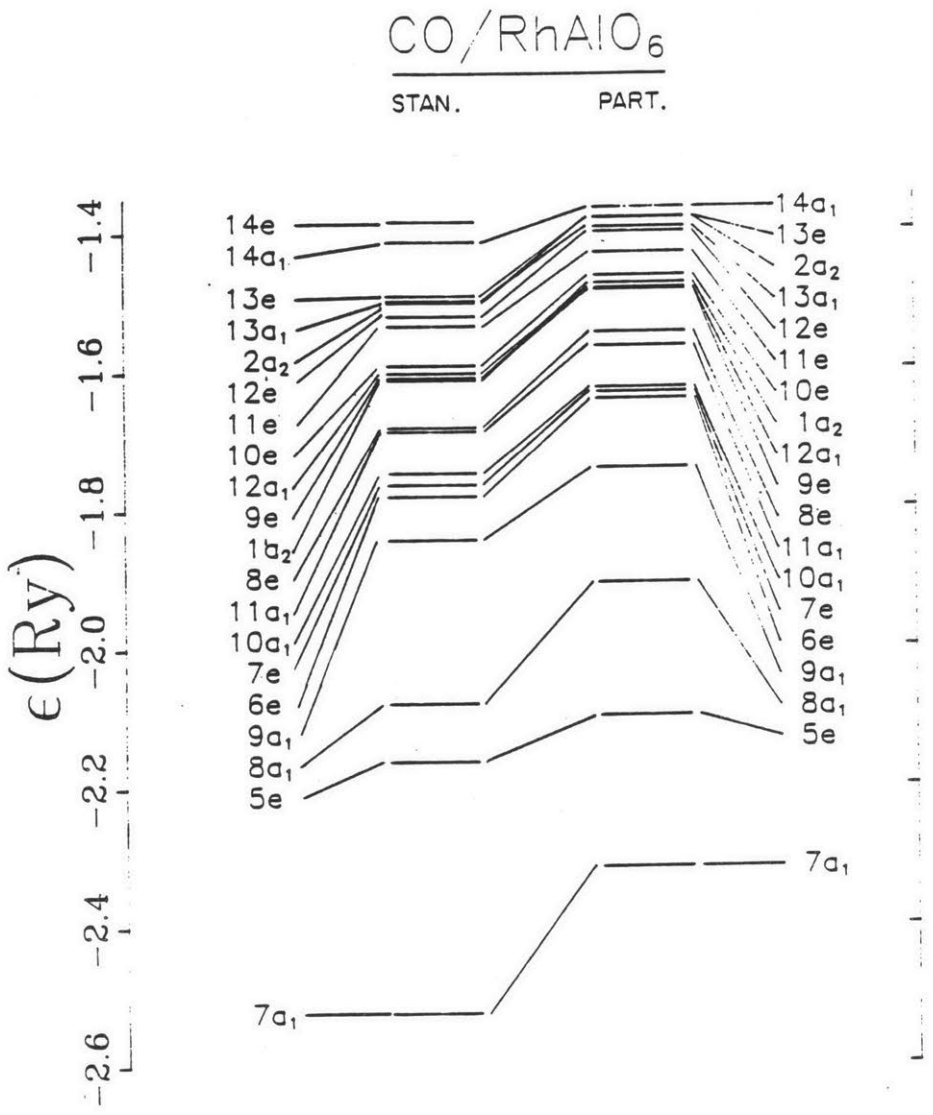

Fig. 4.10. Comparison of the energy level diagrams of the CO/RhAlO$_6$ cluster using the standard SCF-Xα-SW method (left) and the partitioning method (right). Note the differences in the three primary CO orbitals (7a1, 8e, and 8a1). The energy scales are the same for both calculations.

spheres is to shift the energy levels to higher energy. This shift is the expected result of containing more of the electronic charge closer to the atomic nuclei (see the discussion in Chapter 2). The constant potentials in the three different interatomic regions are markedly different from the value of -1.738 rydbergs found in the standard SCF-Xα-SW case. For the partitioned case, the constant potential of the CO sub-cluster was -2.300 rydbergs, that of the $RhAlO_6$ sub-cluster was -1.505 rydbergs, and that of Region II (i.e., outside the two partitioning spheres) was -1.728 rydbergs. Note that the overall shift in the energy levels was roughly about 25% less than the shift in the constant potential of the $RhAlO_6$ sub-cluster. This agrees with previous observations that the one electron energy levels tend to track the value of the intersphere potential [11].

A distinct, and possibly significant, difference between the partitioned results and the standard SCF-Xα-SW results is found in the relative splitting of the CO levels. In the standard SCF-Xα-SW case, the energies corresponding to the CO 4 sigma, 1 pi, and 5 sigma levels are -2.53, -2.16, and -2.08 rydbergs respectively. The corresponding energies for the partitioned case are -2.31, -2.10, and -1.90 rydbergs. For the partitioned case, the sigma levels are shifted upwards by about 0.2 rydbergs, while the pi level is shifted by only 0.06 rydbergs. In the methanol studies of Chapter Two, it was found that a partitioning sphere placed around a CO fragment improved the ordering of and splitting between pi and sigma levels. Thus, it can be expected that the partitioned calculation for the $CO/RhAlO_6$ cluster gives a more accurate picture of the splitting between these three CO levels.

Although there are no photoemission data on CO chemisorbed on supported rhodium, R.J. Baird and co-workers [12] have performed UPS experiments with CO chemisorbed on Rh(110). They observed two prominent CO derived lines at 7.6 eV and 10.6 eV below the Fermi level. Baird identifies these lines with the CO 4 sigma (more tightly bound) and the combined 5 sigma, 1 pi levels (less tightly bound line). Earlier studies of CO chemisorbed on Ni and Pd have made the same identification of similar features [5]. These earlier identifications were in good agreement with standard SCF-Xα-SW calculations.

Rigorously speaking, a direct comparison cannot be made between photoemission data and Xα one electron eigenvalues. Transition state energies are the relevant quantities for comparison. Nevertheless, in practice the Xα eigenvalues have often proved to be a useful guide. With this caveat, it seems that neither the standard SCF-Xα-SW or partitioned calculations presented here can be reconciled with the assignments that Baird has made.An alternative assignment would identify the UPS line at 7.6 eV with the 1 pi level and place the 5 sigma level buried within the rhodium d levels. This assignment would agree with expectations that forward donation from CO to rhodium should be weaker (and back donation stronger) than for the case of nickel or palladium, which are to the right of rhodium in the periodic table. For nickel and palladium, the transition metal-CO interaction is strong enough to pull the 5 sigma level below the 1 pi level. In the case of rhodium, however, this interaction is relatively weak, and the orbitals retain the ordering of the isolated CO molecule. Additional support for this assignment lies in the lack of any

observable structure in the 7.6 eV line. Because Baird and co-workers claim an instrumental resolution of 0.4 eV, identifying both the 5 sigma and the 1 pi levels with the 7.6 eV line implies that they are almost exactly degenerate. Such a degeneracy is not observed in either of the calculations presented here.

Another difference between the partitioned and standard SCF-Xα-SW calculations is the distribution of electronic charge. The charges on the individual atoms for the $RhAlO_6$ cluster are shown in Table 4.2. The absolute values of these charges are not accurate, because they depend strongly on the somewhat arbitrary values of the atomic sphere radii. However, some insight can be gained by examining the relative values among the various calculations, as they have all used the same atomic radii.

The oxidation state of isolated rhodium atoms on an alumina support has been discussed by several workers [8,13]. The consensus opinion is that species I rhodium (with two attached carbon molecules) should be in an oxidation state of +1. While the total charges of Table 4.2 do not show an oxidation state of +1, it is interesting to note that when the CO is attached, the charge on the rhodium atom decreases by 0.28 electrons for the standard SCF-Xα-SW case and by 0.58 electrons for the partitioned case. The difference between the two calculations is primarily acounted for by greater back donation to the CO molecule in the partitioned calculation. The back bonding e level is 6.4% C, 4.9% O for the standard SCF-Xα-SW case, and 9.6% C, 10.2% O for the partitioned case. Furthermore, an additional 0.1 electron is transferred to the aluminum atom in the partitioned case.

Assuming that the charge transfer to CO is the primary cause of

TABLE 4.2

Total Atomic Charges in $RhAlO_6$ and $CO/RhAlO_6$ Clusters

	$RhAlO_6$	$CO/RhAlO_6$	
Atom	(stan. Xα) [a]	(stan. Xα)	(part.) [b]
C	--	5.39	5.51
O3	--	8.65	8.88
Rh	46.12	45.84	45.54
Al	11.85	11.99	12.07
O1	9.30	9.28	9.25
O2	9.71	9.77	9.75

[a]. The intersphere and outer sphere charge was divided among the atoms in proportion to their valence charge.

[b]. The intersphere charge within each partitioning sphere was divided among the atoms of that sphere in proportion to their valence charges. The charge in the outer sphere region and in region II (outside the partitioning spheres) was divided among all of the atoms in proportion to their valence charges.

the decrease of rhodium charge in both cases, one can speculate that a cluster with two attached CO molecules (representing species I) would roughly double the decrease of charge on the rhodium atom. If the charge transfer to the aluminum were discounted, this would lead to Rh(+0.28) for the standard SCF-Xα-SW calculation, and Rh(+0.92) for the partitioned case. Thus, the partitioned calculation tends to support the widely held belief that species I rhodium is in the +1 oxidation state, and adds the new information that the missing charge is transferred to the chemisorbed CO. However, these numbers must be considered speculative, as many important determinants of the charge state are not considered here. For example, the above estimate assumes that the rhodium in the $RhAlO_6$ cluster is close to being neutral; the calculations give us no reliable information on this point.

In summary, it can be seen that the inclusion of the partitioning spheres does lead to significant differences in electronic structure. The partitioned calculations for $CO/RhAlO_6$ lead to spectral assignments that differ from those of the experimental literature. However, additional research would be helpful to confirm these results. In particular, a molecular orbital study of CO chemisorbed on an unsupported rhodium surface would resolve the question of the effect of the metal-support interactions on the CO levels.

Approximate Coupling Treatment of $CO/RhAlO_6$

Approximate coupling calculations have been performed on the partitioned $CO/RhAlO_6$ cluster. Because this cluster is tractable with the fully coupled method, these calculations serve primarily as a test of the approximate coupling method. The results will not give new information on the $CO/RhAlO_6$ cluster, but they will give information on the range of the applicability of the approximate coupling technique. The $CO/RhAlO_6$ chemisorption problem provides a particularly good test case for the approximate coupling method described in Chapter Three. There are several reasons for this; first, the adsorbate-surface system is very easily divided into two sub-clusters, as discussed in the third section on the partitioned calculation. It is quite natural to think of the adsorbate molecule as the principal sub-cluster, with its properties being somewhat modified by the surface sub-cluster (i.e., the "environment"). Of course, it is also possible to treat the surface as the principal sub-cluster. In either case, most of the molecular field energy levels should be unaltered by interaction between the two sub-clusters. The only orbitals that should be noticeably affected are those for which the adsorbate-surface interaction has significant bonding or antibonding character.

Another reason for the use of the approximate coupling method is found in the way that chemisorption studies are often done. Typically one may be interested in trends that develop when a series of different types of molecules are chemisorbed on a single type of

surface (or vice versa: a single type of molecule on different surfaces). In principle, it is possible to converge a large surface cluster only once (using the standard SCF-Xα-SW method), and use the resulting potential as a starting point for a whole series of adsorbate-surface calculations using the approximate coupling method. Use of this procedure would save very substantial amounts of computer time, and make systematic chemisorption studies practical even with large surface clusters.

A third reason for the use of of the approximate coupling method in chemisorption problems is the potential ability to treat very large surface clusters. While standard SCF-Xα-SW techniques have been widely and successfully applied to surface problems, its use still encounters controversy from theorists schooled in band structure techniques. In particular, criticism is directed at the modelling of an infinite surface by a cluster consisting of a small number of atoms. Most standard SCF-Xα-SW calculations of transition metal surfaces are limited to a dozen or so atoms by practical and numerical considerations. To use the approximate coupling method for a molecule adsorbed on a very large surface cluster, the system would probably be divided differently. The principal sub-cluster would consist of the adsorbed molecule and a few atoms of the adjoining surface. The environment would consist of the more distant atoms of the surface cluster. Although this type of calculation has not yet been performed, it holds out the possibility of laying this controversy to rest.

The potentials for the $CO/RhAlO_6$ approximate coupling calculations were obtained from self-consistent, converged, fully coupled partitioned calculations described earlier in this chapter.

Two sets of approximate calculations were performed: one with the CO as the principal sub-cluster, and one with the $RhAlO_6$ as the principal sub-cluster. The molecular field calculations used the formalism of (3.6) in which scattering from the system outer sphere is included. The iteration procedure used a slightly different weighting scheme for finding the new trial environment energies, in which the old energy was multiplied by 0.75 and the eigenvalue by 0.25; the next trial environment energy was obtained from their sum. The procedure used for the methanlo molecule in Chapter Three simply used the mean of the two energies for the next trial energy.

The resulting energy levels are shown in Fig. 4.11. Because the orbitals localized on the $RhAlO_6$ cluster are virtually unchanged from their molecular field values, they are not explicitly given; only those orbitals with substantial CO character are shown in Fig. 4.11. It is interesting to note that even those orbitals with substantial CO-Rh interaction are shifted only slightly from their molecular field levels. The Rh-CO sigma bonding orbital (the a1 level at E=-1.90) is shifted by less than 0.02 rydbergs, even though the charge distributions for this level are 16% O, 64% C, and 17% Rh, indicating substantial Rh-C bonding. The back-bonding orbital (the e level at E=-1.43 rydbergs) is shifted by less than 0.04 rydbergs; its charge distributions are 10% O, 10% C, and 15% Rh. This is the only occupied orbital with substantial CO character that cannot be derived from the CO sub-cluster (i.e., with CO as the principal sub-cluster). The molecular field CO e level at E=-1.36 (corresponding to a CO 2 pi antibonding level) which might lead to the back-bonding level instead develops

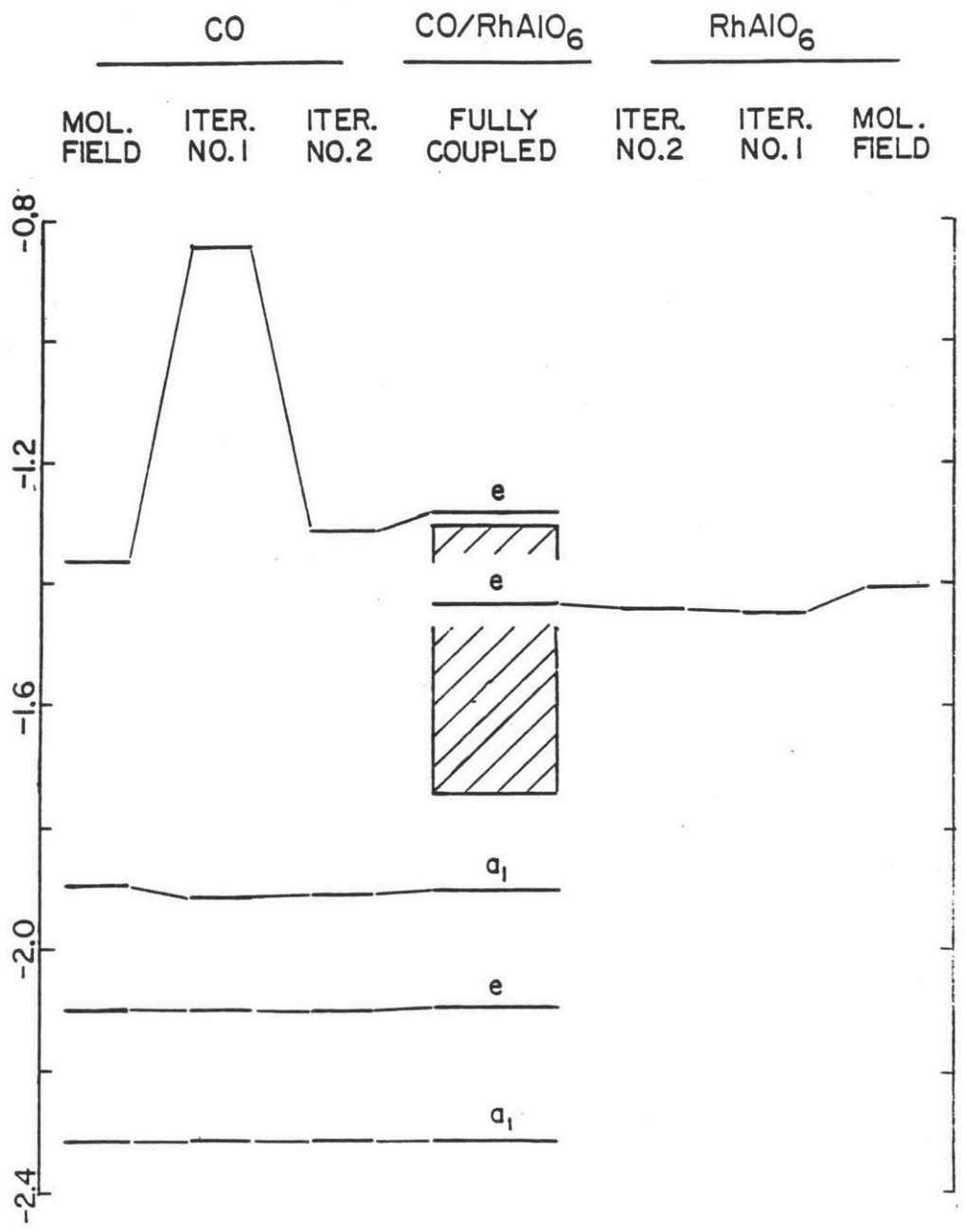

Fig. 4.11. Energy level diagram for the approximate coupling calculations for $CO/RhAlO_6$. Only the levels with substantial CO character are shown; the other orbitals are represented by the shaded box. The calculations using the CO as the principal sub-cluster are on the left, while those using the $RhAlO_6$ as the principal sub-cluster are on the right. In the center are the "exact" energy levels from the partitioned calculations.

into an unoccupied state which is antibonding with respect to the C-Rh interaction. The absence of the back-bonding orbital from the CO sub-cluster can be explained, perhaps, by the relative weakness of the back-donation.

In discussing the interaction of the CO molecule with the $RhAlO_6$ cluster, this method allows distinctions to be made between "electrostatic" interactions and "electronic coupling" interactions. The molecular field calculations can be said to include electrostatic effects, because the potentials reflect the presence of the nuclei and electronic charge of the atoms in the environment. The difference between the molecular field levels and the fully coupled levels reflect the degree of electronic coupling between the two sub-clusters. Using this differentiation, it can be said that the electrostatic interaction between CO and $RhAlO_6$ is strong, because the CO molecular field levels are quite different from those of an isolated CO molecule. On the other hand, it could be said that the electronic coupling is weak, because the CO levels (and the rhodium level involved in the back-bonding orbital) are shifted by a small amount.

The weak electronic coupling implies that the approximate coupling scheme is appropriate for this type of chemisorption problem. However, the fact that the electrostatic interactions are large raises the question of the importance of self-consistency. The results of this chapter have generally shown that charge transfer between the sub-clusters is important. If this were not a test calculation in which converged self-consistent potentials are available, a starting potential would be created by superimposing potentials (or charge

densities) of converged sub-clusters. Would such a starting potential include enough of the electrostatic effects? The answer isn't known because such potentials have not yet been created. If it were not adequate, some facility for self-consistent calculation of potentials must be added to the approximate coupling procedure to allow for charge re-arrangement both between and within the sub-clusters. As mentioned in Chapter Three, there is, in principle, no obstacle to self-consistent calculations within the approximate coupling scheme.

In summary, it has been shown that the approximate coupling method successfully reproduces the eigenvalues found in fully coupled calculations, both in the test case of methanol and in the more demanding (and realistic) application to chemisorption. Thus, this method has the potential of opening up new areas of application of the $X\alpha$-SW method, applications which are otherwise impractical or impossible due to large cluster size. This potential can be confirmed only by further investigation.

REFERENCES

1. N.D. Spencer and G.A. Somorjai, Reports on Progress in Physics 46, 1 (1983).

2. K.H. Johnson in The New World of Quantum Chemistry, edited by B. Pullman and R. Parr (D. Reidel) Publishing Co., Boston 1976).

3. A.C. Balazs, K.H.Johnson, and G.M. Whitesides, Inorganic Chemistry 21, 2162 (1982).

4. K.H. Johnson, A.C. Balazs, and H.J. Kolari, Surface Science 72, 733 (1978).

5. B. CHen, D.C. foyt, and J.M. White, Surface Science 67, 218 (1977).

6. T.M. Duncan, J.T. Yates, and R.W. Vaughn, J. Chem. Phys. 73, 975 (1980).

7. A. Theolier, A.K. Smith, M. Leconte, J.M. Basset, G.M. Zanderighi, R. Psaro, and R. Ugo, J. of Organometallic Chemistry 191, 415 (1980).

8. C.A. Rice, S.D. Worley, C.W. Curtis, J.A. Guin, and A.R. Tarrer, J. Chem. Phys. 74, 6487 (1981).

9. D.J. Yates, L.L. Murrell, and E.B. Prestridge, J. Catal. 57, 41 (1979).

10. G.V. Samsonov, The Oxide Handbook (Plenum, New York, 1973).

11. D.A. Case, M. Cook, and M. Karplus, J. of Chem. Phys. 73, 3294 (1980).

12. R.J. Baird, R.C. Ku, and P. Wynblatt, Surface Science 97, 346 (1980).

13. K.L. Watters, R.F. Howe, T.P. Chojnacki, C. Fu, R.L. Schneider, and N. Wong, J. of Catal. 66, 424 (1980).

14. J.A. Appelbaum and D.R. Hamann, Rev. Mod. Phys. 48, 479 (1976).

CHAPTER 5 - MOLECULAR ORBITAL MODELS OF METALLIC GLASSES

Since Duwez and co-workers first demonstrated that the alloy Au-Si could be solidified in the amorphous state using rapid solidification techniques, countless other metallic glasses have been prepared and their properties studied [1]. The motivation for these investigations has been more than pure scientific curiousity in a novel state of matter; it has included the numerous practical applications that some of these materials may possess. Metallic glasses have exhibited unique magnetic, chemical, structural, and electronic properties. In some cases, metallic glasses have properties which cannot be obtained with crystalline alloys; in other cases, they can substitute for crystalline alloys that are prohibitively expensive. The wide range of compostitions from which metallic glasses can be formed allows their properties to be "fine-tuned", while also providing new materials or the study of the physics of alloys.

Fundamental to the understanding of the properties of a material is an understanding of its electronic structure. Electronic structure calculations of crystalline substitutional alloys have long been a thorny problem in solid state physics [2]. The band structure techniques which have been very effective in elemental and compound solids cannot be applied to alloys in which the translational symmetry

is broken. Electronic structure calculations of metallic glasses present even greater difficulties than crystalline substitutional alloys. In addition to the compositional disorder characteristic of a substitutional alloy, metallic glasses have topological disorder as well. In fact , the definition of a metallic glass is generally taken to be a material with no evidence of microstructure in x-ray diffraction experiments. Thus, methods used for substitutional alloys which rely on the existence of a crystal lattice are not necessarily applicable to glasses.

There have been a variety of techniques used by other workers to calculate the electronic structure of amorphous materials. The Bethe lattice technique has been applied to a wide variety of semiconductor problems, but its reliance on tight-binding formalism makes it inappropriate for use with transition metals [3]. A number of studies have been done in which the geometric structure of a large disordered cluster has been determined by dense-random-packing-of-hard-spheres (DRPHS) or similar techniques [4]; this cluster can then be used as a starting point for an electronic structure calculation, either as an isolated cluster using tight-binding techniques or as a large unit cell in a band structure calculation. Yet another method has been to postulate a hypothetical crystal structure for an alloy having roughly the same composition as the metallic glass under consideration [5]. Band structure calculations performed on such hypothetical crystal structures yield densities of states which are generally consistent with spectroscopic data obtained from the corresponding metallic glass.

This study uses small clusters of atoms as a model for the

metallic glass. The clusters are constructed to incorporate what is known lf the glass's local chemical environment. Unlike the cluster studies described above, no attempt is made to include the effects of disorder: the proposed clusters consist of four to nineteen atoms in relatively symmetrical configurations. These "ordered" clusters cannot model the effects caused by long range disorder, and this failure is unfortunate; undoubtedly there is interesting physics caused specifically by the randomness of the material. However, the lack of convincing structural information on the nature of the disordered state makes it difficult to include the effects of disorder. The disordered clusters referred to previously consist of 100-1000 atoms arranged according to various structural theories of the metallic glass, typically being a modified version of the DRPHS model. While DRPHS does provide a plausible simulation of the disordered state, many other proposed structures of the glass can also reproduce the experimentally obtained pair distribution functions. Thus, the relationship of DRPHS or any model to the structure of the actual metallic glass is speculative at this time.

A justification for omitting consideration of the disorder is found in the observation that photoemission studies comparing metallic glasses and their crystalline counterparts reveal many similarities in the electronic densities of states. This suggests that many essential features of the electronic structure are determined by the local chemical environment, certain aspects of which remain unchanged when the material goes from an ordered to an amorphous state. Electronic structure calculations of amorphous semiconductors have relied on similar assumptions; for example, amorphous Si is commonly modelled as

a network of tetrahedral bonds to insure that the Si atom has the same coordination number as the atoms of crystalline Si.

In spite of the similarities of the spectra of metallic glasses and their crystalline counterparts, the use of small clusters has clear advantages over band structure calculations. First, many metallic glasses have no crystalline analogue. To perform a band structure calculation on these glasses, one must assume a hypothetical crystal structure. A cluster allows much more flexibility in coordination number and interatomic distance because there are no constraints imposed by the periodicity of a lattice. In addition, alloys with three or more types of atoms can be easily modelled with clusters, while corresponding crystal structures would become quite complex. Finally, while disorder is not explicitly included in the small cluster model, neither is long range order; in this respect, the cluster calculations are more realistic than band structure calculations. The periodicity which must be assumed for band structure calculations may introduce artifacts in the resultant densities of states.

How should the structure of the small clusters be chosen? Because the precise structure of the glass is unknown, plausible guesses must be made of an appropriate structure for the cluster. However, these guesses are informed by two important sources of information. First, knowledge of the behavior of similar alloys in the crystalline state may qualitative information on the nature of the bonding of the constituent atoms, as well as more quantitative information on coordination numbers and interatomic distances. Second, many metallic glasses have been experimentally studied with

EXAFS, x-ray scattering, neutron scattering scattering, and other structural probes. Experimentally obtained pair distribution functions can sometimes provide important constraints on interatomic distances and coordination numbers. Nevertheless, the relationship of the clusters to the structure of the actual metallic glass must be regarded as tentative and speculative. The results of calculations using these clusters should not be regarded as rigorous, but rather as a guide to the interpretation of experimental data.

Once a given cluster is specified, its electronic structure is computed, from first principles, by the self-consistent-field $X\alpha$ scattered-wave (SCF-$X\alpha$-SW) molecular orbital method. This method has been used in the past to show that cluster molecular orbitals can provide a good description of many features of the electronic structure of bulk materials, including elemental metals, alloys, and amorphous semiconductors [6-10]. In this chapter, the results of such calculations are reported for amorphous Pd-Si and Zr-Cu, two alloys which are representative of the transition metal-metalloid (TM-M) and transition metal-transition metal (TM-TM) types of glasses, respectively.

Zr-Cu Metallic Glasses

To model the TM-TM alloy Zr-Cu, a series of clusters have been studied which have the symmetry and structure of the close packed lattices FCC and HCP. Close packed structures are appropriate for Zr-Cu because the bonding of Zr and Cu is considered to be relatively non-directional. Furthermore, these crystal structures correspond to those of the pure metals Cu (FCC) and Zr (HCP). It might be noted

that the use of clusters which are close packed is in the spirit of the DRPHS model of the metallic glass, which can be considered as a type of disordered close packing.

The FCC cluster is shown schematically in Figure 5.1. It is a nineteen atom cluster having Td symmetry; this type of cluster has been widely used in studies of crystalline metals and alloys [6,13]. The interatomic distance, 5.48 (au), was obtained from the interatomic distance between Cu and Zr in crystalline Zr_2Cu. The cluster's central atom and the six outer atoms are Zr; the twelve first nearest neighbors of the central Zr are Cu atoms. This cluster can be considered to represent a Cu rich Zr-Cu alloy, with composition of roughly Zr_{37}-Cu_{63}.

Figure 5.2 shows a schematic representation of a 13 atom HCP cluster having D3h symmetry. The central plane consists of seven Cu atoms, while the upper and lower planes consist of three Zr atoms each. The lower symmetry of this cluster allows more flexibility of interatomic distances in comparison to the FCC cluster. In particular, distances between like and unlike atom pairs can differ. Results from EXAFS studies have been used to assign a length of 2.67 Å to the Zr-Cu bond, and a length of 3.10 Å to the Zr-Zr bond [11]. The Cu-Cu bond length in this cluster is also 3.10 Å, although this length was not determined in the EXAFS study. This cluster corresponds to an alloy with composition of roughly $Zr_{46}Cu_{54}$.

Figure 5.3 shows a diagram of the molecular orbital energy levels of the HCP cluster, labelled according to the irreducible representations of the D3h point group. The highest occupied orbital, the 9e', has a population of 2 electrons. Figure 5.4 is a plot of the

density of states of this cluster, obtained by Gaussian broadening of

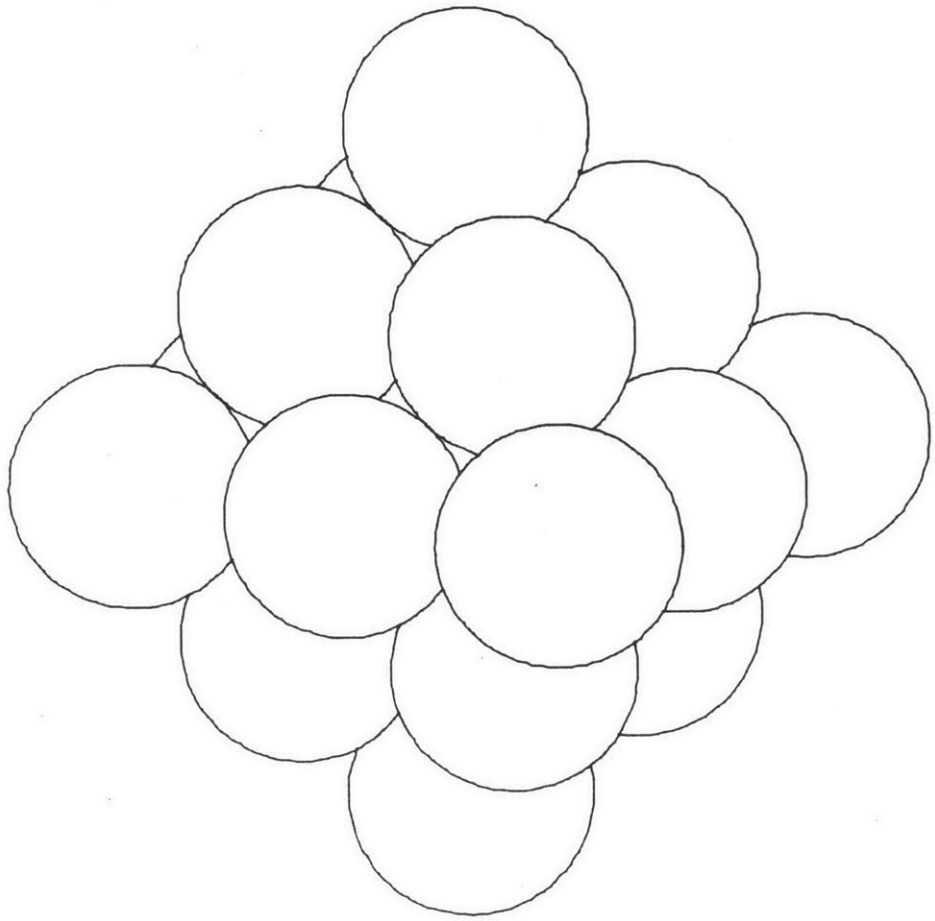

Fig. 5.1. Schematic drawing of the nineteen atom cluster modelling tne local structure of the Zr-Cu metallic glass. This cluster has the geometric arrangement of an FCC lattice.

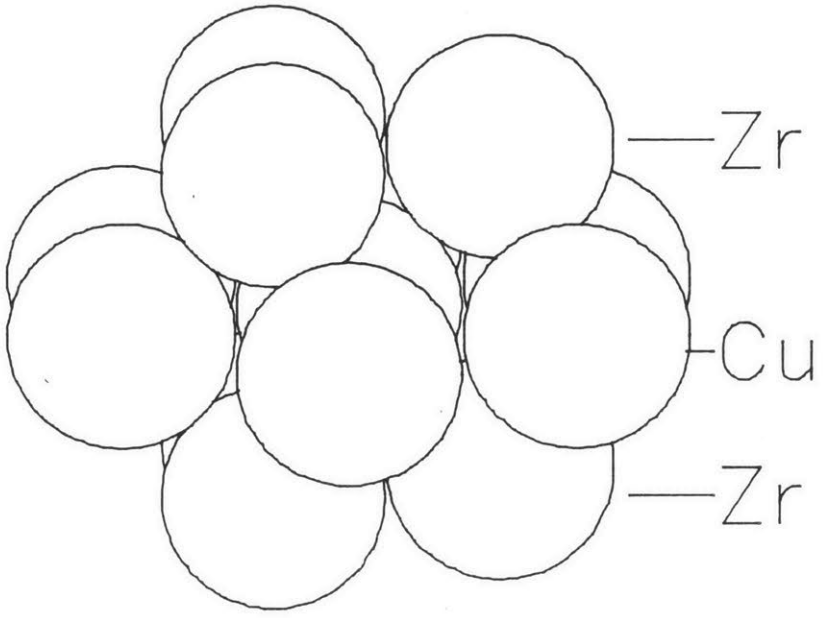

Fig. 5.2. Schematic drawing of the thirteen atom cluster modelling the local structure of the Zr-Cu metallic glass. This cluster has the geometric arrangement of an HCP lattice.

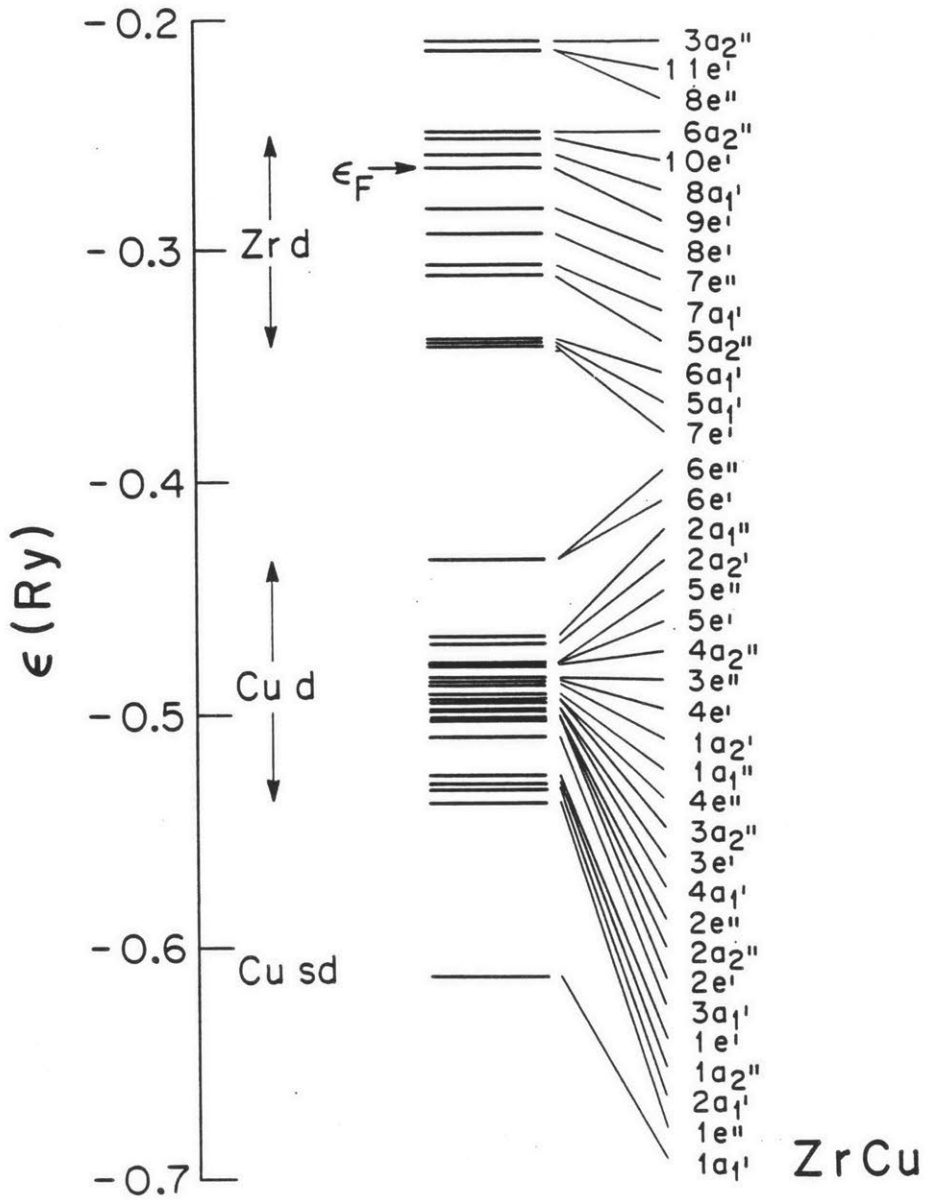

Fig. 5.3. The SCF-Xα-SW energy eigenvalues of the thirteen atom HCP cluster representing the Zr-Cu metallic glass.

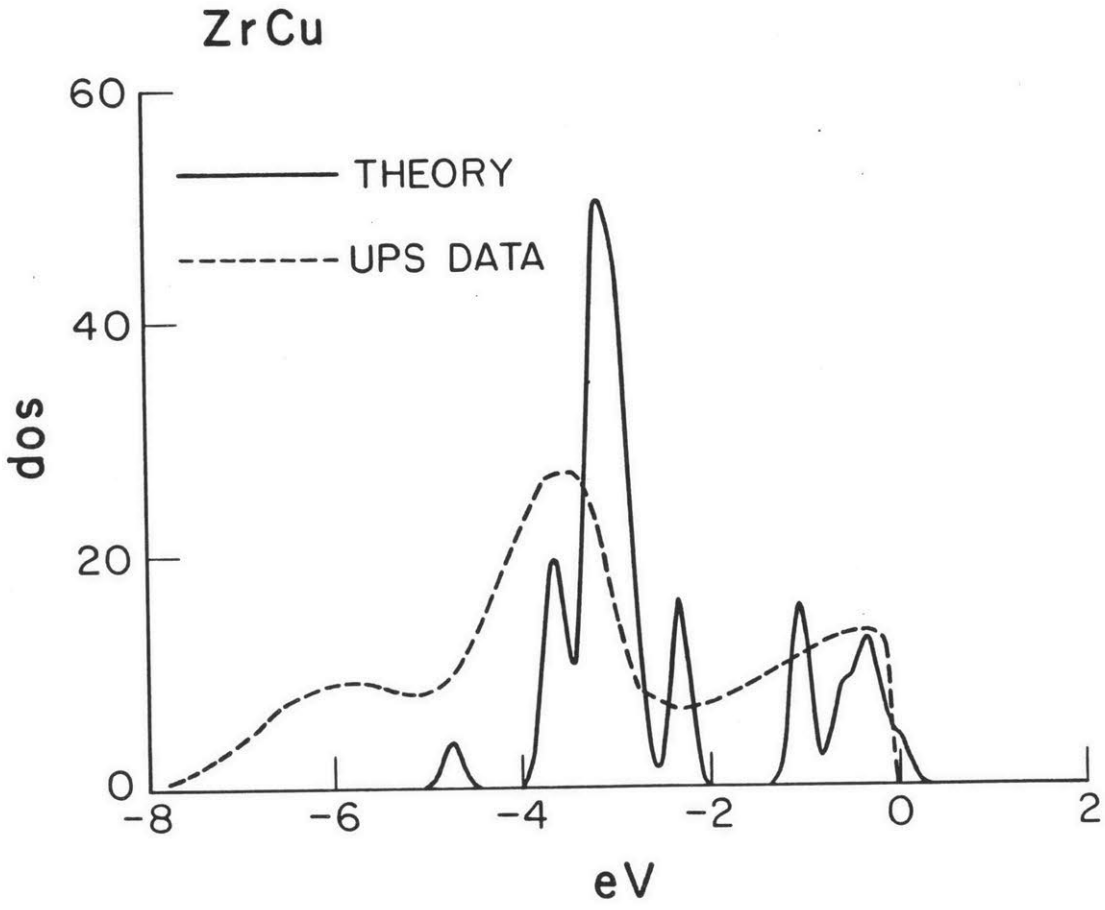

Fig. 5.4. Comparison of the Gaussian-broadened density of states from the thirteen atom HCP cluster with data from photoemission experiments (see Ref. [12]). Density of states units are arbitrary.

the discrete levels according to the relationship

$$N(E) = \sum_i \frac{n_i}{(2\pi\sigma)^{\frac{1}{2}}} \, EXP\left(-\frac{(E-E_i)^2}{2\sigma^2}\right) \qquad (5.1)$$

In this expression, E_i is the $X\alpha$ orbital eigenvalue, n_i is the orbital occupation number, and σ is the width of the broadening, chosen in this case to be 0.25 eV. Figure 5.4 also shows the results of a published photoemission study of the metallic glass $Zr_{60}Cu_{40}$ (hv= 21.2 eV) [12]. For purposes of comparison, the Fermi level of the calculated density of states has been aligned with the zero of energy. Plotted in Figure 5.5 is the decomposition of the total density of states into partial Cu and Zr densities of states. These were obtained by weighting the occupation number in (5.1) by the fraction of the charge density of the given molecular orbital on the given atomic species. The energy level diagram of the FCC cluster is shown in Figure 5.6. The highest occupied orbital of the FCC cluster is the $4t_{1g}$, with a population of 2 electrons.

The calculated results for these two systems are qualitatively quite similar. In the energy level diagrams and in the densities of states the division of the spectrum into two distinct bands is evident. While the lower consists primarily of Cu d levels, it has a significant amount of Zr-Cu bonding character. Similarly, the upper band is mainly composed of Zr d levels, but it has a significant amount of Zr-Cu antibonding character. In both of these clusters, there is characteristic similarity in the nature of the highest or nearly highest occupied molecular orbitals; they exhibit a delocalized

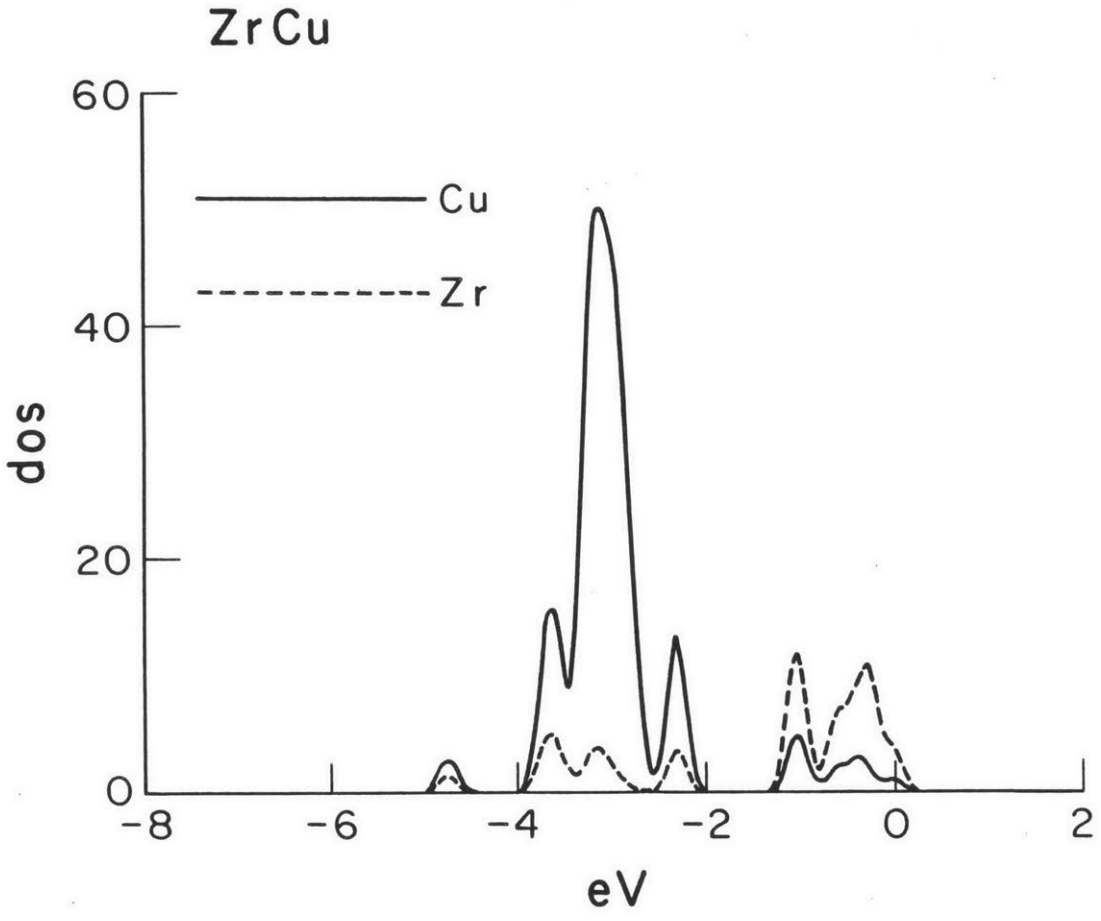

Fig. 5.5. Decomposition of the density of states of the thirteen atom HCP cluster into partial Cu and Zr character.

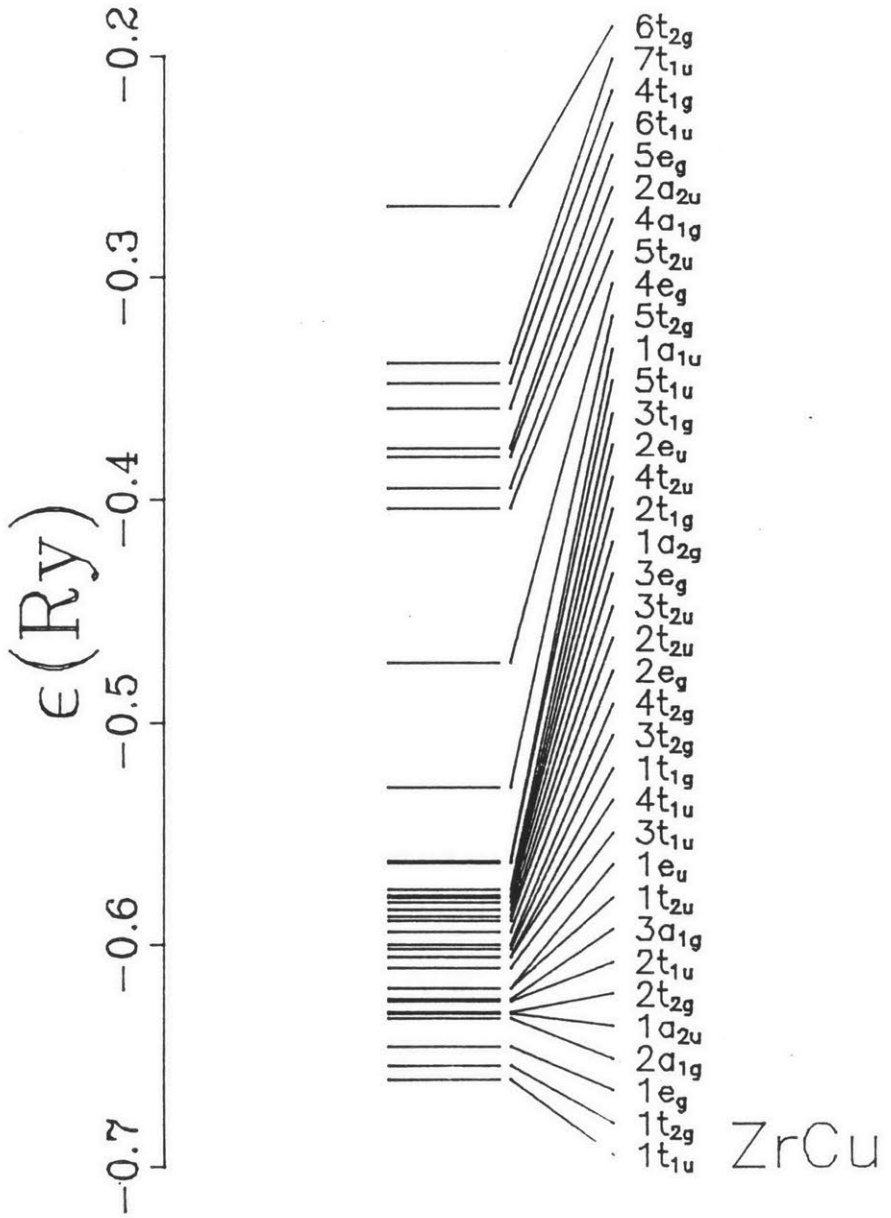

Fig. 5.6. Energy eigenvalues of the nineteen atom FCC cluster representing the Zr-Cu metallic glass.

Zr-Zr bonding structure, promoted in part by Zr-Cu antibonding. A plot of a wavefunction of one of these orbitals is given in Figure 5.7. It is possible that such networks of Zr-Zr bonds may play a role in the stabilization of the glass.

By examining Figure 5.4, it can be seen that the calculated densities of states are in good quantitative agreement with the photoelectron spectra. In particular, a noteworthy feature of the photoemission data is the downward shift of about 1 eV observed in the Cu d band in comparison to elemental Cu. If the position with respect to the Fermi level of the Cu d bands in these alloy cluster calculations are compared to the position of the d band in a pure Cu cluster [13], shifts of 1.5 eV and 1.0 eV are seen for the FCC and HCP clusters respectively.

Pd-Si Metallic Glasses

In this section, studies of Pd-Si, a representative of the TM-M type of metallic glass, are presented. Recent experimental work has revealed a distinction between the local environments of the TM-M and the TM-TM glasses [14,15]. In the TM-TM alloys, the nearest neighbor of a given constituent may be a like or unlike atom. While there may be a slight statistical preference for like or unlike pairs, x-ray diffraction studies have shown that the constituents can best be considered as randomly distributed. In contrast, the metalloid atoms in TM-M systems exhibit strong interactions with the transition metal atoms. Experimental evidence seems to support the widely held belief that there are no metalloid-metalloid nearest neighbor pairs in TM-M

$5e_g$

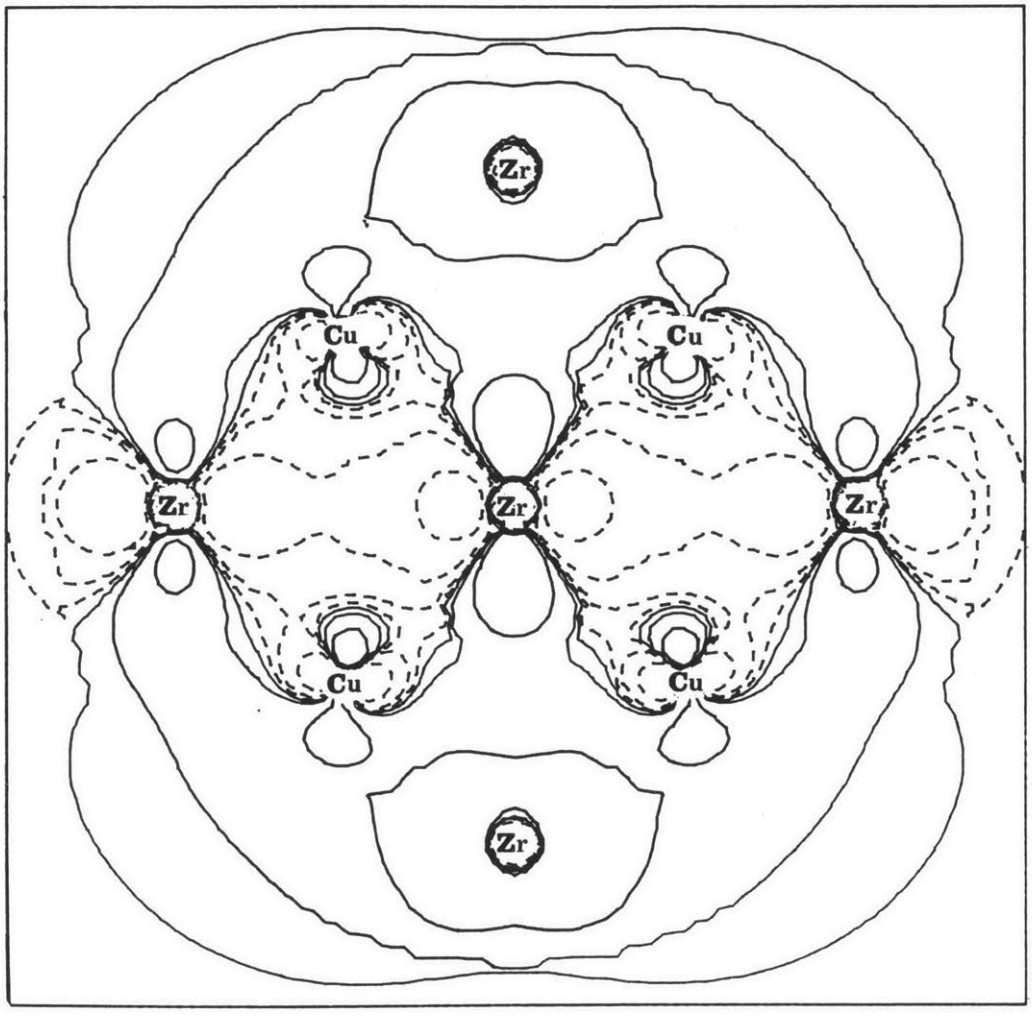

Fig. 5.7. Plot of the wavefunction of the 5eg orbital from the nineteen atom FCC cluster, showing second nearest neighbor Zr-Zr bonds.

metallic glasses.

Further insight into the nature of the local chemical environment can be obtained by considering the nature of the bonding in crystalline alloys, such as Pd_3Si. The range over which Pd-Si forms a glass (14 to 22 %Si) is reasonably close to the concentration of Si in crystalline Pd Si. The coordination of Si in Pd Si can be described as six Pd atoms forming a trigonal prism about the central Si, with three additional Pd atoms capping the square faces at a larger Pd-Si distance. This general type of coordination is also seen in crystalline alloys of Si, B, P, or C with many other transition metals [16].

It is interesting to note that x-ray and neutron diffraction experiments [17] on glassy Pd-Si give the number of nearest neighbors of Si as six at the highest Si concentration (22%); for low SI concentrations, the number is seven, which extrapolates to nine at 0% Si. Clearly, these numbers are consistent with trigonal prismatic coordination of the Si in the Pd-Si glass. It is tempting to speculate that the glass is formed from non-periodic arrangements of these trigonal prismatic units, and that the strength of the bonding and relative stability of these units may play an important role in the stability of the glass. It is, in general, more difficult to form a periodic structure from large assymetrical structural units than from spherically symmetrical atoms.

Three clusters representing Pd-Si alloys are depicted in Figures 5.8, 5.9, and 5.10. The Pd_3Si cluster in Figure 5.8 is tetrahedral, representing half of a trigonal prism, while the Pd_6Si cluster of Figure 5.9 represents the full trigonal prism. These two clusters

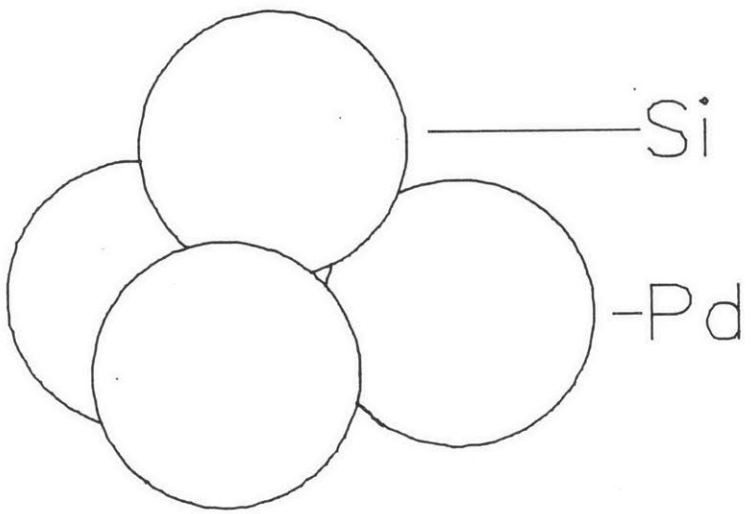

Fig. 5.8. Schematic drawing of the Pd_3Si cluster representing the Pd-Si metallic glass.

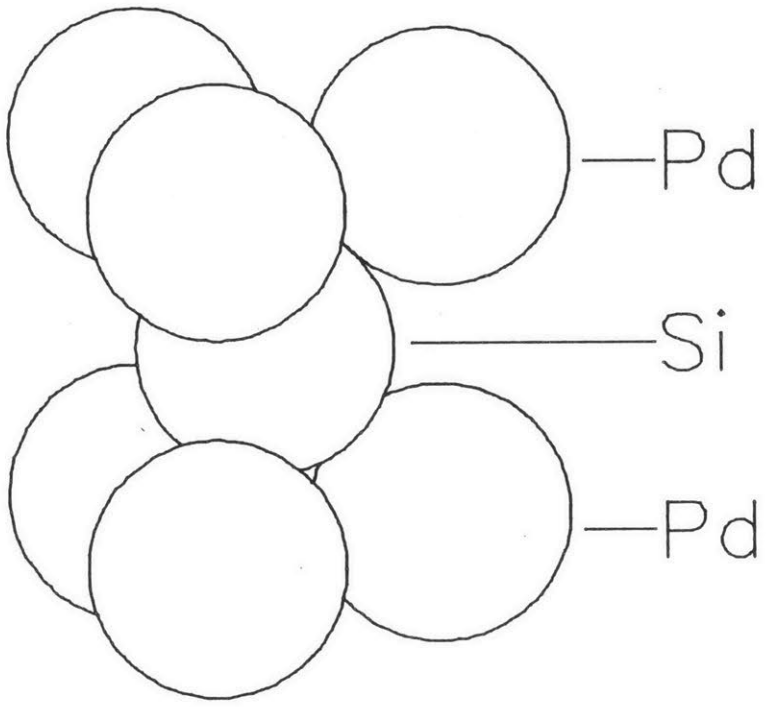

Fig. 5.9. Schematic drawing of the Pd_6Si cluster. The trigonal prism of Pd atoms surrounding the Si atom is similar to the coordination of Si in crystalline Pd_3Si.

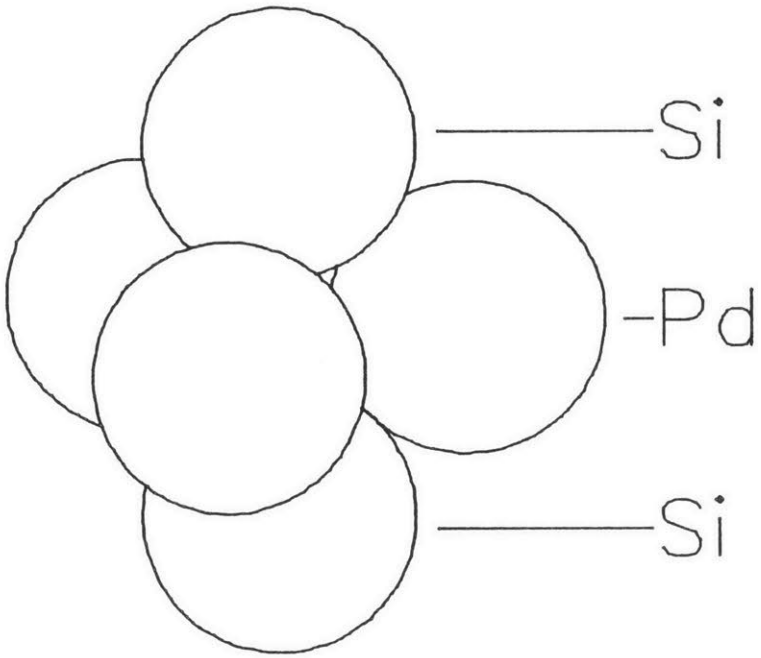

Fig. 5.10. Schematic drawing of the Pd_3Si_2 cluster. This cluster was studied to investigate the possibility of second nearest neighbor Si-Si bonds.

nearly span the range of concentrations for which Pd-Si can be formed into a glass . The Pd_3Si_2 cluster in Figure 5.10 has been investigated with the intention of studying the possibility of second nearest neighbor Si-Si interaction. The coordinates of all three clusters were chosen to be consistent with partial pair distribution functions obtained from published x-ray and neutron diffraction studies [15,18]. However, the Si-Si distance in the third cluster is simply a guess based on observations suggesting that the Si-Si distance must be greater than that of a second nearest neighbor.

The basic nature of the interaction between Pd and Si can be seen in the electronic structure of the Pd_3Si cluster. As seen in the energy level diagram in Figure 5.11 and the plot of the component densities of states in Figure 5.12, there is a manifold of Pd d states centered at about -0.5 rydbergs. The Si p states interact with the Pd at the top and the bottom of this Pd d band. The $2a_1$ and 3e levels, at the bottom of the band, are bonding between Pd and Si. The plot of the wavefunction of the $2a_1$ level is shown in Figure 5.13. The $5a_1$ level, at the top of the Pd d band, consists of a Si p state which is antibonding with respect to Pd. A plot of the wavefunction of this level, showing its very diffuse character, is given in Figure 5.14. The Si s state at -0.91 rydbergs is completely detached from the Pd d and Si p valence states.

The Pd_6Si cluster differs from the Pd_3Si cluster in that the Si is now completely coordinated, i.e., it has six nearest neighbor Pd atoms, as it does in crystalline Pd Si. Examining the energy levels in Figure 5.15, the most dramatic differences from the Pd_3Si results are the Si-Pd bonding (1a2" and 1e') and antibonding (4a2" and 6e')

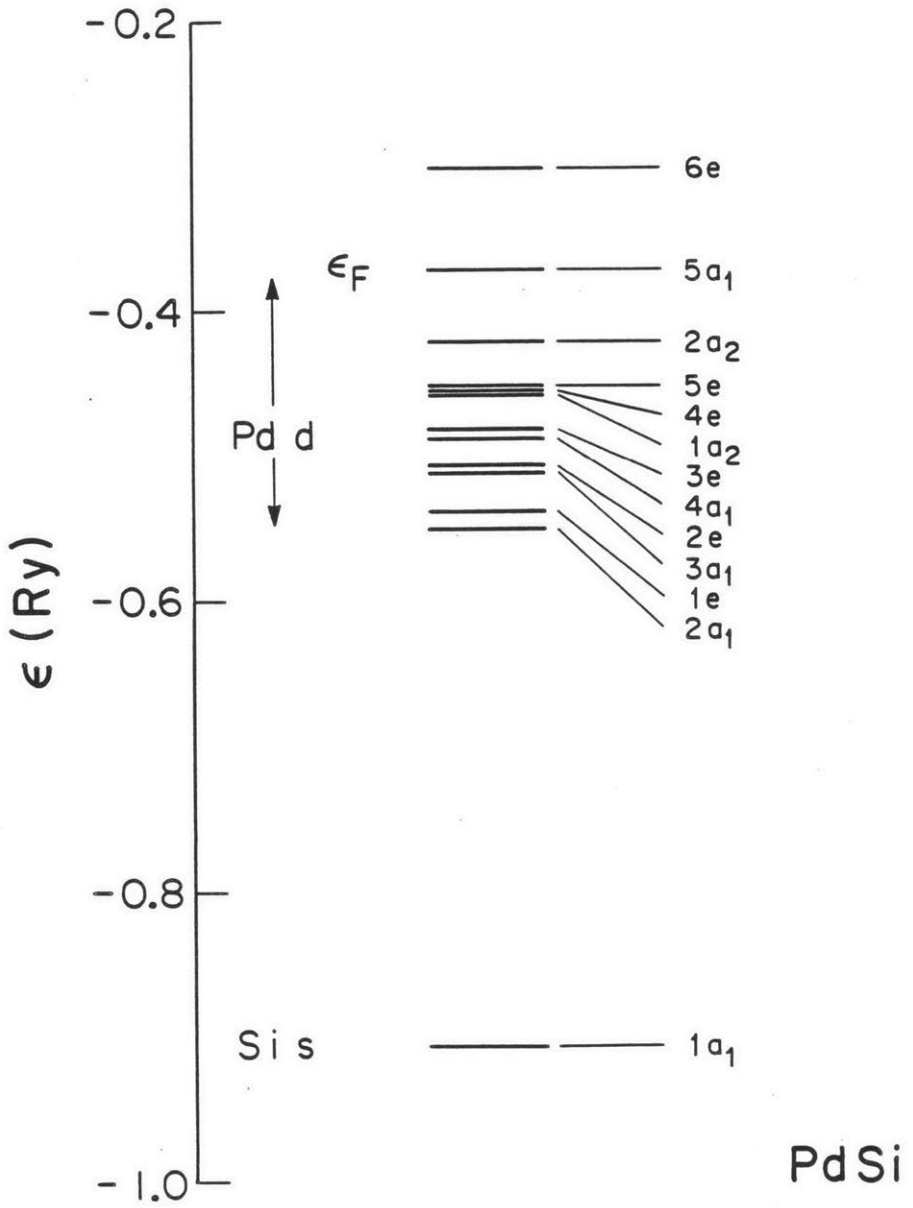

Fig. 5.11. Energy level diagram of the Pd_3Si cluster.

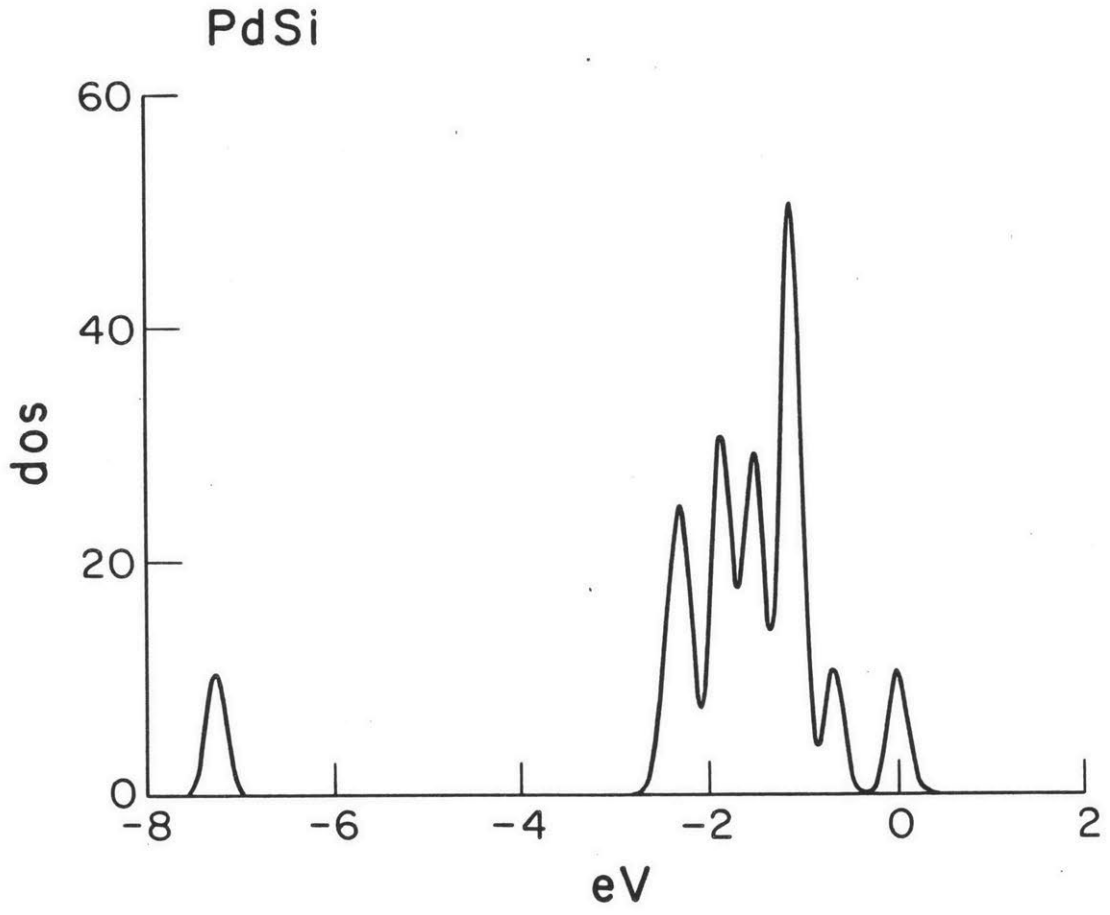

Fig. 5.12. Gaussian broadened density of states of the Pd_3Si cluster (arbitrary units).

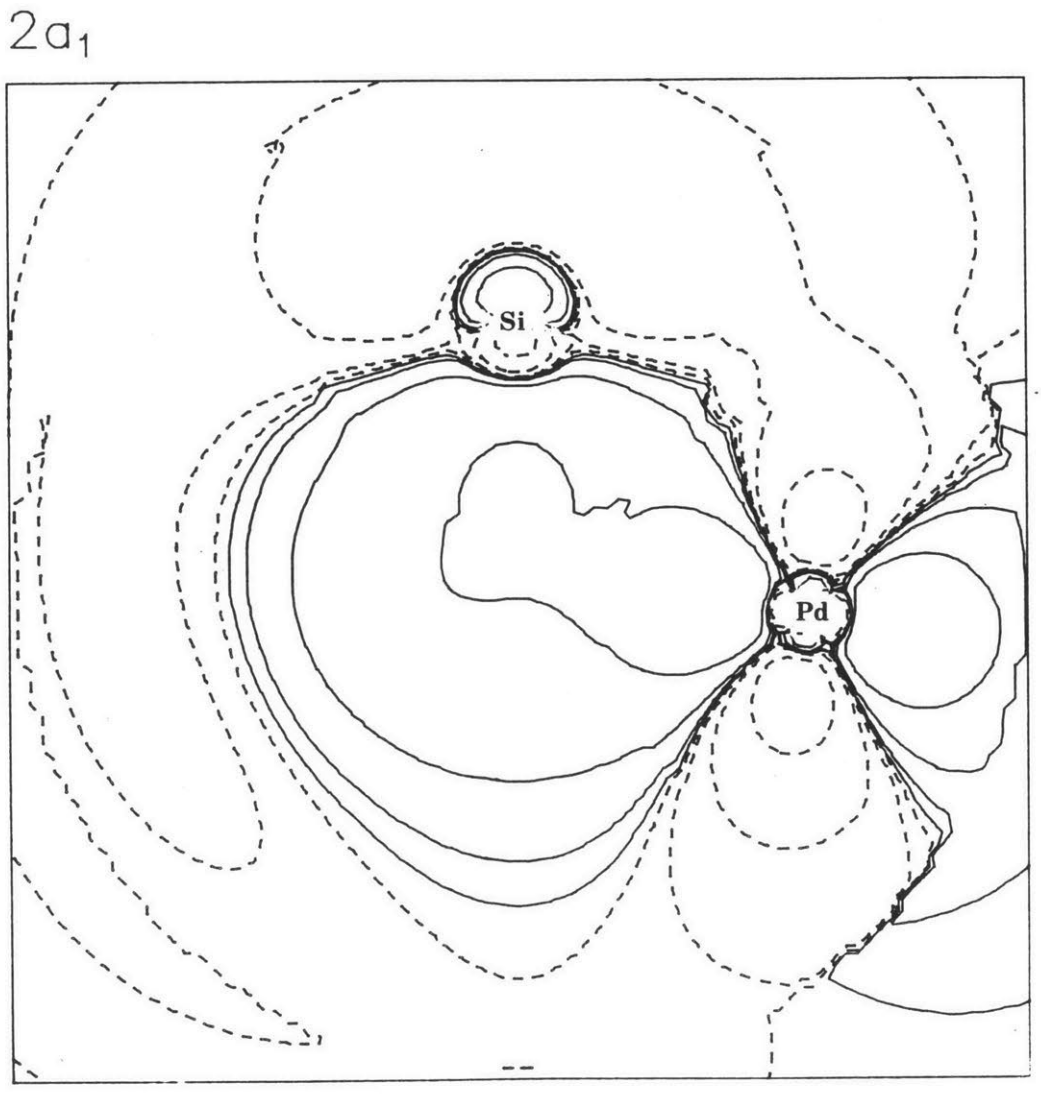

Fig. 5.13. Plot of the wavefunction of the 2a1 orbital of the Pd_3Si cluster showing Si p, Pd d bonding interaction.

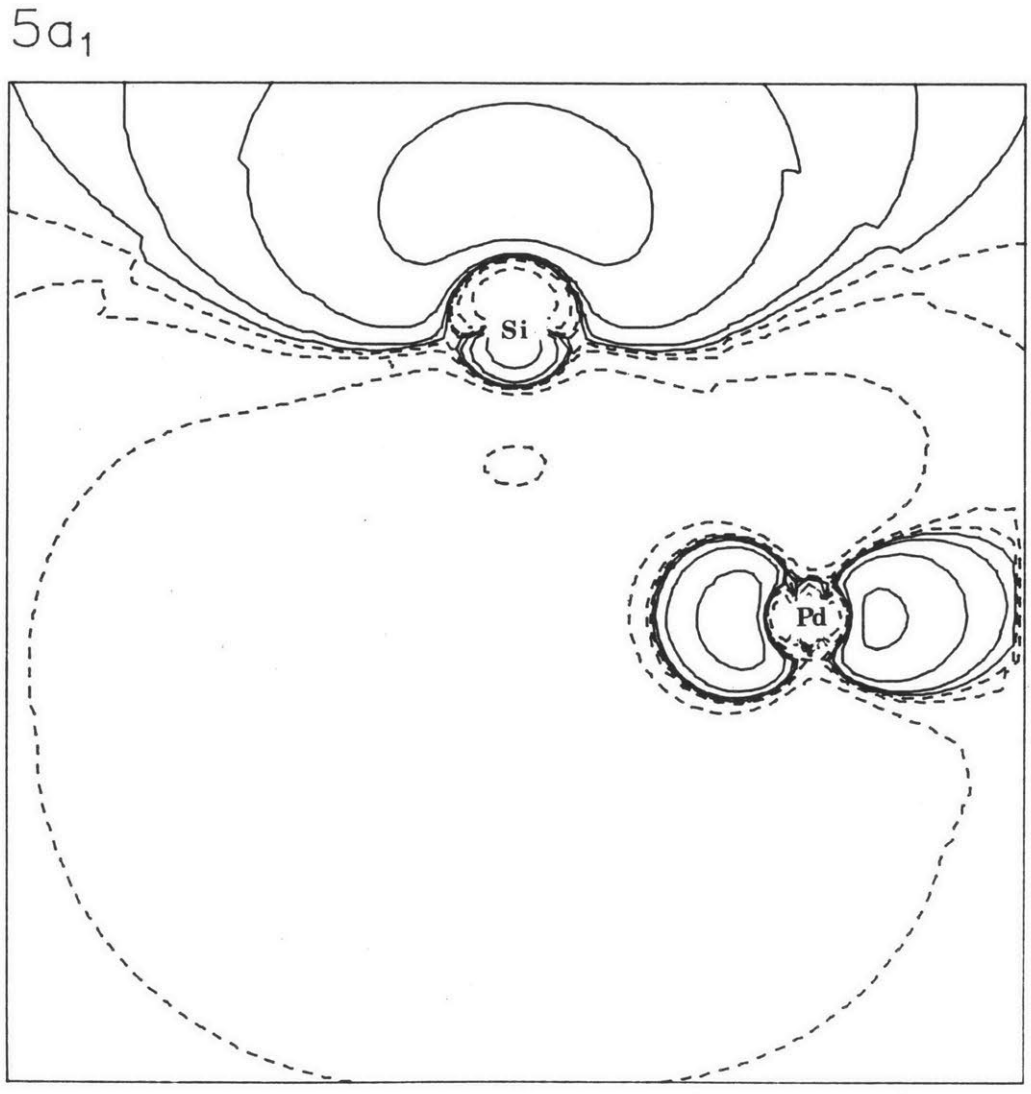

Fig. 5.14. Plot of the highest occupied molecular orbital of the Pd_3Si cluster showing the diffuse Si p character.

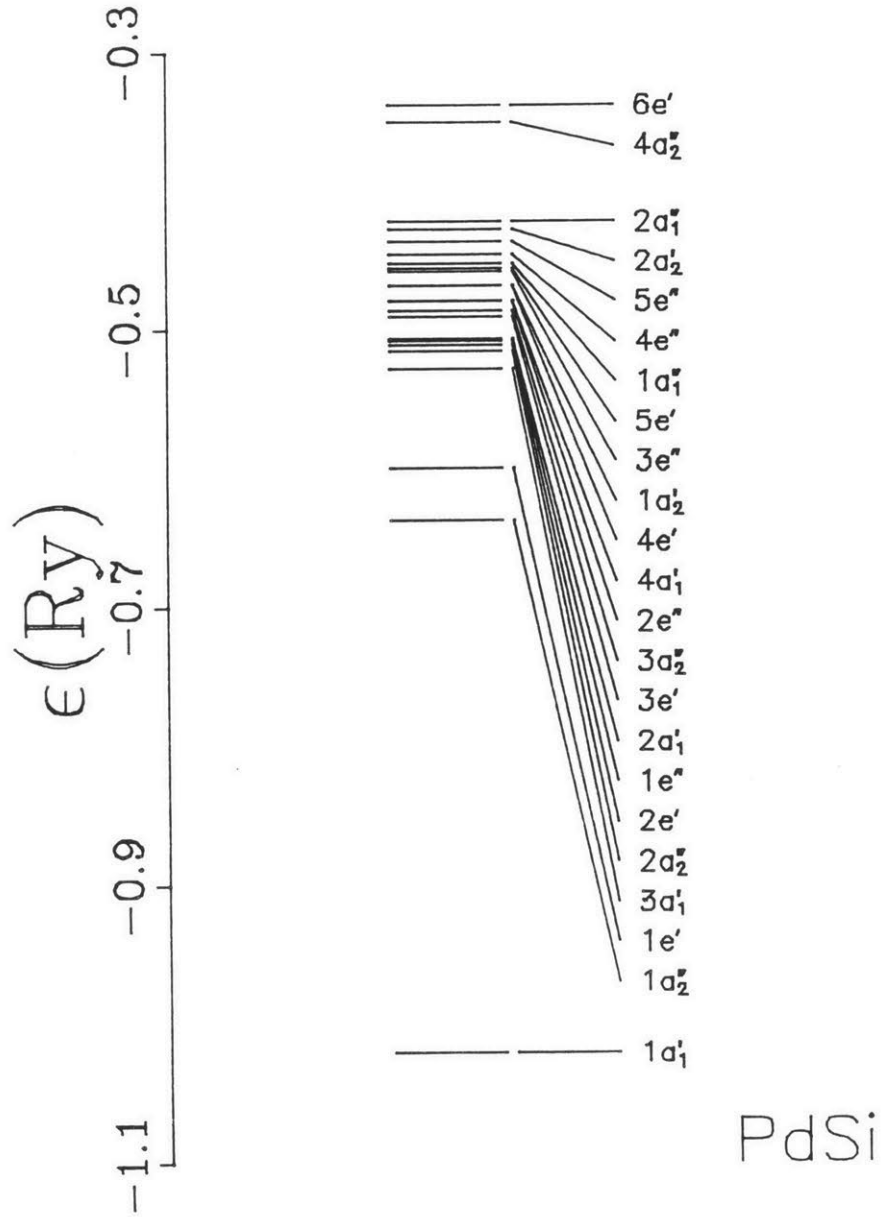

Fig. 5.15. Energy level diagram of the Pd_6Si cluster. Note how the two main Si-Pd bonding orbitals (1e′ and 1a2″) have been pulled substantially below the manifold of Pd d states.

levels, which are now more definitely split off from the Pd d band. The 1a2" and 2e' levels are pulled much lower in energy than the corresponding orbitals (2a1 and 1e) of the Pd_3Si cluster. Because the Pd-Si interatomic distances are identical in the two clusters, the degree to which the 1a2" and 2e' levels are lowered is a measure of the strength of the chemical bonding between the Si and the additional three Pd atoms.

The strong chemical interaction between the Pd and Si has implications for the mechanism of glass formation. Bernal [19] first described the structure of a liquid metal as a dense random packing of hard spheres. This theory is notable for the appearance of characteristic interstitial voids, called "Bernal holes." Later, Polk and others [20] explained the stability of TM-M glasses by assuming that the smaller metalloid atoms would fill the Bernal holes created by the dense random packing of the larger transition metal atoms. From this viewpoint, the difference in the atomic sizes is crucial to the stability of the glass. Chen and Park [21], using arguments based on volumetric studies, argued that factors other than atomic size (such as chemical bonding) must be important for the stability of TM-M glasses in general and the Pd-Si glasses in particular. While the cluster calculations reported here can shed no light on the relative importance of the atomic size differential to glass formation, they do lend weight to the claim that strong chemical bonding between the transition metal and metalloid is important to the formation of the of TM-M glasses.

The energy levels of the Pd_3Si_2 cluster are shown in Figure 5.16. While the general features are similar to those of the first two

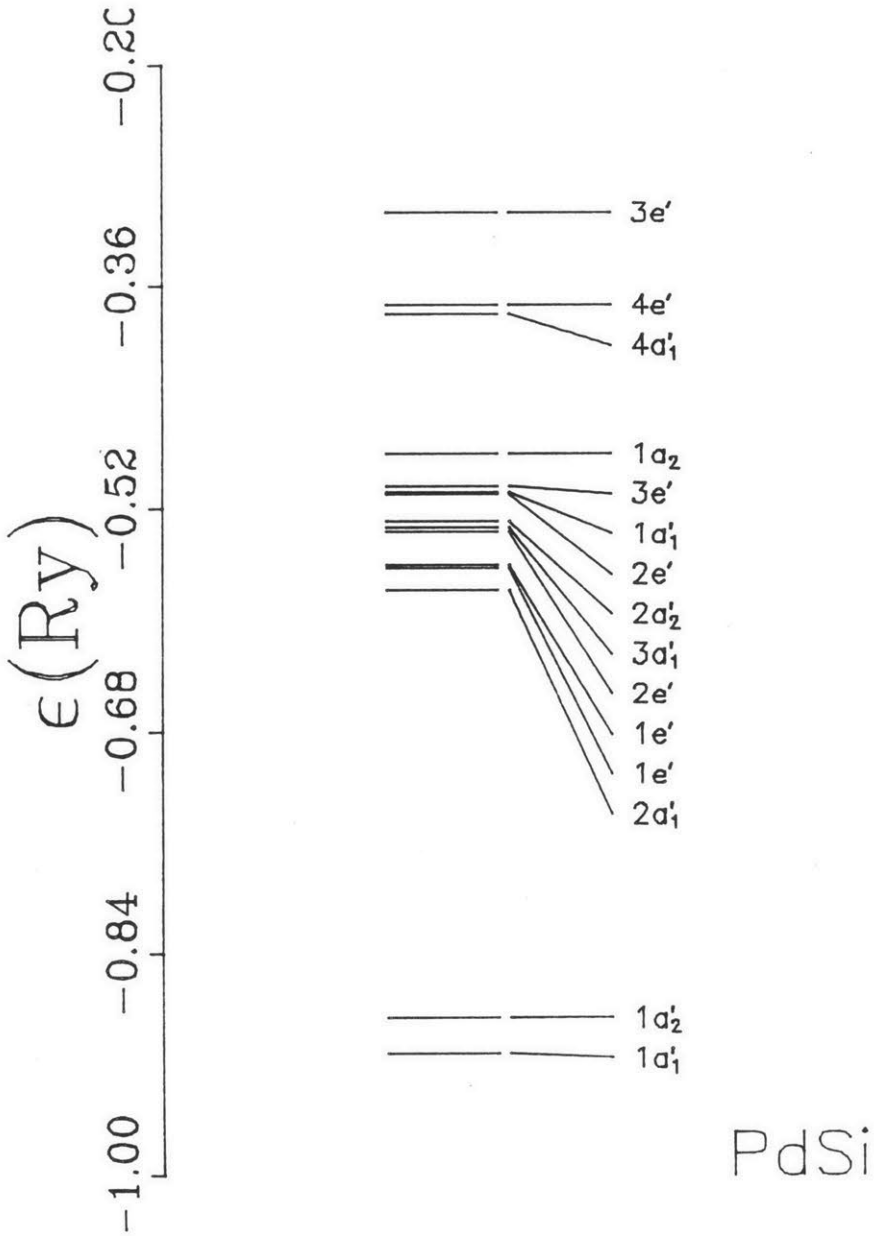

Fig. 5.16. Energy level diagram for the Pd_3Si_2 cluster.

clusters, the highest occupied orbitals (4e' and 4a1') are of interest. These orbitals are antibonding between the Si and Pd, but bonding between the two Si atoms. The diffuse nature of this second nearest neighbor bond is seen in the plot of the 4a' wavefunction in Figure 5.17. Although the strength of such a bond is uncertain, one might speculate that a network of such Si-Si bonds may have a role in the stabilization of of the glass. In addition, because orbitals of this type are at the Fermi level, they must determine the transport properties of the alloy. It is interesting to note that these orbitals can be considered to correspond to the Si conduction band, while the lower Pd-Si bonding levels (1e' and 2a' in the Pd Si cluster) correspond to the Si valence band.

Both UPS and high resolution XPS studies of Pd-Si metallic glasses have identified a shoulder in the density of states at the the Fermi level that does not appear in pure Pd [22,23]. Cartier and co-workers claim that this shoulder arises from Pd d states; the calculations presented here lead to the identification of the shoulder with the Pd-Si antibonding orbitals. In all three clusters the Pd-Si antibonding orbitals consist of Si p character and varying degrees of Pd s-d hybridization. In the Pd_3Si cluster, the partial wave decomposition of the Pd character of the 5a1 level is 57% s, 6% p, and 36% d. The 4a2" level of the Pd_6Si cluster has a partial wave decomposition of 32% s, 5% p, and 64% d. The corresponding figures for the 4a1' and 4e' levels of the Pd_3Si_2 cluster are 40% s, 5% p, and 55% d for 4a1'; 18%s, 4% p, and 77% d for the 4e' state. For all three clusters, significant Pd s-d hybridization is seen only in those orbitals having substantial Si character.

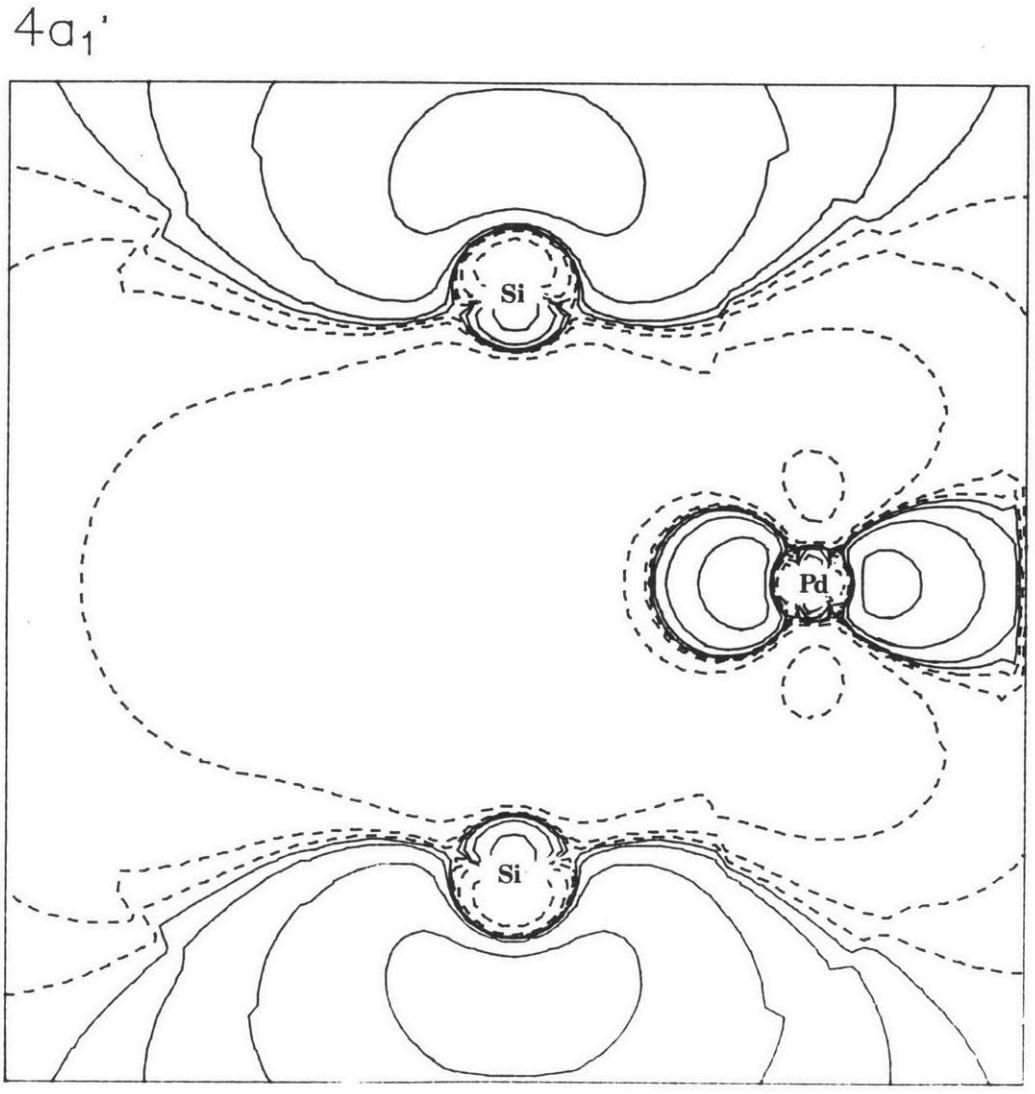

Fig. 5.17. Plot of the wavefunction of the 4a1' orbital of the Pd_3Si_2 cluster, showing diffuse second nearest neighbor Si-Si bonds.

To summarize, small clusters of atoms have been shown to provide useful models for the calculation of the electronic structures of TM-TM and TM-M metallic glasses. The calculated electronic structures are in good quantitative agreement with, and provide an interpretation of, published photoelectron spectra of amorphous Zr-Cu and Pd-Si. In addition, these calculations provide information on the chemical bonding in these alloys, giving into their glass forming ability.

REFERENCES

1. H. Beck and H.-J. Guntherodt, in Glassy Metals I, edited by H.-J. Guntherodt and H. Beck (Springer-Verlag, Berlin, 1981).

2. H. Ehrenreich and L.M. Schwartz, in Solid State Physics, Vol. 31 (Academic Press, New York, 1976).

3. J.D. Joannopoulos and M.L. Cohen, in Solid State Physics, Vol. 31 (Academic Press, New York, 1976).

4. M.J. Kelley and D.W. Bullett, J. Phys. C (GB) 12, 2531 (1979).

5. J. Kubler, K.H. Bennemann, R. Lapka, F. Rosel, P. Oelhafen, and H.-J. Guntherodt, Phys. Rev. B 23, 5176 (1981).

6. R.P. Messmer, S.K. Knudsen, K.H. Johnson, J.B. Diamond, and C.Y. Yang, Phys. Rev. B 13, 1396 (1976).

7. D.R. Salahub and R.P. Messmer, Phys. Rev. B 16, 2526 (1977); R.P. Messmer and D.R. Salahub, Phys. Rev. B 16, 3415 (1977).

8. K.H. Johnson, D.D. Vvedensky, and R.P. Messmer, Phys. Rev. B 19, 1519 (1979).

9. T.E. Fischer, S.R. Kelemen, K.P. Wang, and K.H. Johnson, Phys. Rev. B 20, 3124 (1979).

10. K.H. Johnson, H.J. Kolari, J.P. deNeufville, and D.L. Morel, Phys. Rev. B 21, 643 (1980).

11. J. Wong, private communication.

12. P. Oelhafen, E. Hauser, H.-J. Guntherodt, and K.H. Benneman, Phys. Rev. Lett. 43, 1134 (1979).

13. D.D. Vvedensky, Ph.D. Thesis (Massachusetts Institute of Technology, 1980).

14. H.S. Chen and Y. Waseda, Phys. Stat. Sol. (a) 51, 593 (1979).

15. J. Wong in Glassy Metals, Vol. 1, edited by H.-J. Guntherodt and H. Beck (Springer-Verlag, Berlin, 1980).

16. P.H. Gaskell, Nature 276,484 (1978).

17. T. Fukunaga, M. Misawa, K. Fukamichi, T. Masumoto, and K. Suzuki, in Proceedings of Rapidly Quenched Alloys Conference (1978).

18. K. Suzuki, T. Fukunaga, M. Misawa, and T. Masumoto, Mater. Sci. Eng. 23, 215 (1976).

19. J.D. Bernal, Nature 185, 68 (1960).

20. D.E. Polk, Scripta Met. 4, 117 (1970).

21. H.S. Chen and B.K. Park, Acta Met. 21, 395 (1973).

22. P. Oelhafen, M. Liard, H.-J. Guntherodt, K. Berresheim, and H.D. Polaschegg, Solid State Comm. 30, 641 (1979).

23. E. Cartier, Y. Baer, M. Liard, and H.-J. Guntherodt, J. Phys. F 10, L21 (1980).

ACKNOWLEDGEMENTS

I am very grateful to Professor Keith Johnson for his suggestion of the thesis, and for his continual support, encouragement, and enthusiasm. I am also grateful to Dr. Scott Wallace, who introduced me to computers and the lore of quantum chemistry. Finally, I would like to acknowledge the moral support of friends and colleagues at M.I.T., in particular Anna Balazs and Dave Root.